AFRL-RH-FS-TR-2017-0024

MATILDA Version-2: Rough Earth TIALD Model for Laser Probabilistic Risk Assessment in Hilly Terrain – Part II

Paul K. Kennedy
711th Human Performance Wing
Airman Systems Directorate
Bioeffects Division
Optical Radiation Bioeffects Branch

Brian K. Flemming
Leonardo MW Ltd, 2 Crewe Road North,
Edinburgh EH5 2XS, United Kingdom

Daniel F. Huantes
Engility, Inc., JBSA Fort Sam Houston, TX, USA

Matthew D. Flower
UK Ministry of Defence, MOD Abbey Wood, Bristol
BS34 8JH, United Kingdom

July 2017

Interim Report for March 2016 to June 2017

Air Force Research Laboratory
711th Human Performance Wing
Airman Systems Directorate
Bioeffects Division
Optical Radiation Bioeffects Branch
JBSA Fort Sam Houston, Texas
78234

NOTICE AND SIGNATURE PAGE

Using Government drawings, specifications, or other data included in this document for any purpose other than Government procurement does not in any way obligate the U.S. Government. The fact that the Government formulated or supplied the drawings, specifications, or other data does not license the holder or any other person or corporation; or convey any rights or permission to manufacture, use, or sell any patented invention that may relate to them.

This report was cleared for public release by the 88th ABW Public Affairs Office and is available to the general public, including foreign nationals. Copies may be obtained from the Defense Technical Information Center (DTIC) (http://www.dtic.mil).

"MATILDA Version-2: Rough Earth TIALD Model for Laser Probabilistic Risk Assessment in Hilly Terrain – Part II"

(AFRL-RH-FS-TR- 2017-0024) has been reviewed and is approved for publication in accordance with assigned distribution statement.

KENNEDY.PAUL.K.1231446318 Digitally signed by KENNEDY.PAUL.K.1231446318
DN: c=US, o=U.S. Government, ou=DoD, ou=PKI, ou=USAF, cn=KENNEDY.PAUL.K.1231446318
Date: 2017.07.28 12:23:09 -05'00'

PAUL KENNEDY, Ph.D.
Work Unit Manager
Optical Radiation Bioeffects Branch

MILLER.STEPHANIE.A.1230536283 Digitally signed by MILLER.STEPHANIE.A.1230536283
Date: 2017.10.15 13:46:23 -05'00'

STEPHANIE A. MILLER, DR-IV, DAF
Chief, Bioeffects Division
Airman Systems Directorate
711th Human Performance Wing
Air Force Research Laboratory

This report is published in the interest of scientific and technical information exchange, and its publication does not constitute the Government's approval or disapproval of its ideas or findings.

REPORT DOCUMENTATION PAGE

Form Approved
OMB No. 0704-0188

1. REPORT DATE *(DD-MM-YYYY)*	2. REPORT TYPE	3. DATES COVERED *(From - To)*
28-07-2017	Technical Report	March 2016 to June 2017

4. TITLE AND SUBTITLE

MATILDA Version-2: Rough Earth TIALD Model for Laser Probabilistic Risk Assessment in Hilly Terrain – Part II

5a. CONTRACT NUMBER
FA8650-14-D-6519

5b. GRANT NUMBER

5c. PROGRAM ELEMENT NUMBER

6. AUTHOR(S)

Paul K. Kennedy, Brian K. Flemming, Daniel F. Huantes, Matthew D. Flower

5d. PROJECT NUMBER

5e. TASK NUMBER

5f. WORK UNIT NUMBER
H0S0

7. PERFORMING ORGANIZATION NAME(S) AND ADDRESS(ES)

Air Force Research Laboratory
711th Human Performance Wing
Airman Systems Directorate
Bioeffects Division
Optical Radiation Bioeffects
JBSA, Fort Sam Houston, Texas 78234

Engility Corp
4141 Petroleum Rd
Fort Sam Houston, Texas 78234

8. PERFORMING ORGANIZATION REPORT

9. SPONSORING / MONITORING AGENCY NAME(S) AND ADDRESS(ES)

711th Human Effectiveness Wing
Airman Systems Directorate
Bioeffects Division
Optical Radiation Branch
JBSA, Fort Sam Houston, Texas 78234

10. SPONSOR/MONITOR'S ACRONYM(S)
711 HPW/RHDO

11. SPONSOR/MONITOR'S REPORT NUMBER(S)
AFRL-RH-FS-TR-2017-0024

12. DISTRIBUTION / AVAILABILITY STATEMENT

Pending Distribution A: Approved for public release; distribution unlimited. PA Case No: TSRL-PA-2017-0228

13. SUPPLEMENTARY NOTES

14. ABSTRACT

Over the past 15 years, the United Kingdom (UK) Ministry of Defence (MoD) and the United States (US) Air Force Research Laboratory (AFRL) have collaborated to develop a US-UK laser range safety tool, the Military Advanced Technology Integrated Laser hazarD Assessment (MATILDA) tool. MATILDA uses Probabilistic Risk Assessment (PRA) techniques to perform laser safety and hazard analysis in support of airborne laser designator use during test and training exercises on military ranges. The initial MATILDA tool, MATILDA PRO Version1.6.1, was based on the 2007 PRA model developed to perform range safety clearances for the UK Thermal Imaging Airborne Laser Designator (TIALD) system. The 2007 TIALD model was an approximation that assumed flat terrain on the range (Smooth Earth TIALD Model), a conservative approximation valid in all terrain. Over the past five years, however, an enhanced version, MATILDA PRO Version-2.0.3, has been produced. The enhanced tool is based on an updated (2012) TIALD model that has more complex PRA algorithms appropriate for hilly terrain (Rough Earth TIALD Model). For reasons of length, documentation of the mathematical algorithms and computational procedures incorporated in MATILDA PRO Version-2.0.3 has been divided between two AFRL Technical Reports. This Technical Report, designated Part II, contains documentation of the computational procedures for the fault-free laser hazard analysis. The first Technical Report, designated Part I, documented the probabilistic fault/failure laser hazard analysis.

15. SUBJECT TERMS

16. SECURITY CLASSIFICATION OF:			17. LIMITATION OF ABSTRACT	18. NUMBER OF PAGES	19a. NAME OF RESPONSIBLE PERSON
Unclassified					Paul Kennedy
a. REPORT	b. ABSTRACT	c. THIS PAGE			19b. TELEPHONE NUMBER *(include area code)*
U	U	U	Unclassified	74	NA

Standard Form 298 (Rev. 8-98)
Prescribed by ANSI Std. 239.18

This Page Intentionally Left Blank

TABLE OF CONTENTS

LIST OF FIGURES

ACRONYMS

UK/MoD	United Kingdom Ministry of Defence
US/AFRL	United States Air Force Research Laboratory
MATILDA	Military Advanced Technology Integrated Laser hazarD Assessment
PRA	Probabilistic Risk Assessment
TIALD	Thermal Imaging Airborne Laser Designator
DoD	Department of Defense
HEL	High Energy Laser
MPE	Maximum Permissible Exposure
PA	Project Arrangement
CRA	Controlled Range Area
GUI	Graphic User Interface
GIS	Geographic Information System
DTED	Digital Terrain Elevation Data
NASA	National Aeronautics and Space Administration
NOHD	Nominal Ocular Hazard Distance
ALARP	As Low As Reasonably Practicable
MOVL	Minimum Ophthalmoscopically Visible Lesion
LSP	Laser Safety Paper
PCRM	Probabilistic Range Clearance Model
PDF	Probability Distribution Function
MSD	Minimum Separation Distance
FFLFZ	Fault-Free Laser Firing Zone
MKS	Meters, Kilograms, Seconds
MICS	MATILDA Internal Coordinate System
CALF	Circle of Allowed Laser Firing
GPS	Global Positioning System
AMSL	Above Mean Sea Level
MPTS	Most Prominent Terrain Step
BNG	British National Grid

ABSTRACT

Over the past 15 years, the United Kingdom (UK) Ministry of Defence (MoD) and the United States (US) Air Force Research Laboratory (AFRL) have collaborated to develop a US-UK laser range safety tool, the Military Advanced Technology Integrated Laser hazarD Assessment (MATILDA) tool. MATILDA uses Probabilistic Risk Assessment (PRA) techniques to perform laser safety and hazard analysis in support of airborne laser designator use during test and training exercises on military ranges. The initial MATILDA tool, MATILDA PRO Version1.6.1, was based on the 2007 PRA model developed to perform range safety clearances for the UK Thermal Imaging Airborne Laser Designator (TIALD) system. The 2007 TIALD model was an approximation that assumed flat terrain on the range (Smooth Earth TIALD Model), a conservative approximation valid in all terrain. Over the past five years, however, an enhanced version, MATILDA PRO Version-2.0.3, has been produced. The enhanced tool is based on an updated (2012) TIALD model that has more complex PRA algorithms appropriate for hilly terrain (Rough Earth TIALD Model). For reasons of length, documentation of the mathematical algorithms and computational procedures incorporated in MATILDA PRO Version-2.0.3 has been divided between two AFRL Technical Reports. This Technical Report, designated Part II, contains documentation of the computational procedures for the fault-free laser hazard analysis. The first Technical Report, designated Part I, documented the probabilistic fault/failure laser hazard analysis.

1 INTRODUCTION

Over the past 20 years, the US Department of Defense (DoD) has funded the development of airborne, ground-based, and ship-borne High Energy Laser (HEL) weapons systems, primarily for Counter-Rocket, Artillery, and Mortar applications. The development, and potential deployment, of an increasingly wide range of military laser systems with higher energies, and hence, greater hazard potential, is leading to a requirement for more sophisticated means of assessing the real risk of hazardous exposure to operational personnel and strategic assets. Standard deterministic risk analysis methods [1,2], based on Maximum Permissible Exposure (MPE) limits [3,4], are inadequate to assess the potential risk posed by test and deployment of HEL systems. Deterministic models do not account for the unpredictable errors that inevitably occur in outdoor range tests, training, and/or operational use. They also give only a binary safe/unsafe assessment, without providing a quantitative risk assessment for “unsafe” scenarios.

Recently, attention in the DoD has turned to Probabilistic Risk Assessment (PRA) models [5,6] as an alternative for performing laser hazard analysis for high output lasers in outdoor environments [7-12]. These models can incorporate errors and uncertainties, using probability distribution functions, and they can provide a quantitative probability of injury to personnel or damage to hardware. Over the past 15 years, in response to DoD requirements, the United States (US) Air Force Research Laboratory (AFRL) has collaborated with the United Kingdom (UK) Ministry of Defence (MoD) to develop a jointly-owned, PRA-based, laser range safety tool, the Military Advanced Technology Integrated Laser hazarD Assessment (MATILDA) tool [13-17]. This collaboration has been covered, sequentially, by two US-UK Project Arrangements (PAs): No. DOD-MOD-AF-06-0004 (2007-2012) and No. DOD-MOD-AF-12-0004 (2012-2017).

The UK MoD has been using laser PRA models to support military laser tests at UK ranges for the past 40 years. PRA analysis is essential for range testing in the UK, where ranges are typically quite small and located near to populated areas. Only by quantifying laser hazards using PRA, and comparing these to a maximum acceptable risk level, can the MoD authorize laser testing on small ranges, where the beam has a finite probability of escaping the Controlled Range Area (CRA). The US-UK collaboration was initiated because the USAF considered it highly desirable to leverage UK expertise in this area, with the long term goal of producing probabilistic laser safety tools to meet future DoD laser safety needs. The quid pro quo was a trade of UK expertise in probabilistic laser hazard analysis and PRA mathematical modeling for US expertise in the development of advanced software tools for laser hazard analysis and laser range safety.

Initial MATILDA code development (2007–2012) was based on the PRA "partition" model developed to perform range safety clearances for the UK Thermal Imaging Airborne Laser Designator (TIALD) system. The TIALD model "fault-free" laser hazard analysis is geometrically similar to the standard risk analysis methods currently used for laser safety clearances on US ranges [1]. However, the TIALD model contains an additional probabilistic hazard analysis component, which assesses probability of injury to an unprotected person outside of the CRA in the event of a fault or failure in the laser directional control system. The TIALD model was chosen as the basis for the initial MATILDA tool because it was the most advanced UK laser PRA model available at the time when code development began (2007).

The final deliverable (2012) under the first PA was a code designated MATILDA PRO Version-1.6.1, which was a tested and validated software tool containing the complete 2007 TIALD model. It included a calculation of safe firing zones for fault-free operation, calculation of the probability of injury to an observer off the range in the event of system fault/failure, and a sophisticated graphics and terrain mapping package to illustrate the results. The Graphic User Interface (GUI) was based on open-source Geographic Information System (GIS) technology that integrates relevant laser system performance parameters with environmental data appropriate to the range location where the system is being operated. A previous AFRL Technical Report [16] documented the mathematical algorithms and computational procedures incorporated in MATILDA PRO Version-1.6.1, and provided the mathematical basis for future code development and improvements.

Advanced MATILDA code development (2012-2017), under the second PA, has been based on incorporation of an updated TIALD model. The 2007 TIALD model was an approximation that assumed flat terrain on the range (Smooth Earth Model). The Smooth Earth Model is a conservative approximation in laser safety terms, since hills and elevated terrain generally provide shielding and reduce risk. A less conservative and more realistic model was desirable, however, since it would produce reduced hazard estimates and fewer constraints on range tests. By 2012 an updated TIALD model had been developed, with more complex PRA algorithms appropriate for hilly terrain (Rough Earth TIALD Model). This model uses input data from the Digital Terrain Elevation Data (DTED) database, data taken by the National Aeronautics and Space Administration (NASA). The final deliverable under this second PA will be a code designated MATILDA PRO Version-2.0.3, which is a tested and validated software tool containing the complete Rough Earth TIALD Model.

For reasons of length, documentation of the mathematical algorithms, calculations, and analytical procedures incorporated in MATILDA PRO Version-2.0.3 has been divided between two AFRL Technical Reports, which will once again provide the mathematical basis for future code development. The first Technical Report, designated Part I [18], documented the computational procedures for probabilistic fault/failure laser hazard analysis. This Technical Report, designated Part II, documents the computational procedures for the fault-free laser hazard analysis. Section 2 of this report gives a brief summary and overview of the UK Laser PRA Model, the Smooth Earth TIALD Model, and the computational structure of the Rough Earth TIALD Model. This overview material was also presented in the first TR; it is repeated here to provide background material for readers who have not read the first report. Sections 3 and 4 document the Flat Earth and Curved Earth algorithms for the 3D-CALCZONE module, which calculates the Fault-Free Laser Firing Zones (FFLFZ) in hilly terrain for no-fault laser operations. Section 5 documents the 3D-CALCTERT module, which modifies the FFLFZ to mitigate hazards from low probability/high consequence events. Sections 6 and 7 give conclusions and references.

2 UK LASER PRA MODEL AND MATILDA COMPUTATIONAL MODELS

The UK Laser PRA Model, and the risk-based approach to laser hazard assessment that underlies it, has already been extensively documented in past open source publications [11-17]. A detailed description of the UK technical approach and solution reporting can be found within the initial AFRL Technical Report [16], which documented MATILDA PRO Version-1.6.1 and its Computational Model (Smooth Earth TIALD Model). Only a brief overview and summary of the UK Laser PRA Model and the Smooth Earth TIALD Model is given in Sections 2.1 and 2.2 of this report, with the reader directed to past work for a more extensive and detailed description. Section 2.3 gives a brief overview of the Computational Model underlying MATILDA PRO Version-2.0.3 (Rough Earth TIALD Model), with an eye to setting the stage for the detailed documentation of this model given in later Sections.

2.1 UK Laser PRA Model

The primary hazard associated with the use of low-to-moderate power lasers on military ranges is potential injury to exposed tissue, in particular the eye. While protective measures can be applied for persons within the CRA, the main concern – particularly in the case of airborne laser target designators and rangefinders – is avoidance of possible ocular injury to unprotected members of the general public, should laser energy escape the confines of the range. The goal of the UK Laser PRA Model is to quantify the expectation value of ocular damage to unprotected observers outside the CRA, based on range geometry, target location on the range, location and population density of surrounding urban areas, laser system parameters (including laser pointing errors during no-fault operation and fault conditions), and the planned laser firing locations during the test or training scenario. For airborne laser-target designators, which have been the primary focus of UK PRA hazard analysis, the flight height and attack track of the aircraft carrying the laser designator defines possible firing locations [16].

Traditionally, the ocular hazards associated with a laser's output have been assessed in terms of the MPE, from which a corresponding Nominal Ocular Hazard Distance (NOHD) is determined [3,4]. The NOHD represents a safe viewing distance, and the area or volume inside the NOHD is a hazard zone, within which an unprotected observer is at risk of ocular injury. Where sufficient real estate is available, it is possible to ensure confinement of the hazard zone within the CRA, without imposing onerous restrictions on the permitted laser firing envelope. In such cases, the laser energy is said to have been "back-stopped" within the range. Should laser energy escape the CRA, however, it is possible that an unprotected observer could have an ocular injury. In such cases the zero risk criterion, implicit in standard deterministic risk analysis, creates a significant problem for those generating range safety clearances for laser testing and training.

The UK Laser PRA Model acknowledges that there is always a finite risk of laser energy escaping the CRA, especially during laser fault conditions, and that the actual risk of injury is always non-zero, although it may be negligible. The relatively small size of UK ranges enhances this risk. Thus, the stringent limitations on laser firing, required to satisfy a zero risk criterion, make standard MPE-based risk analysis too inflexible for UK range clearance requirements. Instead, UK range clearance models are probabilistic, and based on the principle of residual risk being "As Low As Reasonably Practicable" (ALARP) [2]. The use of the ALARP principle in UK hazard assessment arises from the provisions of the UK *Health and Safety at Work Act* of 1974 [19]. Given non-zero risks, use of the NOHD as a criterion for risk analysis is unsatisfactory, since it does not *quantify* the probable risk of injury for unprotected observers inside the hazard zone. The UK Laser PRA Model thus uses a probabilistic ocular damage model for 1064 nm laser energy, a "dose-response" model, to assess probability of injury. The model is based on biological injury data, and relates the dose (total intra-ocular energy) to the response to determine the probability of causing a Minimum Ophthalmoscopically Visible Lesion (MOVL) [7].

ALARP requirements can only be satisfied by the use of a risk-based approach to laser hazard assessment. The outcome of such a risk-based approach is a risk management process, by which adverse events, and the inherent uncertainties with which they occur, can be rigorously identified and mitigated. The UK risk assessment process comprises two distinct stages. The *risk analysis stage* constitutes a hazard assessment of the laser system *performance* when operating either as intended, or in the event of a laser sightline directional control system fault or failure. The laser system hazard assessment in the UK is expressed formally in a Laser Safety Paper (LSP). The hazard assessment for the laser system *operation* is the subject of the *risk management and control stage*. The Probabilistic Range Clearance Model (PRCM) provides a means by which hazards arising from the laser system *operation* can be evaluated, and is based on the performance assessment described in the LSP. Laser firing restrictions for a given range, target and attack profile combination are generated by application of the PRCM, as encoded in the MATILDA tool.

The risk of an adverse event, such as a laser-induced ocular injury in an unprotected population, can be expressed in terms of a "risk chain" comprising three main components [20]: (i) a risk source, (ii) an exposure process and (iii) a causal process. This concept is illustrated in Figure 1. Uncertainty persists within both the exposure and causal processes over the occurrence of given events, such as the misdirection of laser energy in a specific direction or the sustaining of an ocular injury. The likeliness of an event occurring may be defined by a fixed value, for simple

models, or by a Probability Distribution Function (PDF) for more complex ones. The General Risk Model thus falls naturally into a probabilistic structure, the "P_E-P_I-P_{OD}" catastrophic chain of events structure, also shown in Fig. 1. The PCRM, mentioned previously, is the mathematical implementation of the "P_E-P_I-P_{OD}" chain of adverse risk events model. Here the "P_E-P_I" couplet represents the exposure process and the "P_{OD}" element represents the causal process. The "P_E-P_I-P_{OD}" structure provides the mathematical basis for the UK probabilistic laser hazard assessment.

As a start to constructing a mathematical model of the probabilistic laser hazard assessment, the risk chain must be broken down into its individual probabilistic elements. The three main components of such a risk chain are: (i) the probability of laser energy being fired in an inappropriate direction outside the Controlled Range Area (P_E), (ii) the probability of an unprotected observer having an ocular irradiation by the laser energy (P_I), and (iii) the subsequent probability of the irradiated observer sustaining an ocular injury (P_{OD}). These three components can be further decomposed into five distinct elements: i) the risk of laser energy being directed outside the CRA; ii) the risk of an unprotected observer being irradiated; iii) the risk of the unprotected observer looking in the direction of the laser energy (ocular irradiation); iv) the risk of atmospheric scintillation increasing the radiant exposure entering the eye; and v) the risk of the received radiant exposure causing ocular damage. Here, the first element is associated with P_E, the second and third with P_I, and the fourth and fifth with P_{OD}.

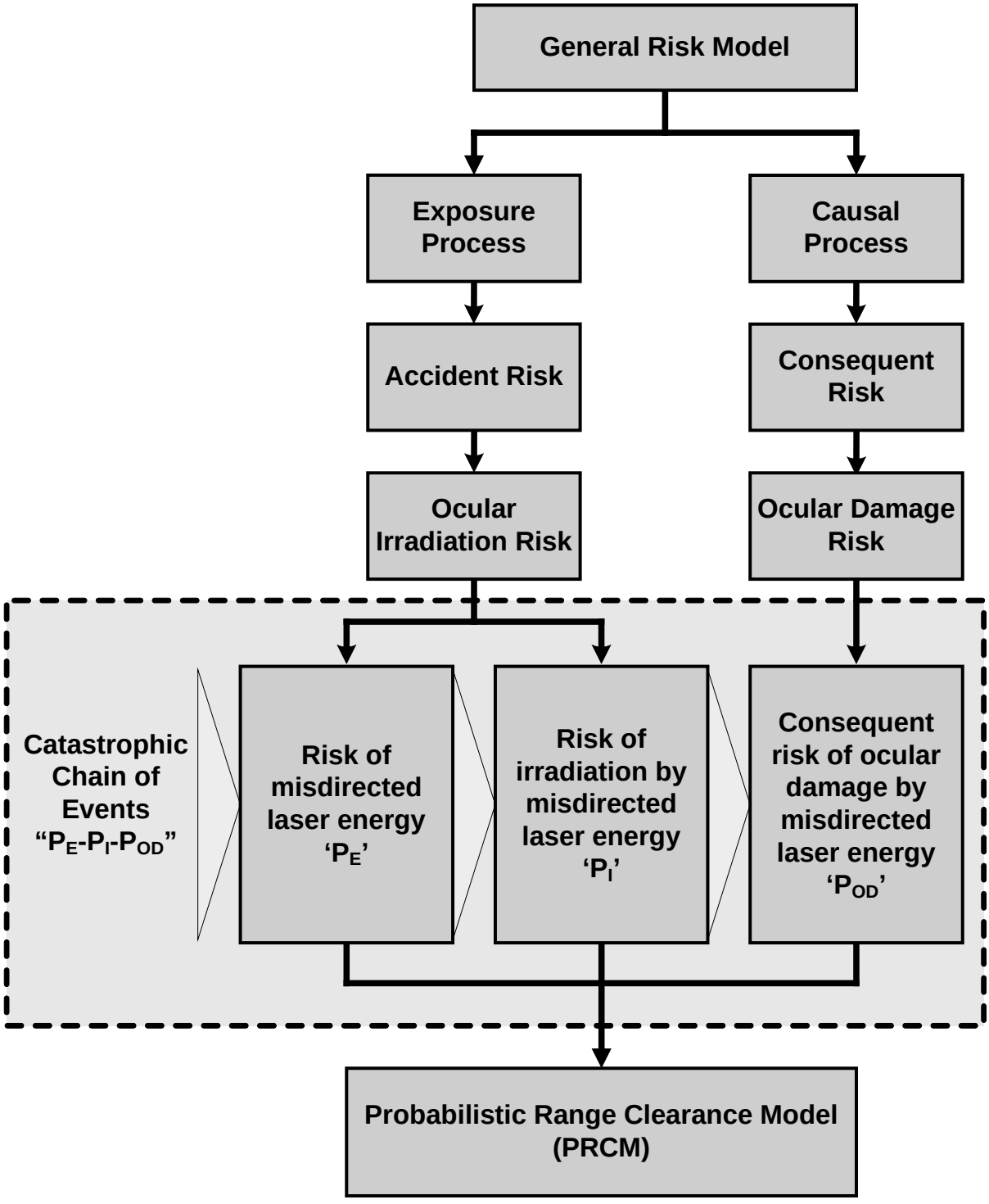

Figure 1: The "PE-PI-POD" Catastrophic Chain of Events Model

UK risk-based range clearance models have been based primarily on two of the three components: a probabilistic laser pointing error model (P_E), coupled with a probabilistic ocular

damage model for 1064 nm laser energy (P_{OD}). These have been described in detail in previous documentation [16]. In contrast, due to the complexity of accurately determining the probability of an observer being at a particular location, or looking into the laser beam, the P_I component has usually been implemented in a highly simplified version; i.e., these probabilities are typically set to unity. The inherent pessimism of this approach can then be mitigated by estimating the *expected number* of observers sustaining a given level of ocular damage in any given laser firing direction, based on the size of the beam footprint and the local population density. For this reason the UK probabilistic hazard assessment model is also referred to as the UK Expectation Model.

As indicated above, the UK Expectation Model, which incorporates the P_E-P_I-P_{OD} structure, is based on an evaluation of the expected number of unprotected observers who sustain a MOVL during an airborne laser firing maneuver, a quantity defined as E_{MOVL}. The Primary Criterion for clearance of a laser firing maneuver is that the expected number of cases of MOVL does not exceed a pre-defined maximum acceptable value, $E_{MOVLMAX}$. A typical maximum acceptable expectation value for UK range clearances is 10^{-8} probability of MOVL per attack. (In comparison, a typical NASA acceptable expectation value, for injury by falling inert debris, is 10^{-6} probability of injury per launch.) If the Primary Criterion is exceeded, then restrictions on the laser firing envelope are imposed to reduce risk to acceptable levels. Note that the very low risk levels set by the Primary Criterion are principally achieved by ensuring that most of the laser energy falls within the CRA.

Once the Primary Criterion is met then two additional precautions, the Secondary and Tertiary Precautions, are applied to identify any additional restrictions on the laser firing envelope. The Secondary and Tertiary Precautions guard against the possibility of a low likeliness, high impact event, in which a high probability of ocular damage to an irradiated observer could be masked by a low frequency of occurrence. The Secondary Precaution evaluates the expected hazard for a scenario in which it is assumed that laser energy is misdirected towards a populated area outside the CRA. The acceptable criterion for the Secondary Precaution is that – should laser energy be inadvertently misdirected outside the CRA – the expected number of cases of MOVL does not exceed a maximum *conditional* expectation value, E_{CONMAX}. For the UK, a typical maximum value for the Secondary Precaution is on the order of 10^{-3} to 10^{-4} probability of MOVL per attack.

The Tertiary Precaution assumes that an unprotected observer has actually been irradiated by a single pulse of laser energy. The acceptable criterion for the Tertiary Precaution is that the probability of a MOVL for an irradiated individual does not exceed a pre-defined maximum value, $P_{MOVLMAX}$. For the UK, a typical maximum value for the Tertiary Precaution is 10^{-1} probability of MOVL per attack. The effect of the Tertiary Precaution is to impose a probabilistically defined Minimum Separation Distance (MSD) between the laser and any unprotected observer outside the CRA. In summary, appropriate restrictions are imposed on the laser firing envelope to ensure that the Primary Criterion, Secondary Precaution, and Tertiary Precaution, are satisfied.

The final topic dealt with in this brief overview of the UK Laser PRA Model is the UK Partition Model, which determines both the computational structure of the UK TIALD model and its implementation in the MATILDA tool. The UK Partition Model is a specific implementation of the UK Expectation Model described above, in which the hazard contributions arising from fault-

free and fault/failure operation of the laser directional control system are "partitioned" and evaluated separately. The overall clearance restrictions defining the permitted laser firing envelope are a composite of the separately and sequentially evaluated restrictions for fault-free and fault/failure operation.

The fault-free portion of the Partition Model is fundamentally a geometric implementation of the hazard analysis, based on where in the terrain laser pulses are expected to fall. Laser pulses emitted during fault-free laser operation, which will be the majority of pulses fired during most attack runs, will be constrained to fall within the CRA by geometric restrictions on aircraft operations generated during the fault-free analysis. Consequently, any hazard to the population surrounding the range will come from the relatively small number of pulses, which could be emitted during fault/failure operation and which might fall outside the CRA. The hazard from these pulses is determined by a full probabilistic hazard analysis incorporating the P_E-P_I-P_{OD} structure described above.

The primary products of the fault-free laser hazard analysis are the Fault-Free Laser Firing Zones for aircraft flying at each altitude of interest. A Fault-Free Laser Firing Zone (FFLFZ) is a geometric area within which an aircraft flying at a designated altitude can fire freely at the target. For any given attack altitude, the FFLFZ is defined in such a way that all fault-free laser pointing errors, which are less than or equal to the maximum fault-free pointing error, produce laser beams that fall within the CRA. Typically, the FFLFZ are evaluated for all compass directions around the target, and over a range of aircraft altitudes, in accordance with laser system user requirements. Each designated aircraft altitude produces a different FFLFZ. The geometry of the FFLFZ calculation is similar to the standard risk analysis methods currently used by the USAF to establish a safe laser firing envelope [1]. However, the FFLFZ calculation is designed to maximise the range-to-target at which the laser can be fired, given the extent of CRA available.

The hazard analysis for fault/failure operation is the fully probabilistic portion of the overall laser hazard assessment. It follows computation of the FFLFZ, considers laser pointing errors in excess of the maximum fault-free pointing error and is only performed for specific laser firing maneuvers on specific aircraft attack tracks. Thus, the first step in the fault hazard analysis is to define the aircraft attack track, attack altitude, and laser firing positions. A check is then made to ensure that the attack scenario complies with FFLFZ restrictions. Any laser firing maneuvers that do not comply with FFLFZ restrictions are eliminated prior to the fault hazard analysis. Next, the probabilistic Expectation Model is used to evaluate E_{MOVL}, and this is compared to the maximum acceptable value, $E_{MOVLMAX}$, to determine whether the specified laser firing maneuver meets the Primary Criterion for safety clearance. Finally, if the Primary Criterion is met, then the Secondary and Tertiary Precautions are applied, to identify any additional restrictions on the laser firing envelope.

2.2 MATILDA Version-1.6.1 and the Smooth Earth TIALD Model

In MATILDA Version-1.6.1, the Partition/Expectation Model is implemented by means of a Computational Model known as the Smooth Earth TIALD Model, from which the applicable laser firing restrictions are derived. The Smooth Earth TIALD Model is composed of three main modules, executed sequentially, called RBPROG, CALCZONE, and CALCFAULT. Prior to execution of these modules the input data required for the hazard assessment are first specified.

There are five types of input data required for a full MATILDA analysis: i) population data for the urban and rural areas surrounding the range; ii) laser system parameters; iii) aircraft attack track data; iv) terrain mapping and terrain elevation data; and v) geometric and geographic data defining the range and areas surrounding it. The latter includes range boundaries, target position on the range, location and boundaries of Urban Areas, and natural geographic features such as rivers, lakes, and coastlines.

The MATILDA tool is currently designed for PRA analysis of air-to-ground laser-target engagements, with an airborne laser designator that is a multiple pulse "all-round line-of-sight" system mounted on a strike aircraft. Important MATILDA input parameters for the laser system include: i) pulse energy, peak irradiance, and beam energy distribution; ii) other key beam parameters such as wavelength, beam divergence, pulse duration, and pulse repetition frequency; iii) Fault-Free and Fault Pointing Error Distributions; and iv) the Probability of Fault for the laser system. These laser system parameters are obtained by the laser system manufacturer, through testing of multiple laser units and averaging of performance data. The data is provided to laser safety officers in the Laser Safety Paper.

The five data types described above may initially be available to the analyst in a variety of physical units. For consistency a single system of units must be used in computations. The Meters, Kilograms, Seconds (MKS) unit system has been chosen for MATILDA and, with some specific exceptions, all data not initially available in MKS units are transformed into them prior to input. Another potential problem is that some geographic data types may initially be available in a variety of coordinate systems, typically local (grid-based) map coordinate systems. For computational consistency these are transformed into a single common coordinate system, termed the MATILDA Internal Coordinate System (MICS). In order to bring such local map data into the MICS, three different coordinate transformations are performed. These coordinate transformations have been described in earlier documentation [16] and will not be discussed here.

After data input and data transformations are complete, there is one additional set-up procedure which must be performed prior to initiating the computational analysis: generation of a mathematical model termed the Terrain Profile Surface, using the digital terrain elevation data and target location supplied. Although the Smooth Earth TIALD Model assumes a flat range, a conservative safety analysis requires that *some* allowance must be made for terrain elevation in the area surrounding the target, if only to guard against the possibility of short-range irradiation of elevated terrain areas where unprotected persons might be present. The Terrain Profile Surface is a simplified representation of the terrain elevation in the area surrounding the target. This theoretical surface has the target location as its lowest point. From that point it rises, in terrain steps of steadily increasing height, as we move radially outward from the target in all directions. Terrain Profile step heights are defined such that the actual terrain heights are always below the surface. The Terrain Profile Surface thus guards against short-range irradiation of elevated terrain areas under the laser-target vector. It is used in the CALCZONE module, to aid in the proper definition of the FFLFZ, which can be affected by the underlying terrain step profile.

Following data input, preliminary computations, and definition of the range test scenario to be analysed, the three computational modules mentioned above are executed. The initial module is the Range Boundary Program, known as RBPROG for short. The main purpose of the RBPROG algorithm is to define the Controlled Range Area, which will be used in the CALCZONE module

to define the FFLFZ. The CRA is a sub-set of the total Range area, which is "star-shaped" with respect to a given target. A CRA is defined to be star-shaped when any radial vector, ω, emanating from the target, crosses the Range boundary only once. Frequently the initial Range area does not satisfy the star-shaped condition, so a portion of it is truncated to form the star-shaped CRA. Extra coordinates are also inserted around the modified CRA boundary to provide appropriate computation points for the CALCZONE algorithm.

The second module, CALCZONE, performs the fault-free laser hazard analysis. Specifically, it calculates the FFLFZ for each designated target within the CRA and for each designated aircraft altitude. The definition of an FFLFZ begins with a set of radials connecting the target to each of the CRA boundary points. For each radial, ω, emanating from the target, CALCZONE computes a maximum laser firing range-to-target (ground range), $R(\omega)$, such that fault-free laser pointing errors (within the maximum error α_{max} of the laser-target vector) remain within the CRA. This requirement results in two such ranges-to-target, $R_u(\omega)$ and $R_o(\omega)$, corresponding to the need to keep "undershoot" and "overshoot" laser pointing errors, respectively, within the CRA, as shown in Fig. 2.

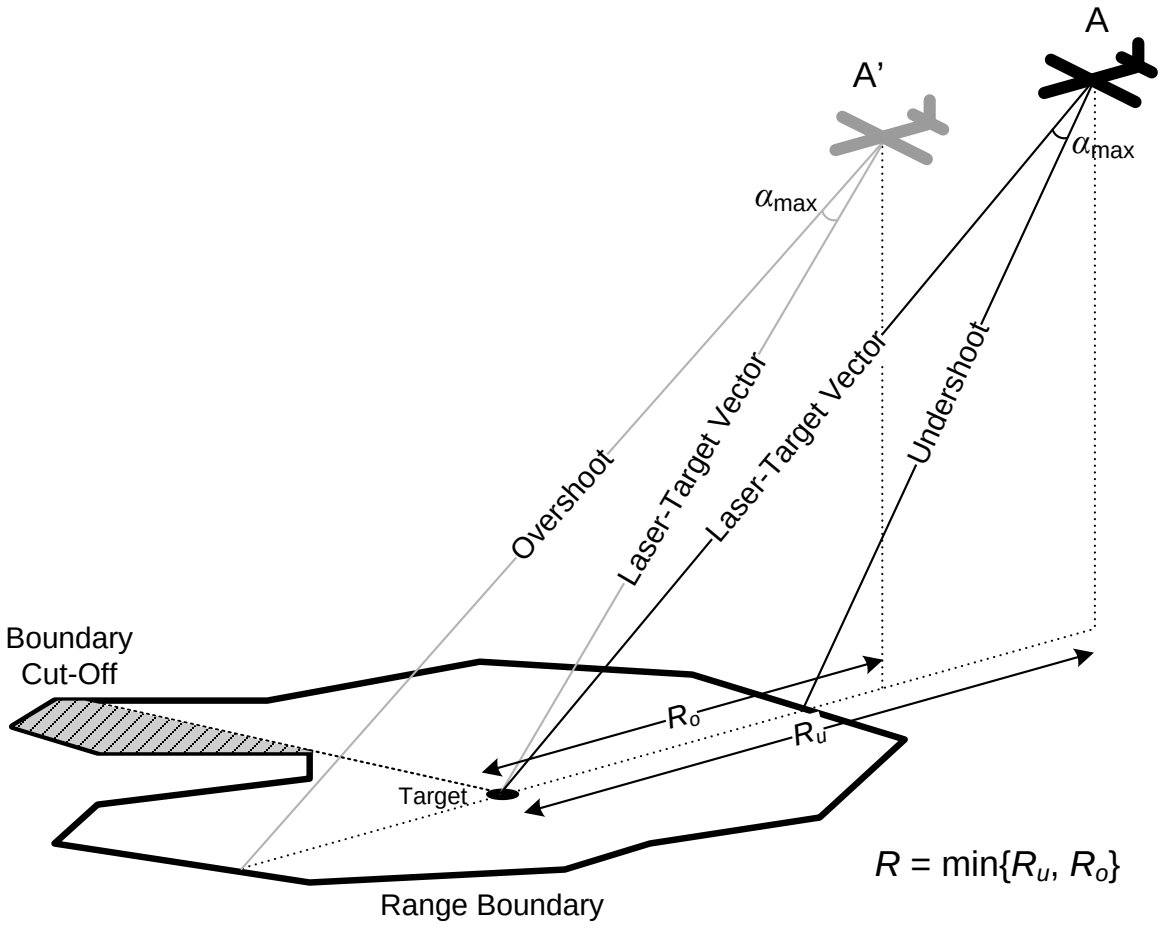

Figure 2: Fault-Free Overshoot & Undershoot

As documented previously [16], the equations for the undershoot and overshoot ranges implemented in Version-1.6.1 do not have analytical solutions, but must be solved by iteration. Once we have calculated the undershoot and overshoot ranges, $R_u(\omega)$ and $R_o(\omega)$, corresponding to aircraft height, H, and to some radial angle, ω, between the target and the near CRA boundary point, the overall maximum firing range, $R(\omega)$, is taken to be the smaller of the two. The FFLFZ for that height can then be defined by calculating the set $\{R(\omega): \omega \in [0,2\pi)\}$, covering all possible radials to any boundary point. The FFLFZ is typically plotted by laying down each range at the proper radial angle on the map, plotting the end point of each range vector, and then connecting all the end points to make a closed contour about the target. This process is repeated for each proposed attack height. The nested series of contours produced defines a three-dimensional envelope for safe firing during fault-free operation of the laser directional control system. For any aircraft maneuver, at any given altitude, the FFLFZ defines the maximum range-to-target at which the laser may be fired, assuming fault-free operation of the laser directional controls.

Generation of the FFLFZ contours completes the fault-free laser hazard analysis and lays the foundation for the probabilistic fault/failure hazard analysis performed in CALCFAULT. Prior to execution of CALCFAULT; however, a specific laser attack scenario must be defined. MATILDA provides a feature, the Attack Track Waypoint Editor that allows an analyst to overlay an attack track, defined by a series of waypoints, onto the map. The data entry for waypoints includes waypoint coordinates, aircraft altitude, aircraft velocity, and whether the laser is firing at that waypoint. With this data, MATILDA compares the proposed attack track against the altitude limitations defined by the FFLFZ and indicates to the analyst those portions of the track that are cleared for laser firing and those where laser firing is prohibited. Only the portion of the attack track that clears FFLFZ restrictions is analysed during CALCFAULT execution.

The third module, CALCFAULT, performs the probabilistic fault/failure hazard analysis for the designated and cleared laser attack scenario, to determine if any additional restrictions must be imposed on the laser firing envelope permitted by the FFLFZ. The CALCFAULT analysis quantifies the actual risk for firing along the designated attack track, in the event of a fault in, or a failure of, the laser directional control system. The probabilistic Expectation Model is used in this analysis. Key input parameters for the CALCFAULT analysis include laser system parameters, attack track data, population densities of the Urban Areas surrounding the range (assumed uniform and outside buildings), the terrain computational grid (points on the ground for which ocular damage probability is computed), and of course, the maximum acceptable value of the overall expectation value, E_{MOVLMAX}.

Since a fault/failure could occur at any point during the course of the cleared laser attack scenario, a large number of failure cases, each representing a possible failure of the directional control system at a different point along the attack track, must potentially be evaluated and their overall expectation values compared to the Primary Criterion. Generally, the number of failure cases evaluated is equal to the number of pulses fired during the attack scenario; i.e., the fault hazard analysis is performed for a possible failure at each of the laser firing positions. For each laser pulse emitted after the fault/failure, the CALCFAULT algorithm evaluates a corresponding expectation value, e_{MOVL}, that a MOVL will occur in the unprotected population surrounding the CRA.

The number of pulses emitted after a fault or failure has occurred depends on the pulse repetition frequency and the length of time required for the laser to cease firing. Consequently, the overall expectation value, E_{MOVL}, for a particular failure case, is the sum of the individual pulse e_{MOVL} values for the period of time during which the laser continues to fire, and before laser firing is inhibited. Restrictions on laser firing are subsequently imposed on those portions of the aircraft attack track for which the calculated value of E_{MOVL} exceeds the acceptable limit, $E_{MOVLMAX}$. Additional laser firing restrictions may also be imposed on those portions of the aircraft maneuver that bring the laser to within the applicable MSD of potentially unprotected populated areas.

Summarizing the material of Section 2.2, hazard analyses done with the Smooth Earth TIALD Model require six main computational steps, performed sequentially, using three major computational modules: RBPROG, CALCZONE, and CALCFAULT. The initial step consists of data input, data transformations, generation of the Terrain Profile Surface, and definition of the range test scenario to be analysed. Second, the RBPROG module is executed to generate the CRA and all range boundary points necessary to support the CALCZONE computations. Third, the CALCZONE module is executed, generating the FFLFZ for every specified aircraft attack height. Fourth, an aircraft attack track is generated, including proposed laser firing positions, and compared to the appropriate FFLFZ restrictions. The attack track is then modified to exclude those portions of the track where laser firing is prohibited by the FFLFZ. Fifth, the CALCFAULT module is executed to perform the probabilistic fault/failure hazard analysis for the designated and cleared laser attack track. Based on the analysis additional restrictions may be imposed on the laser firing envelope permitted by the FFLFZ. Sixth, the Secondary and Tertiary Precautions are applied in CALCFAULT to identify any final restrictions on laser firing.

2.3 MATILDA Version-2.0.3 and the Rough Earth TIALD Model

In the advanced version of MATILDA, MATILDA Version-2.0.3, the Partition/Expectation Model is implemented by means of a Computational Model known as the Rough Earth TIALD Model, which has more complex PRA algorithms appropriate for hilly terrain. Here we give a brief overview and summary of the main computational steps performed, and the major computational modules executed, when hazard analyses are done with the Rough Earth TIALD Model. This overview is intended as a preliminary modelling approach description to those in later Sections, which give detailed documentation of the mathematical algorithms and computational procedures of the major computational modules of the Rough Earth TIALD Model.

Hazard analyses done with the Rough Earth TIALD Model require seven main computational steps, performed sequentially, using four major computational modules: 3D-RBPROG, 3D-CALCZONE, 3D-CALCTERT, and 3D-CALCFAULT. Once again, the initial step consists of data input, data transformations, generation of the Terrain Profile Surface, and definition of the range test scenario to be analysed. Second, the three dimensional RBPROG module (3D-RBPROG) is executed. This process consists of executing the two dimensional RBPROG module, to generate the CRA and all range boundary points, and then creating a three dimensional range boundary (3D-CRA) by assigning an elevation to each boundary point. The elevations assigned are nominally equal to the height of the Terrain Profile Step immediately

above the boundary point. Third, the new three-dimensional CALCZONE module (3D-CALCZONE) is executed, generating the FFLFZ in hilly terrain for no-fault laser operations. A new method, the Circle of Allowed Laser Firing (CALF), is used to determine the FFLFZ in hilly terrain. Unlike the old method, the CALF does not require iterative calculations, producing increased computational efficiency. Once again a FFLFZ is generated for every specified aircraft attack height.

Fourth, the new three-dimensional Tertiary Precaution module (3D-CALCTERT) is executed, which modifies the FFLFZ produced by 3D-CALCZONE to mitigate hazards from low probability/high consequence events. Once again the CALF method is applied, this time to produce FFLFZ restrictions arising from the Tertiary Precaution. Fifth, an aircraft attack track is generated and modified, if necessary, to conform to the appropriate FFLFZ restrictions. Sixth, the new three-dimensional CALCFAULT module (3D-CALCFAULT) is executed, to perform probabilistic fault/failure hazard calculations for the cleared laser attack track in hilly terrain. In 3D-CALCFAULT the probabilistic hazard calculation is changed from one performed in the Ground Plane of the target, using Cartesian Coordinates, to one performed in the Display Plane of the aircraft, using Spherical Coordinates. This approach produces simplification of the algorithms and increased efficiency and speed of computation. Once again, the analysis may impose additional restrictions on the FFLFZ laser firing envelope. Seventh, the Secondary and Tertiary Precautions are applied in 3D-CALCFAULT to identify any final restrictions on laser firing.

The probabilistic fault/failure laser hazard analysis for the Rough Earth TIALD Model, performed using 3D-CALCFAULT, has already been documented in the first Technical Report [18]. Over the remainder of this report, we will document the computational procedures for the fault-free laser hazard analysis, using the first three computational modules: 3D-RBPROG, 3D-CALCZONE, and 3D-CALCTERT. Section 3 briefly discusses the 3D-RBPROG module, before reviewing algorithms for the 3D-CALCZONE module, in a geometry which assumes a Flat Earth, but a hilly terrain on and surrounding the range. The 3D-CALCZONE computation for a Flat Earth Model is inherently conservative, and overestimates the hazard of short range exposure of an observer on a hill, due to neglect of the Earth's curvature. Since the Earth curves away from the Target location, the effective elevation of terrain features relative to the Target is reduced, increasing the laser propagation distance to a hypothetical observer on a hill, and reducing the hazard. Section 4 documents modifications to the 3D-CALCZONE algorithms for a Curved Earth Model, and compares the FFLFZ for the Flat Earth and Curved Earth calculations. Finally, Section 5 documents computational procedures for the 3D-CALCTERT module, which modifies the FFLFZ produced by 3D-CALCZONE by applying restrictions arising from the Tertiary Precaution. The effect of this analysis is to create a Tertiary Precaution "Surface," which effectively puts a "floor" under the FFLFZ, and prevents use of low elevation attack tracks that violate the Tertiary Precaution.

3 3D-CALCZONE: FLAT EARTH MODEL

The basic CALCZONE module, used to calculate the FFLFZ for the Smooth Earth TIALD Model, has been documented in detail in previous work [16] and was summarized in Section 2.2. As illustrated in Fig.2, the CALCZONE computational procedures use the maximum fault-free laser pointing error, α_{max} , the aircraft height, *H*, and the geometry of the Controlled Range Area (CRA) to geometrically calculate the maximum laser firing range-to-target (ground range), $R(\omega)$, along each radial, ω, connecting the target to each of the CRA boundary points. When laser firing is performed at ranges less than or equal to this maximum range, geometric constraints ensure that both overshoot and undershoot laser pointing errors, up to the maximum fault-free value, are kept within the CRA. The FFLFZ for that height is then defined by calculating the set $\{R(\omega): \omega \in [0,2\pi)\}$, covering all possible radials to any boundary point. A typical FFLFZ plot produces a closed contour about the target; a process repeated for each proposed attack height. The result is a nested series of contours that defines a three-dimensional envelope for safe firing of the laser during fault-free operation of the laser directional control system. For any aircraft attack track, at any given altitude, the FFLFZ defines the maximum range-to-target at which the laser may be fired, assuming fault-free operation.

The 3D-CALCZONE module, documented below, is a revised version of the CALCZONE fault-free laser hazard analysis, designed to apply to an environment with hilly terrain on and surrounding the range. As with the old CALCZONE routine, the analysis is essentially geometric, using the geometric parameters defined by the range test scenario to produce an FFLFZ that keeps the beam within the CRA for both overshoot and undershoot errors, and generating an FFLFZ for each specified attack height. A new method, the Circle of Allowed Laser Firing (CALF) geometry, is used to determine the FFLFZ in hilly terrain. Unlike the old method, the CALF approach does not require iterative calculations to produce the maximum laser firing range-to-target.

The initial application of the CALF geometry, described in the remainder of Section 3, is done for the case of a Flat Earth Model. The purpose of the initial Flat Earth application was to provide a simplified context in which the basic algorithms could be developed and tested, prior to application to the more complex Curved Earth Model, described in Section 4. Before proceeding we should note that the material of Sections 3 and 4 is only a condensed summary of the far more extensive documentation produced earlier by Dr. Brian Flemming, the TIALD model developer [21]. Readers are directed to earlier documentation for more mathematical detail and some derivations.

3.1 Terrain Profile Model and 3D-RBPROG

As mentioned in Section 2.3, the initial step in laser hazard analyses done with the Rough Earth TIALD Model consists of data input, data transformations, definition of the range test scenario to be analysed, and generation of the Terrain Profile Surface. The second step is execution of the three dimensional RBPROG module (3D-RBPROG). This subprogram consists simply of executing the two dimensional RBPROG module, to generate the CRA and all range boundary points, and then creating a three dimensional range boundary (3D-CRA) by assigning an

elevation to each range boundary point. The elevations assigned are nominally equal to the height of the Terrain Profile Step immediately above the boundary point.

Accurate use of the CALF method depends on interaction with the Terrain Profile Surface Model, which was briefly described in Section 2.2. On occasion the CALF will intersect with steps in the Terrain Profile Surface, which indicates a risk of short range laser irradiation of observers outside the CRA. These are observers who are occupying elevated terrain features (hills) under the Terrain Profile Surface. In these cases the CALF must be modified to prevent undershoot laser pointing errors from impinging on the Terrain Steps. Since interaction with the Terrain Profile is critical to CALF applications in both the 3D-CALCZONE and 3D-CALTERT modules, a more detailed discussion of the Terrain Profile Model is provided here, prior to description of the CALF method.

The Terrain Profile Model is a simplified representation of elevated terrain outside the CRA. As mentioned, the purpose of the Terrain Profile Model is to guard against potential short range irradiation of observers occupying elevated terrain areas outside the CRA by undershoot laser pointing errors. Figure 3 provides an illustration of the Terrain Profile geometry, in a Flat Earth Model, by showing a cross sectional slice of the Terrain Profile Surface. The Terrain Profile Surface has the target location as its lowest point. From that point it rises, in terrain steps of steadily increasing height, as we move radially outward from the target in all directions. Terrain Profile step heights are defined such that the actual terrain heights are always below the surface.

The laser beam emitted from an aircraft at position "*A*" firing at a target "*T*" could be at risk of intersecting elevated terrain short of the target position, especially from an undershoot pointing error (red cone). The definition of a pessimistic terrain profile relative to the natural terrain enables a new aircraft position "*B*" to be determined. For a laser firing from position "*B*" the risk of short range irradiation of elevated terrain areas outside the CRA, as a result of a laser undershoot within the pointing error cone, can be effectively eliminated (yellow cone).

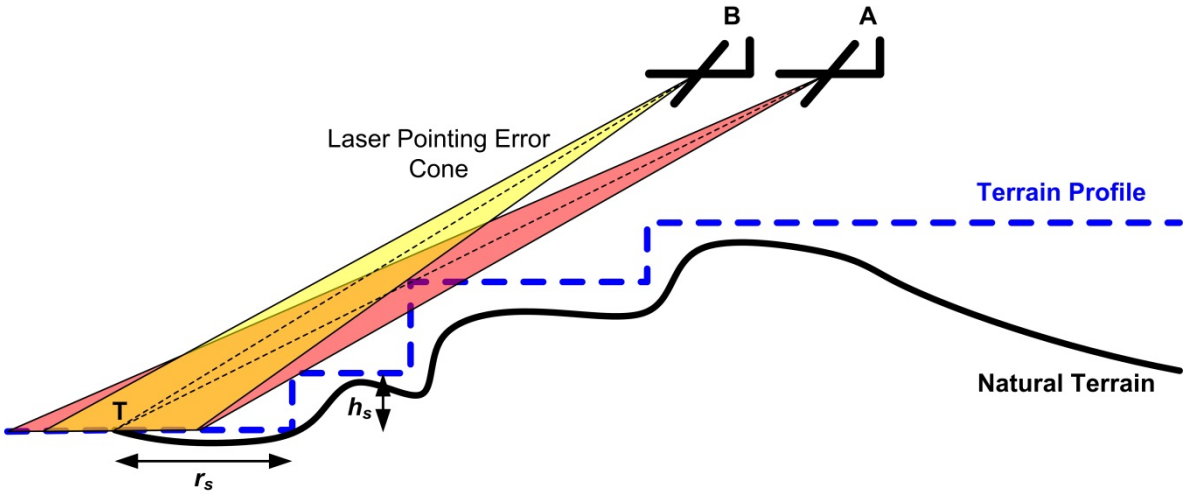

Figure 3: Terrain Profile Cross Section

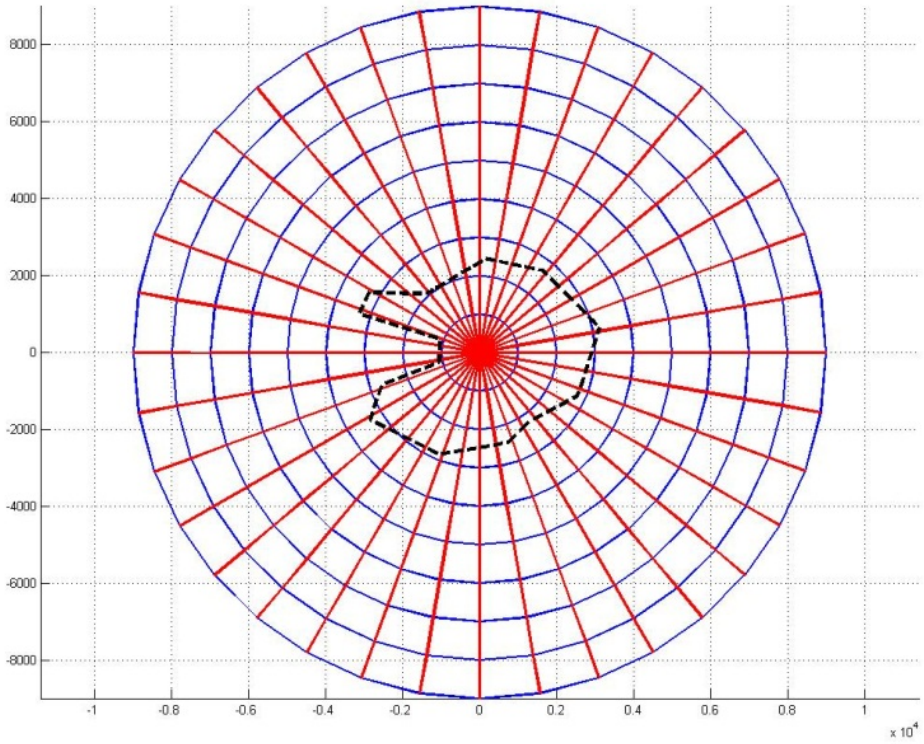

Figure 4: Terrain Profile "Web"

In two dimensions the Terrain Profile Surface is defined within a series of wedge-shaped sectors of angular width ω, with the target at the apex. Within each sector is an ascending series of steps of height h_s defined at regular intervals r_s from the target. Figure 4 provides an illustration of such a two dimensional Terrain Profile "Web" superimposed over a typical CRA, and centered over the target. Each "cell" in the web represents a Terrain Profile Step. The value of the step height h_s is at least that of the highest terrain elevation value within the (r_s, ω) angular segment, or the height of the previous step, whichever is greater. The Terrain Profile Surface is hence defined by the series of (r_s, h_s) pairs within each angular sector. Historically, the step depth r_s has been defined at 1 km intervals, the step height h_s at 10 m intervals, and the width of each angular sector at 10°. Finer resolutions can be defined as necessary.

3.2 Circle of Allowed Laser Firing

The third step in hazard analyses done with the Rough Earth TIALD Model is execution of the three dimensional CALCZONE module (3D-CALCZONE), using the Circle of Allowed Laser

Firing (CALF) geometry. Implementation of the CALF, in either the Flat Earth or Curved Earth Model, is done using the MATILDA Internal Coordinate System (MICS). The MICS has been documented in detail in previous work [16] and will be briefly summarized here for readers unfamiliar with prior work.

The MICS is a Cartesian coordinate system, represented by coordinates (*x, y, z*) and centered on the selected target within the CRA. The MICS origin is the target position. The *z*-axis is oriented perpendicular to the Earth's surface and points locally upwards. The *x* and *y*-axes are directed towards the local east and north, respectively. The MICS *xy*-plane is therefore tangential to the earth's surface at the target position.

The MICS enables data from various sources, such as GPS and Ordnance Survey, to be brought together in a single consistent coordinate system. The MICS is also designed to accommodate either the Flat Earth or the Curved Earth Model, although care must be taken to define what is meant by "height" in the Curved Earth Model. In an Earth-oriented model, "height" is typically defined to be height "above mean sea level" (AMSL) on the Earth's surface. In contrast the definition of "height" in the MICS is typically height above the MICS *xy*-plane, given by the MICS z-coordinate. For the Flat Earth Model the MICS height and the height AMSL will be the same. For the Curved Earth Model they may differ significantly, as shown in Figure 5.

Figure 5 provides an illustration of the MICS geometry for a Curved Earth Model, in the case of an aircraft firing when it reaches the near boundary of the FFLFZ. In this case the aircraft range-to-target, R_O, measured along the surface of the Curved Earth, represents the maximum allowed firing range. This range has been determined by setting the overshoot pointing error, between the target position *T* and the far CRA boundary point, to the maximum fault-free laser pointing error, $\alpha_{\max}$. Note that the aircraft height AMSL, represented by the red arrow, is the distance from the aircraft position to the Earth's surface, measured along a vector pointing towards the center of the Earth, where R_e is the Earth's radius. It clearly differs from the aircraft MICS height above the MICS *xy*-plane. This issue will be revisited in Section 4, when we discuss application of the CALF geometry to the Curved Earth Model.

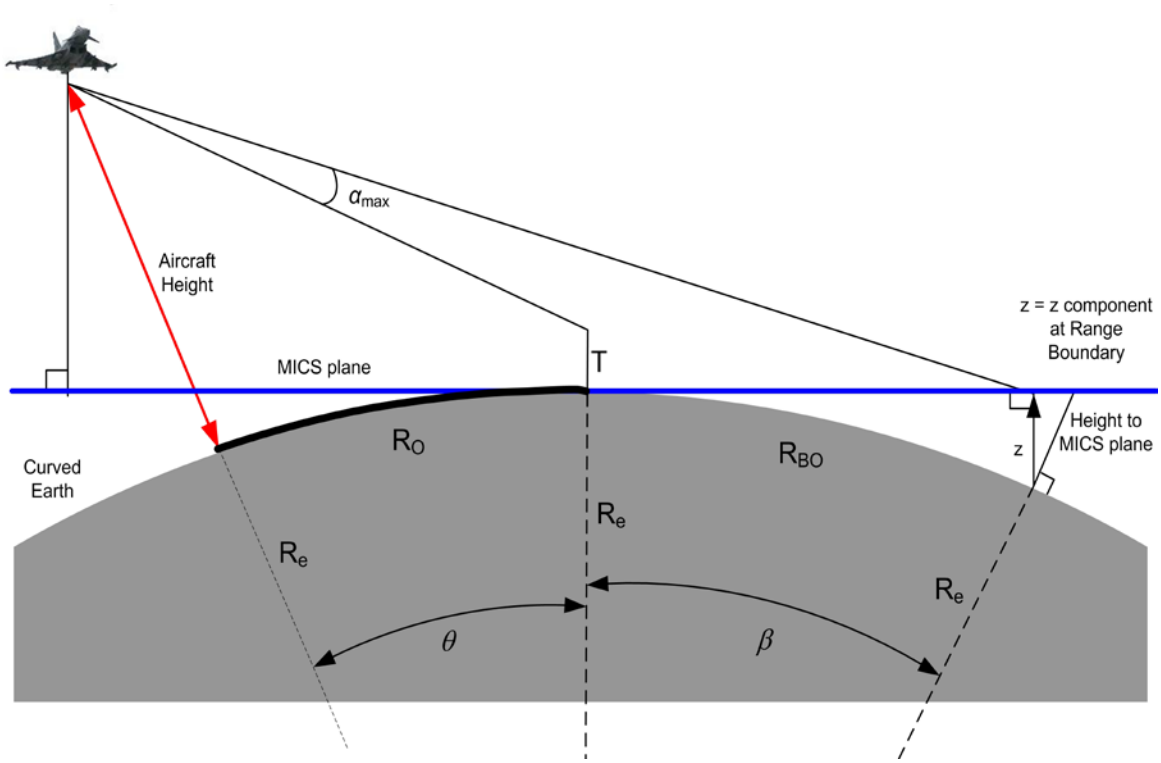

Figure 5: MICS Geometry vs. Curved Earth Model

The Circle of Allowed Laser Firing (CALF), illustrated in Figure 6, is a geometric construct that defines a locus of aircraft positions, from which the laser can be fired at different aircraft heights [21]. For each aircraft height, the laser firing position on the CALF is defined to ensure that, for a fixed fault-free laser pointing error, ϕ, all laser energy will fall between the Target and the CRA boundary. Laser energy will also stay within the CRA for all aircraft firing positions within the CALF. On the other hand, laser energy could irradiate potentially populated areas outside the CRA, if the aircraft laser firing position is outside the CALF.

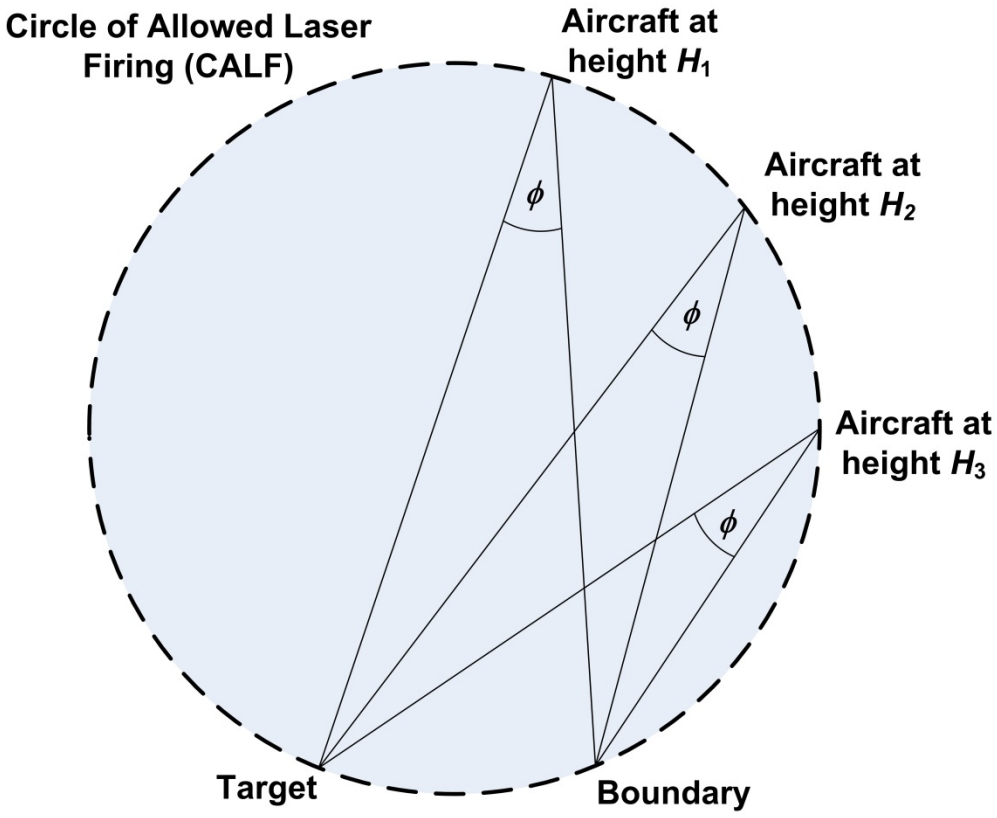

Figure 6: Circle of Allowed Laser Firing

The set of laser firing positions defined by the CALF, as a function of aircraft height, will vary with the aircraft angle of attack; i.e., there will be a different CALF defined for each radial, ω, connecting the target to each of the CRA boundary points. At this point, the similarity between the set of laser firing positions defined by the CALF, and the set of maximum firing range-to-target values that defines the FFLFZ, is obvious. For the special case where the fault-free laser pointing error equals the maximum value, $\phi = \alpha_{\max}$, the CALF can be used to define the FFLFZ.

The CALF is a specific instance of a more general geometrical result in which the loci of equiangular points can be determined. The geometry of the loci of equiangular points is illustrated in Figure 7. In the diagram, *AB* is a fixed line segment. The loci of points *P*, such that the angle *APB* has a constant value, is a circular arc of radius r and center *O*, which will also pass through the points *A* and *B*. The triangles comprising the center point *O* and any two points on the circle are isosceles triangles. From triangle *APB*, the sum of the interior angles is π, so that

$$2a + 2b + 2c = \pi \ , \tag{3.1}$$

where *a* is the angle *OAB*, *b* is the angle *OPA* and *c* is the angle *OPB*.

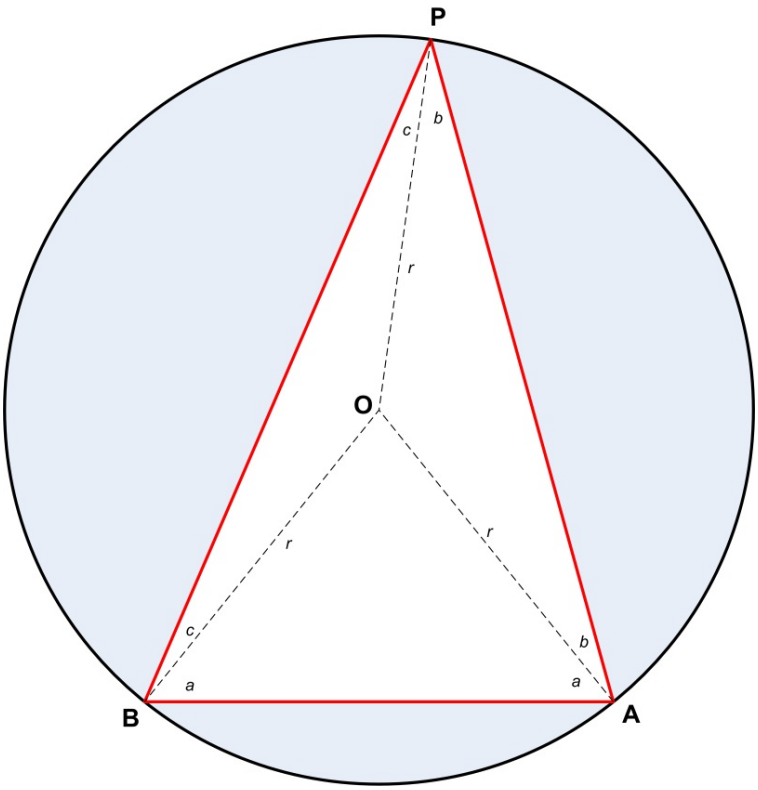

Figure 7: Loci of Equiangular Points

The angle *APB* is thus given by

$$APB = b + c = (\pi/2) - a \ , \qquad (3.2)$$

and is constant for all points *P* on the circle. This relation remains true even if the circle center point *O* is outside the triangle *APB*, as shown in Figure 8, provided the point *P* lies on the larger circular segment created by the chord *AB*. In this case, the angle *c* will effectively be "negative".

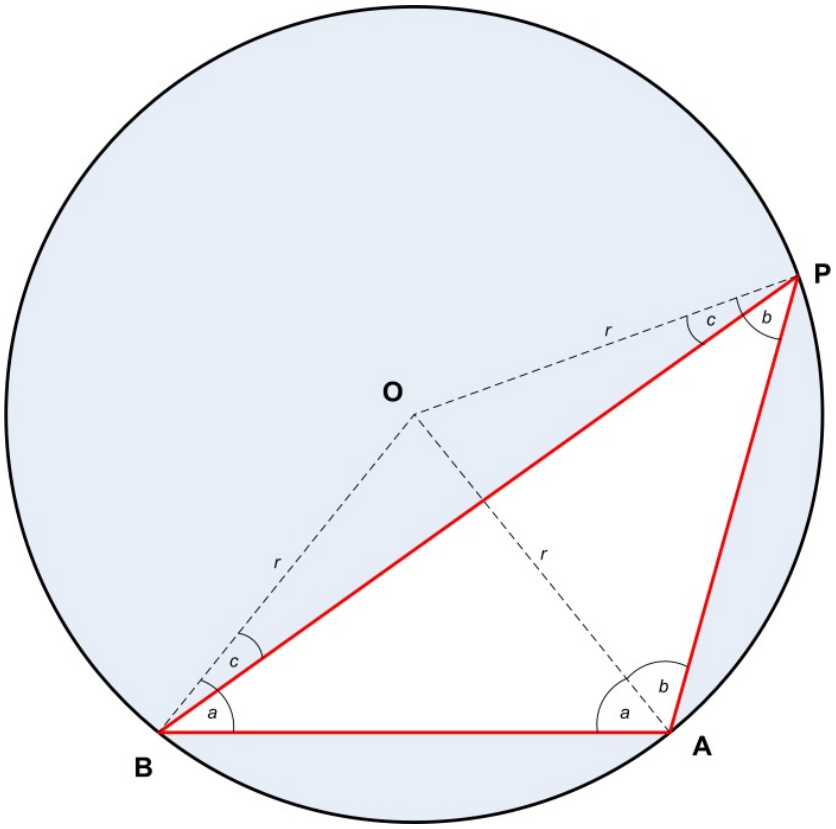

Figure 8: Loci of Equiangular Points: Circle Center not included in APB

When the geometry of the loci of equiangular points in Fig. 7 is compared to the CALF geometry in Fig. 6, it is clear that the angle APB corresponds to the fault-free laser pointing error angle, ϕ. Equation 3.2 now gives

$$b + c = \phi \tag{3.3}$$

and

$$a = \frac{\pi}{2} - \phi \quad . \tag{3.4}$$

As mentioned previously, for the special case where the CALF is used to define the FFLFZ, we set the fault-free laser pointing error equal to the maximum, $\phi = \alpha_{\max}$.

For an undershoot laser pointing error, the points *B* and *A* on the circle will correspond to the target and the undershoot ground point of interest, respectively. In Fig. 6 the undershoot ground point of interest is the CRA undershoot boundary point. The line segment *AP* represents the separation distance between the laser and the undershoot ground point of interest. Conversely, for an overshoot laser pointing error, the target and the overshoot ground point of interest will be represented by *A* and *B*, respectively. Similarly, the line segment *BP* will represent the

separation distance between the laser and the overshoot ground point of interest. It should be noted that, in practice, there will never be a situation where the point *P* would occur "below" the chord *AB*. Hence, this aspect of the CALF geometry need not be considered.

3.3 CALF: Undershoot Risk

We begin our discussion of the application of the CALF geometry to define the FFLFZ by considering use of the CALF to mitigate undershoot laser pointing error risk. The CALF geometry for an aircraft at point P, firing at a target at point B, with respect to an undershoot boundary point A, is shown in Figure 9. As mentioned in the discussion of 3D-RBPROG, the height assigned to a CRA boundary point is equal to the height of the Terrain Step immediately above it. In Figure 9 the edge of a Terrain Step is coincident with the undershoot boundary point *A*.

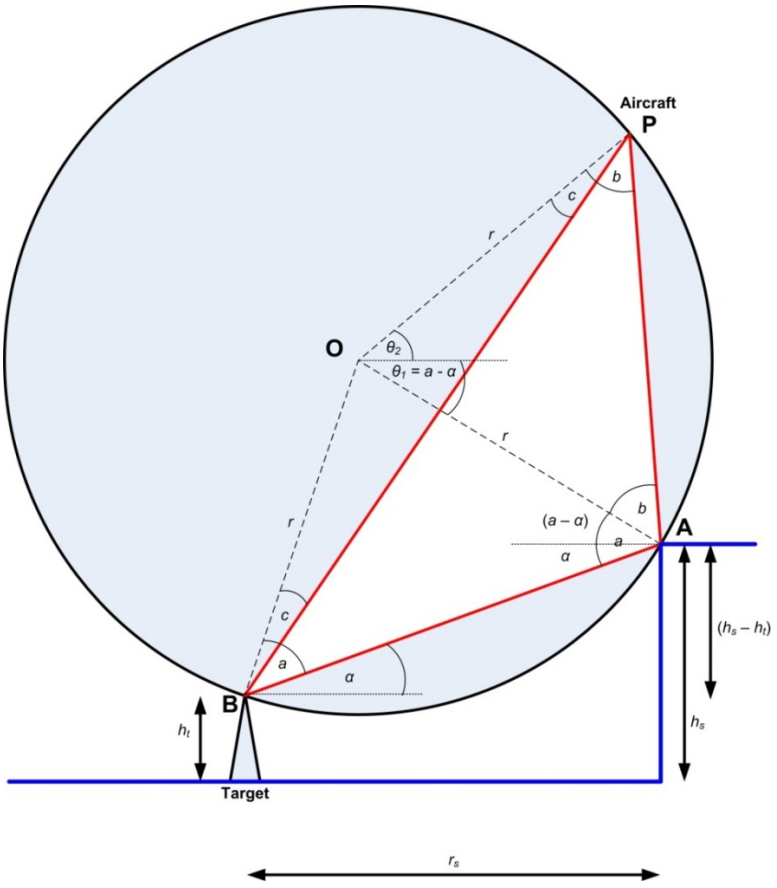

Figure 9: CALF Geometry with Undershoot Boundary Terrain Step

The undershoot boundary parameters and the target height can be used to determine the CALF center point and radius, O and r, respectively, for an undershoot laser pointing error. The chord

distance *AB* is derived from the target height, h_t , the terrain step height, h_s, and the terrain step distance from the target, r_s , so that

$$AB = \sqrt{r_s^{\,2} + \left(h_s - h_t\right)^2} \quad . \tag{3.5}$$

The slope, α , of the chord *AB* with respect to the local horizontal, can also be derived from the terrain step and target parameters:

$$\alpha = \tan^{-1} \frac{\left(h_s - h_t\right)}{r_s} \quad . \tag{3.6}$$

The radius r of the CALF can be calculated as a function of the chord length *AB* and the angle *a*,

$$r = \frac{AB}{2\cos a} \ , \tag{3.7}$$

where *a* is given by Eq. 3.4, with $\phi = \alpha_{\max}$. The coordinates $\left(x_c, z_c\right)$ of the undershoot CALF center point *O*, relative to the target position *B*, are now given by:

$$\begin{aligned} x_c &= r\cos\left(a+\alpha\right) \\ z_c &= h_t + r\sin\left(a+\alpha\right) \end{aligned} \quad . \tag{3.8}$$

The undershoot CALF defines the limiting locus of laser firing positions such that an undershoot fault-free laser pointing error, up to the maximum, will remain within the CRA. The maximum laser firing range-to-target, r_d, determined by the CALF for a given aircraft attack height, h_a, is given by:

$$r_d = \sqrt{r^2 - \left(h_a - z_c\right)^2} + x_c \quad . \tag{3.9}$$

Figure 10 illustrates the application of the CALF for an undershoot laser pointing error. In the diagram, the undershoot CALF appears as a large arc passing through the target and the CRA undershoot boundary point. In this example, the undershoot CALF appears to intersect with a number of steps in the Terrain Profile Surface.

A closer view of the Terrain Profile intersection is illustrated in Figure 11. Intrusion of the Terrain Profile steps into the undershoot CALF indicates a risk of short-range laser irradiation of potentially populated land areas, below the line of attack and outside the CRA. The undershoot CALF must therefore be modified to avoid the possibility of undershoot laser pointing errors impinging on the Terrain Steps.

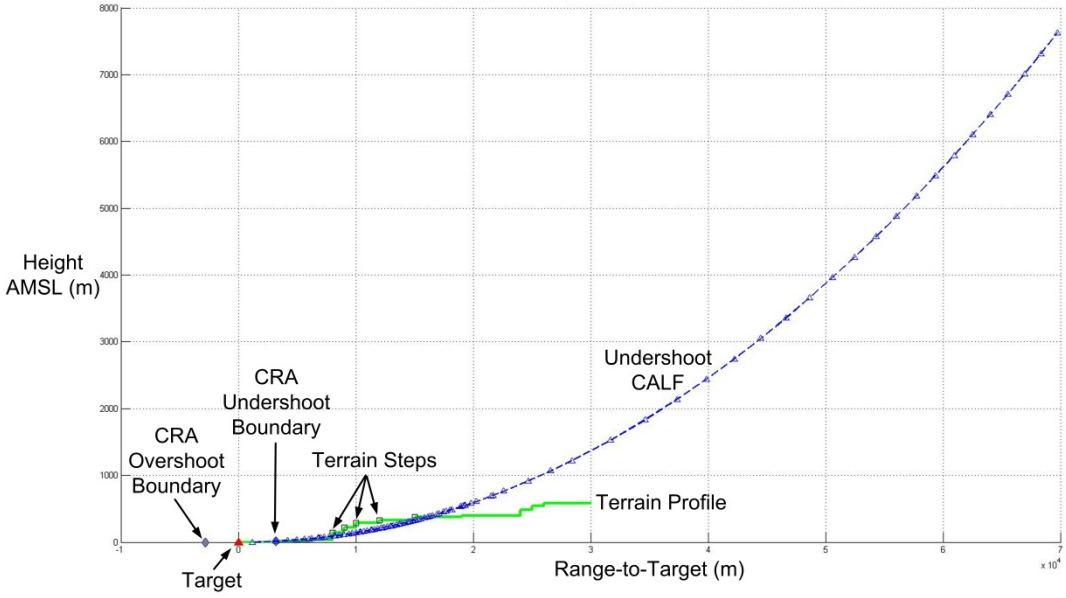

Figure 10: Undershoot CALF

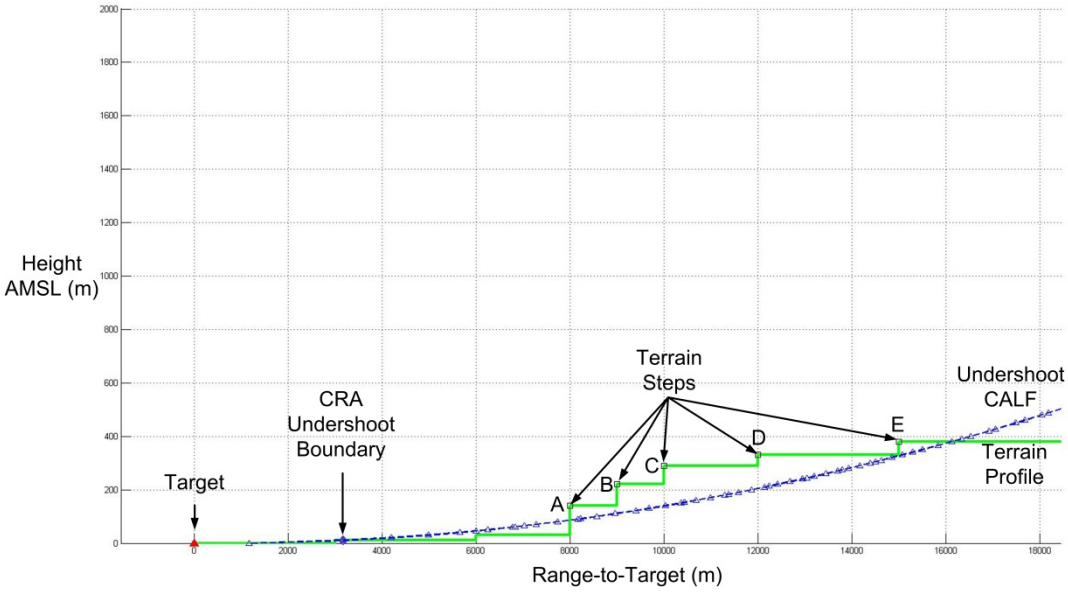

Figure 11: Undershoot CALF Terrain Profile Intersection

In the previous method of determining the undershoot laser firing restriction, used in CALCZONE, the algorithm included the identification of the Most Prominent Terrain Step (MPTS), which was defined as the step having the smallest zenith angle relative to the normal vector at the CRA undershoot boundary point. Any undershoot laser pointing error with a smaller zenith angle would not intersect with any of the terrain steps, and would thus avoid the possibility of short-range irradiation of potentially populated areas. A similar approach is taken in the revised method used in 3D-CALCZONE, but the method of adjustment of the undershoot laser-firing points is different. Figure 12 provides an illustration of the CALF adjustment required for an undershoot laser pointing error not to impinge on any of the terrain steps.

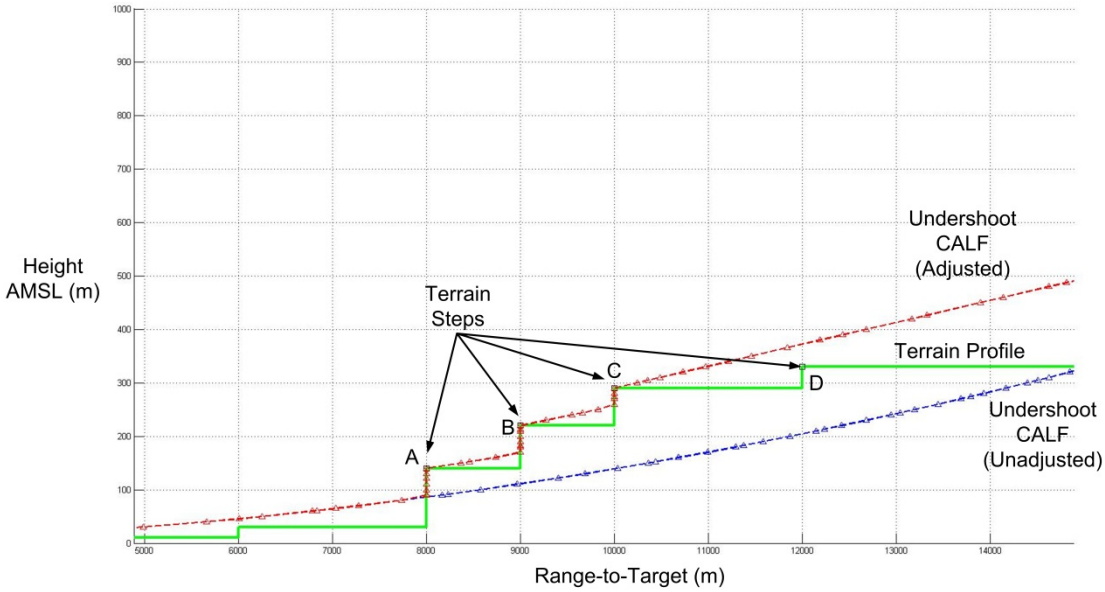

Figure 12: Undershoot CALF Adjusted for Terrain Step Incursions

For the (unadjusted) undershoot CALF there are five terrain steps enclosed, at points A, B, C, D and E. Starting with the lowest enclosed terrain step (Terrain Step A), the adjustment is carried out in two main stages. First, the portion of the CALF that is *lower* than the height of Terrain Step A, but is at a *greater* distance from the target, is cut off at the Terrain Step A distance, where the CALF rises to the top of Terrain Step A. Next, the portion of the CALF that is lower than Terrain Step B, but higher than Terrain Step A, is cut off at the Terrain Step B distance, where the CALF rises to the top of Terrain Step B. This process is repeated for the remaining enclosed terrain steps, as necessary. Note that after the adjustment at Terrain Step C, the resulting (adjusted) undershoot CALF no longer encloses Steps D and E, so no further adjustments are required.

The second stage is to identify all points in the partially-adjusted CALF whose zenith angles with respect to the normal at the CRA undershoot boundary are *greater* than that of the MPTS

(which is Terrain Step C in Figure 12). Starting again with the lowest enclosed step, Terrain Step A, the zenith angles of the CALF, above Terrain Step A, are compared with the zenith angle Terrain Step A makes with the normal at the CRA undershoot boundary. The range-to-target distances of those points with a greater zenith angle are adjusted (that is their range-to-target distances are reduced), until their zenith angles are no greater than that of Terrain Step A. The mathematics of the adjustment is illustrated in the simplified diagram provided in Figure 13.

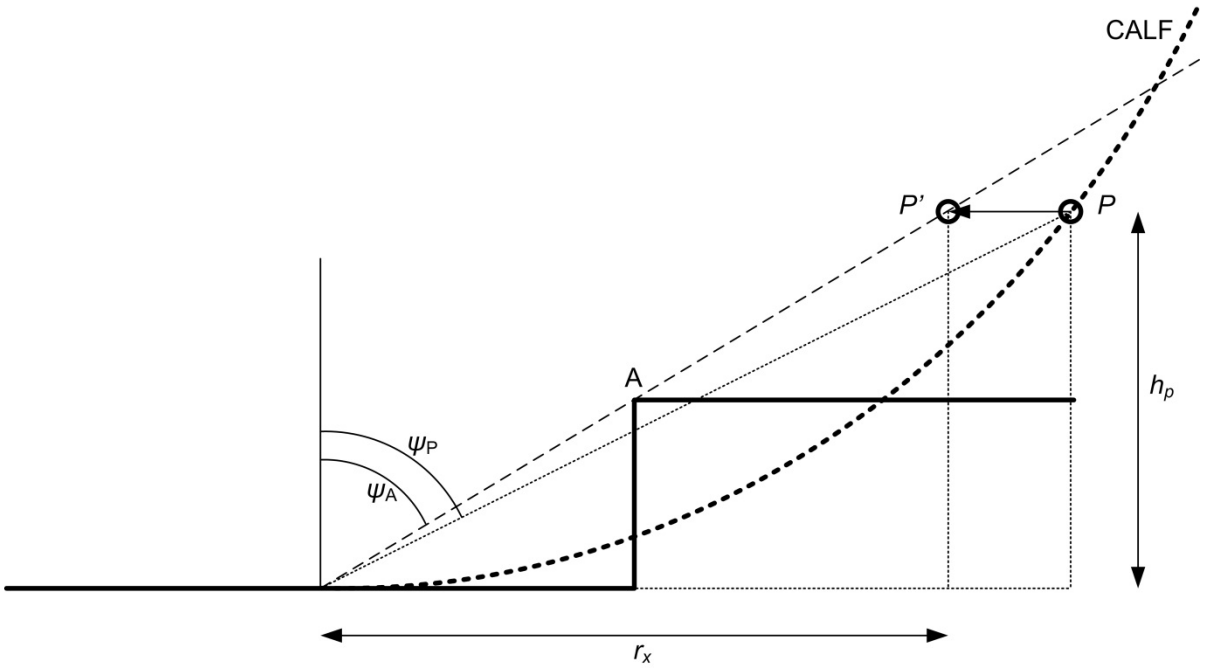

Figure 13: Undershoot CALF Adjustment

In the diagram, the zenith angle for Terrain Step A is ψ_A. Consider a point *P* on the CALF, at height h_p above the boundary point, for which the zenith angle

$$\psi_P > \psi_A \ .$$

In order that an undershoot pointing error does not impinge against the terrain step, the point *P* must be moved to the point *P'*, closer to the target, where the distance r_x from the boundary point is given by:

$$r_x = h_P \tan \psi_A \ . \qquad (3.10)$$

Thus, the (reduced) range-to-target distance, r_d', of the adjusted point *P'*, is

$$r_d' = r_b + r_x \quad , \tag{3.11}$$

where r_b is the distance of the undershoot range boundary point from the target. The process is repeated for zenith angles of the CALF above the remaining enclosed terrain steps (B, C, D, etc.), up to the MPTS. Once again, for the case illustrated in Figure 12, the MPTS is Terrain Step C, and we note that Terrain Steps D and E are well outside the adjusted CALF, as a result of adjustments carried out for the lower, and more prominent, terrain steps. There is, however, one particular circumstance in which the undershoot CALF adjustment described above can be too extreme, which is illustrated in Figure 14.

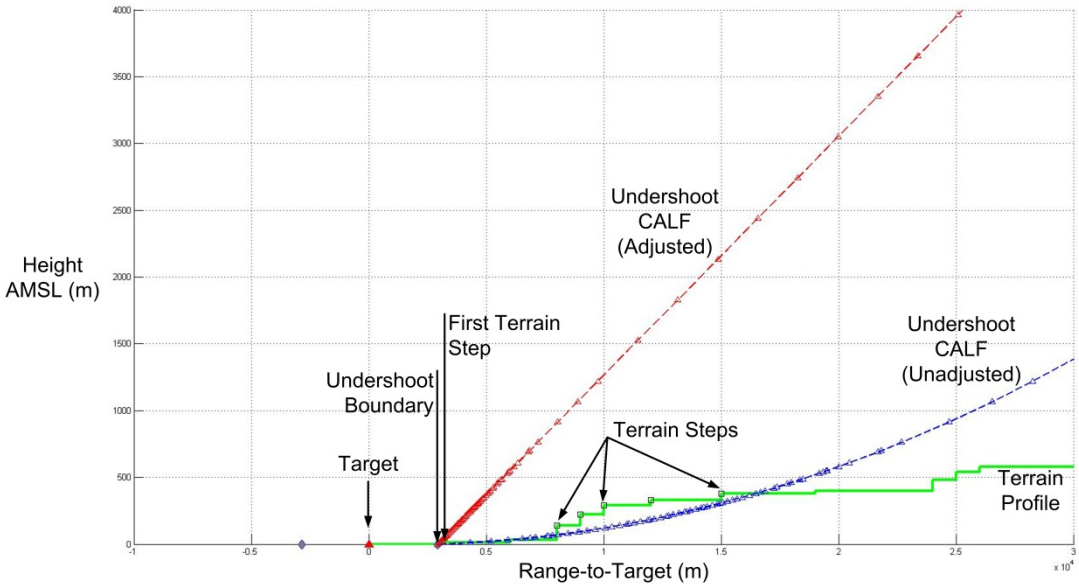

Figure 14: Extreme Undershoot CALF Adjustment

In this case, the CRA undershoot boundary point is very close to the first terrain step, which has resulted in a much smaller zenith angle for Terrain Step A than the angles computed for the points on the (unadjusted) undershoot CALF above Terrain Step A. Consequently, virtually *all* of the points on the (adjusted) undershoot CALF have been overly-adjusted and shifted much closer to the target to avoid undershoot pointing error impingement on the initial terrain step. The practical outcome is that the adjusted undershoot CALF appears as a steeply-inclined straight line rather than a gentle curve.

A practical solution to this conundrum is to set the undershoot boundary height to be the same as that of the *first* terrain step *outside* the CRA, and then to calculate a *second* CALF based on this *heightened* boundary point. As illustrated in Figure 15, this second CALF might itself require adjustment to prevent incursion by terrain steps further along the profile. However, the extreme situation occasioned by the undershoot boundary proximity problem will have been eliminated.

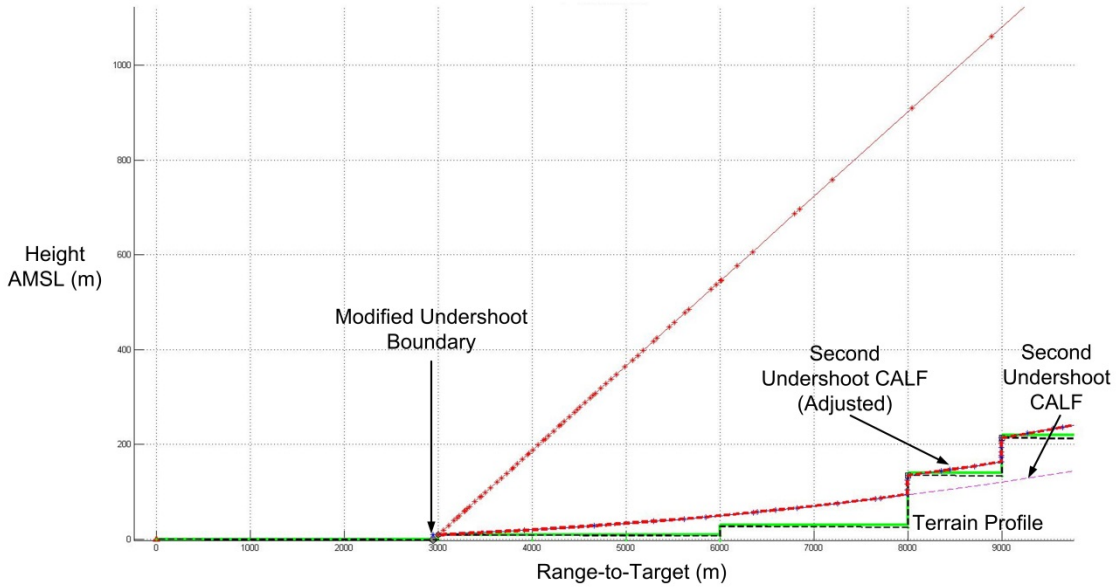

Figure 15: Second Undershoot CALF

Before closing our discussion of adjustments to the undershoot CALF geometry, there is perhaps one point that should be clarified. Using Eqs. 3.4 to 3.9, given previously, the maximum (undershoot) laser firing range-to-target, r_d, can be calculated for a given aircraft attack height, h_a, when the parameter values inserted in these equations are those of the undershoot CALF. To calculate the correct value of the maximum undershoot firing range, however, the parameters used must be those of the *final* undershoot CALF, adjusted to exclude all terrain step incursions by the iterative process just described.

3.4 CALF: Overshoot Risk

The maximum undershoot laser firing range-to-target, obtained using the computational procedures described in Section 3.3, is only one of the two ranges we need to calculate the FFLFZ for a particular attack height. The other is the maximum overshoot laser firing range-to-target. We now turn to application of the CALF geometry to mitigate overshoot laser pointing error risk. The overshoot CALF geometry for an aircraft at point P, firing at a target at point A, with respect to an overshoot boundary point B, is shown in Figure 16. As was true in the undershoot case shown in Figure 9, the edge of a Terrain Step is coincident with the overshoot boundary point *B* and the height assigned to the overshoot boundary point is equal to the height of the Terrain Step.

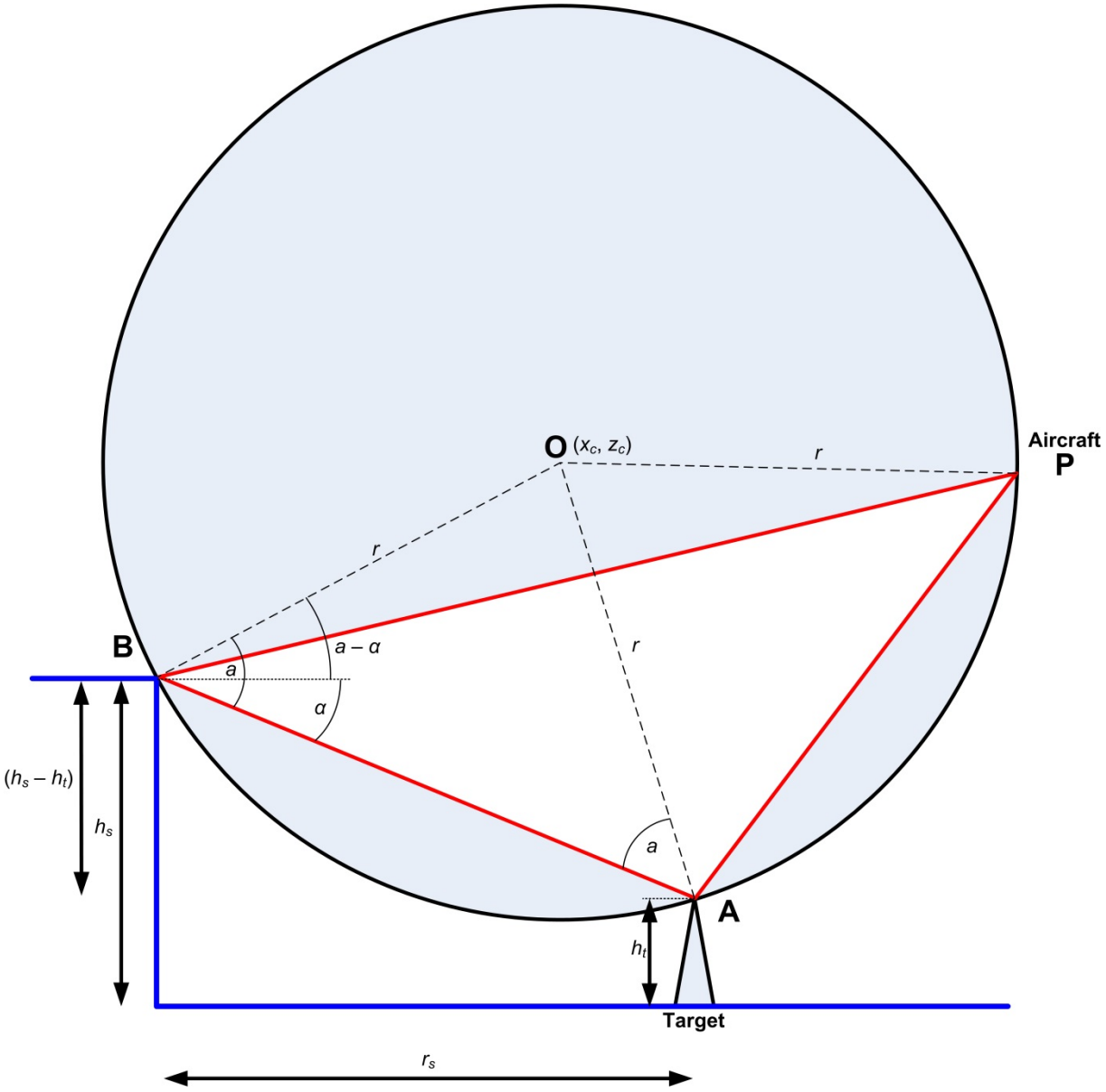

Figure 16: Overshoot CALF Geometry

The overshoot CALF defines the limiting locus of laser firing positions such that any overshoot fault-free laser pointing error, up to the maximum, will remain within the CRA boundary. The geometric similarities between Figures 9 and 16 mean that Eqs. 3.4 to 3.9 can once again be used to calculate the values of a, AB, α, r, x_c, z_c and r_d. Equation 3.9 will give the maximum overshoot laser firing range-to-target, when the parameter values inserted in these equations are those of the overshoot CALF.

As shown in Figure 17, adjustments to the overshoot CALF are sometimes required to avoid terrain step incursions into the permitted laser-firing space. The adjustment methods are identical to those discussed in Section 3.3 for the undershoot CALF application. The purpose of

the overshoot CALF adjustment, however, is not to avoid any risk of short range irradiation of populated areas outside the CRA. Instead, it is merely intended to ensure that the first laser firing point indicated by the CALF does not occur "underground" as defined by the Terrain Profile Surface. Once again, we note that to calculate the correct value of the maximum overshoot firing range from Eqs. 3.4 to 3.9, the parameters used in these equations must be those of the *final* overshoot CALF, adjusted to exclude all terrain step incursions.

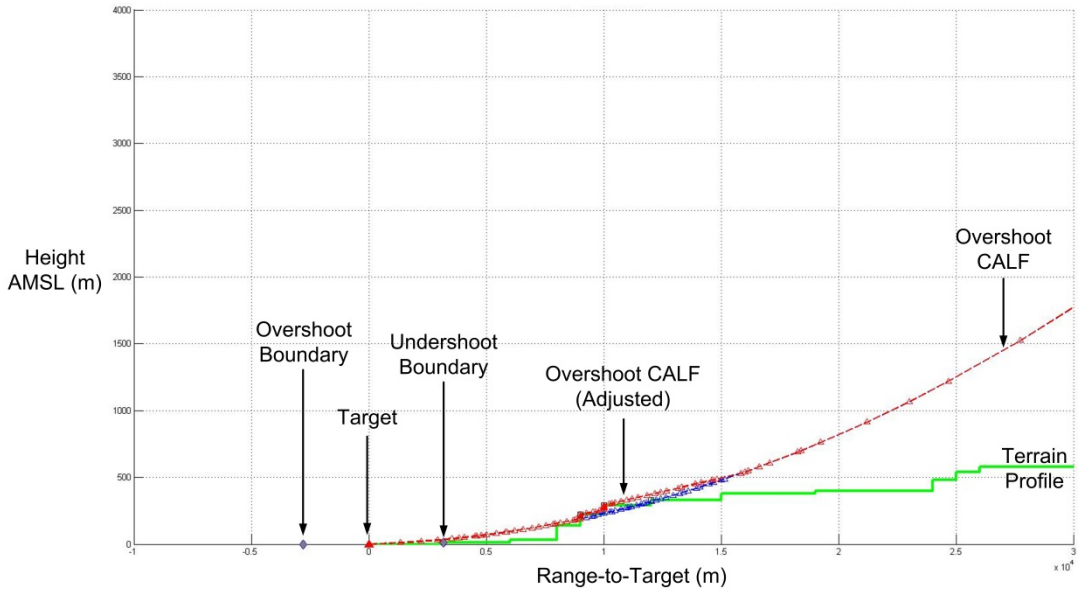

Figure 17: Overshoot CALF Adjustment

3.5 FFLFZ for Flat Earth Model

The computational procedures described in Sections 3.3 and 3.4 can be used to define the (adjusted) undershoot and overshoot CALFs, for a given aircraft attack height and a given pair of undershoot and overshoot CRA boundary points lying along a given attack radial. The undershoot and overshoot CALF geometry parameter values can then be used to calculate the maximum undershoot and overshoot laser firing ranges-to-target, for an aircraft flying along that attack radial at that attack height. This process is repeated for every desired attack height and every radial passing through every CRA boundary point.

The set of maximum undershoot and overshoot firing ranges, computed for all attack heights and all attack radials, can now be used to generate the corresponding FFLFZs, by the same method used in the old CALCZONE module, which was described in Section 2.2. That is, for a given aircraft flying at attack height *H*, along an attack radial of angle θ, the overall maximum permitted laser firing range-to-target, $R_{\text{ffha}}(H,\theta)$, is given by

$$R_{\text{ffha}}\left(H,\theta\right)=\min\left\{R_{\text{under}}\left(H,\theta\right),R_{\text{over}}\left(H,\theta\right)\right\}\ ,\qquad(3.12)$$

where R_{under} and R_{over} are the maximum undershoot and overshoot firing ranges calculated for that attack height and radial. The overall maximum permitted firing ranges for all radials at a given attack height define the FFLFZ for that height.

To illustrate the results of the 3D-CALCZONE module (Flat Earth Model), we have computed the FFLFZs for a sample test range, target location, CRA, Terrain Surface Profile, and set of desired attack heights. For consistency with past work, we have copied the test case previously used to illustrate the results of MATILDA Version-1.6.1: a hypothetical airborne laser designator used in an attack maneuver during a training scenario at the UK's Tain Range in northern Scotland. Readers are referred to prior documentation [16] for details of this test case. Figure 18 provides a three-dimensional illustration of the resulting set of FFLFZs. It should be noted that the scales on the three axes are non-isometric: the FFLFZ "basket" would appear much flatter in reality. Figure 19 provides a "bird's eye" view of the FFLFZs, illustrating the inset that occurs when the target is close to either the undershoot or overshoot boundary.

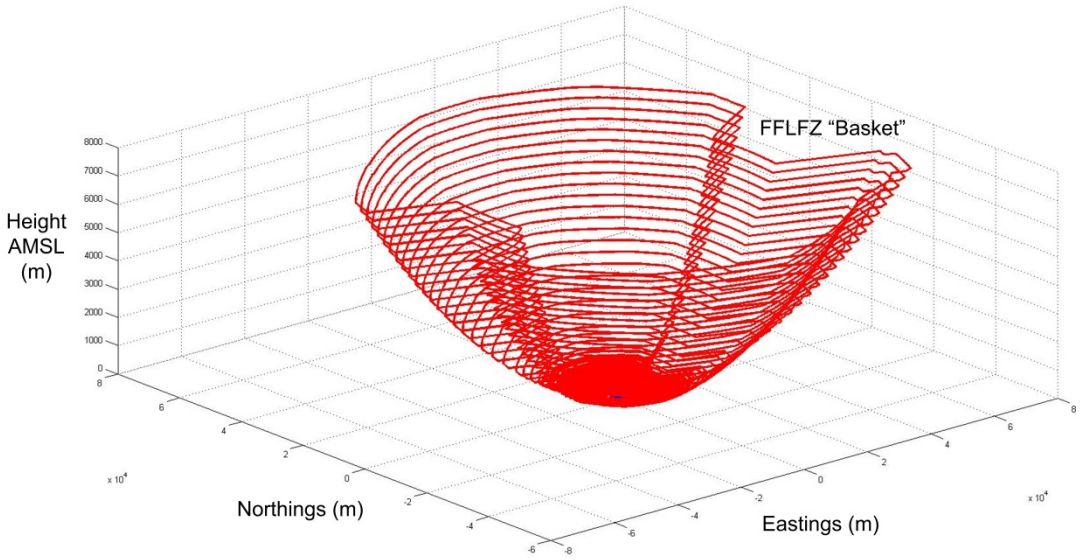

Figure 18: FFLFZ Contours "Basket"

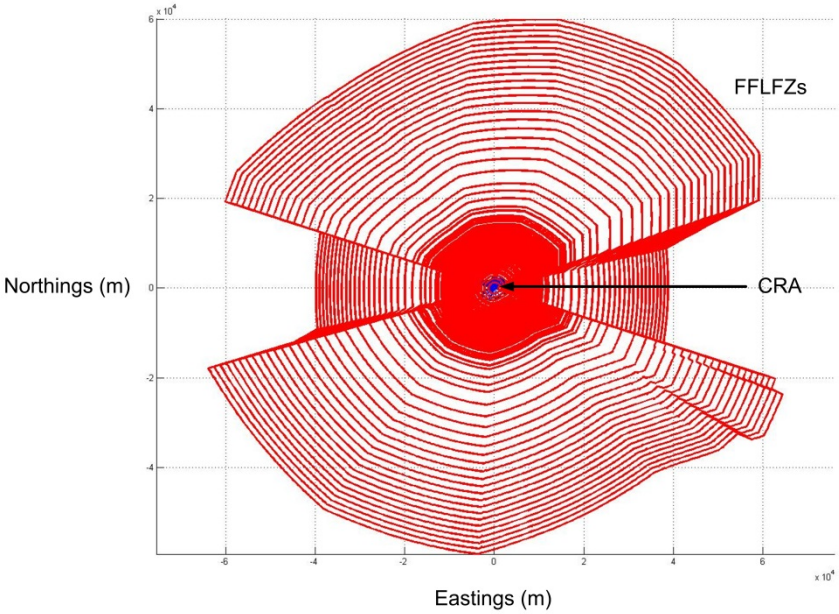

Figure 19: FFLFZ Contours "Bird's Eye" View

4 3D-CALCZONE: CURVED EARTH MODEL

The 3D-CALCZONE computational procedures described in Section 3, used to define the FFLFZs for a Flat Earth Model, are a useful first step in development of similar computational procedures for the more complex Curved Earth Model. We begin with a discussion of the Curved Earth Geometry, its relationship to the MICS, and the modifications it requires in the Terrain Profile Surface.

4.1 Curved Earth Geometry

The geometry of the Curved Earth Model, and its relationship to the MATILDA Internal Coordinate System (MICS), has already been illustrated in Fig. 5 and discussed in Section 2.2. A key point made in that discussion was that, for a Curved Earth Model, the height "above mean sea level" (AMSL) on the Curved Earth's surface differs, in some cases significantly, from the MICS height. The latter is defined as the height relative to the MICS *xy*-plane, given by the MICS z-coordinate, where the MICS *xy*-plane is tangential to the Earth's surface at the target position.

Figure 5 illustrates the difference between MICS height and AMSL height for an aircraft. Just as important is the difference between these two heights for terrain features on the Earth's surface, and for the Terrain Profile Steps that cover them. A key feature of the Curved Earth Model is that all MICS heights associated with terrain features will gradually diminish, relative to that of the target ($z = 0$), as the range-to-target distance increases and the Earth's surface curves away from the MICS *xy*-plane. Thus MICS terrain heights, and in extreme cases even MICS aircraft heights, could eventually become negative ($z < 0$) at large ranges. It should be emphasized,

however, that any systematic variation in height can be handled easily within the MICS, which was specifically designed for this purpose.

Figure 20 illustrates the geometry of a Terrain Step in a Curved Earth Model. Assuming a perfectly spherical Earth, if the angle subtended between the Target and the edge of the Terrain Step, measured relative to the Earth's Center, is ψ, then the height of the Terrain Step relative to the Earth's Center, projected onto the vertical line between the Target and the Earth's Center, is

$$\left(R_{\mathrm{E}} + h_{\mathrm{S}}\right)\cos\psi \ ,$$

where R_{E} is the radius of the Earth and h_{S} is the Terrain Step height AMSL on the Curved Earth surface. Since the radius of the Earth is large compared to the other distances involved here, the angle subtended is small. Using the small angle approximation, the angle ψ is given by

$$\psi = \frac{r_{\mathrm{S}}}{R_{\mathrm{E}}} \quad , \tag{4.1}$$

where r_s is the Terrain Step distance from the Target, meaured along the Curved Earth surface. Similarly, the horizontal distance from the Target to the top of the Terrain Step is

$$\left(R_{\mathrm{E}} + h_{\mathrm{S}}\right)\sin\psi \ ,$$

while the horizontal distance from the Target to the base of the Terrain Step is

$$R_{\mathrm{E}} \sin\psi \ .$$

It should be noted that, strictly speaking, the equations above are only an approximation of the true coordinate transformations required to turn terrain profile data expressed in a two-dimensional Flat Earth coordinate system, like the MICS, into equivalent terrain data expressed in a three-dimensional geodetic (latitude, longitude, altitude) coordinate system [16]. Our purpose here, however, is not to document the mathematics of coordinate transformations, but rather to consider the additional analysis required for CALF derivation of the FFLFZs in a Curved Earth geometry. Thus, for simplicity, it will be assumed that the Terrain Step distances from the Target, r_s , can be taken to be "circumferential" distances (geodesics) in the Curved Earth Model. Although an approximation, this is a fairly close approximation. Now, if the MICS origin is taken to be the target position ($z = 0$), then the MICS height of the Terrain Step relative to the Target, for a Curved Earth Terrain Profile, is

$$\left(R_{\mathrm{E}} + h_{\mathrm{S}}\right)\cos\psi - R_{\mathrm{E}} \ .$$

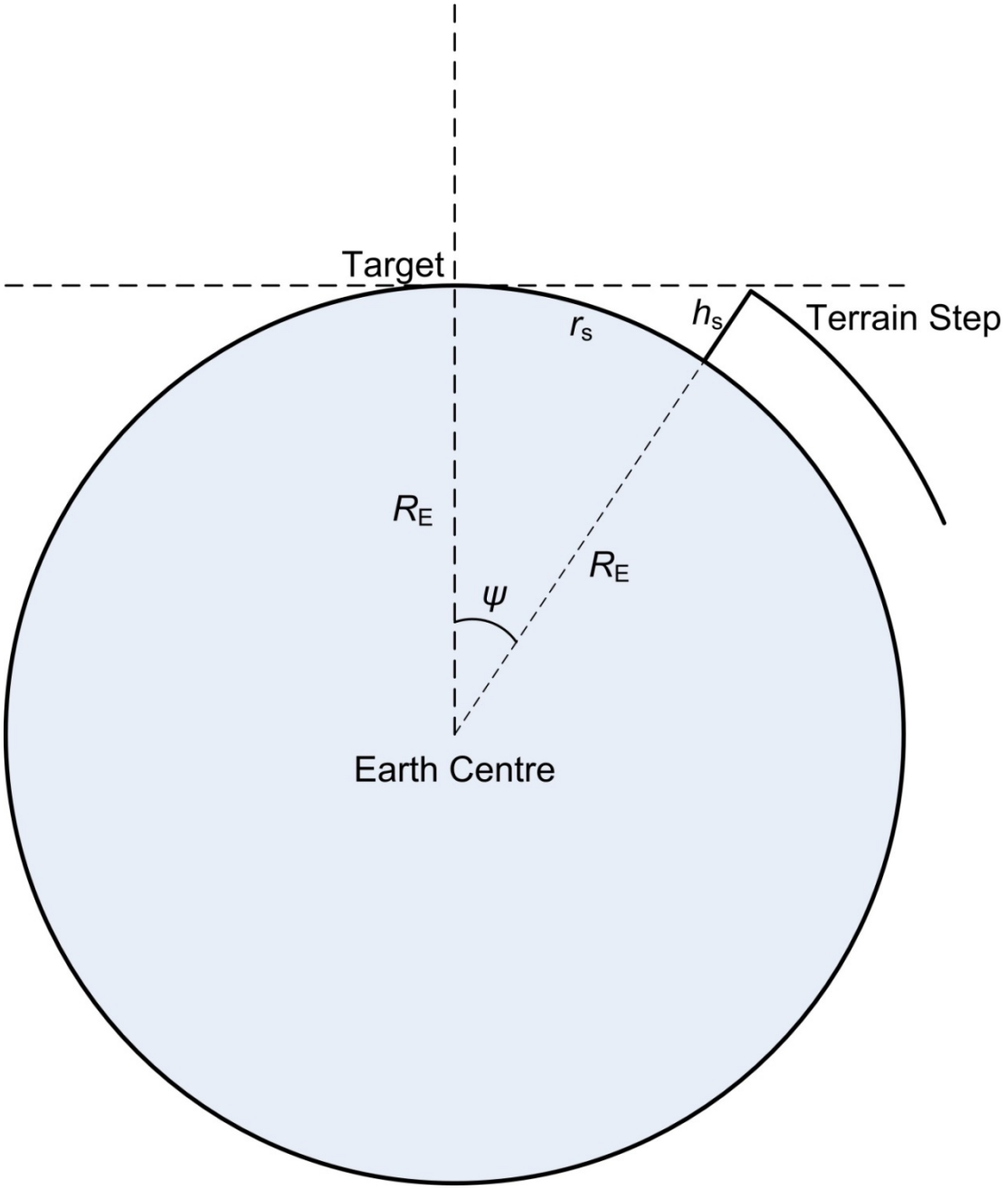

Figure 20: Terrain Step Geometry in a Curved Earth Model

Figure 21 provides a illustration of a modified Curved Earth Terrain Profile compared with the Flat Earth original. We should note the non-isometric scales on the diagram axes in Fig. 21, which accounts for the distortion that makes the Terrain Step risers in the Curved Earth Terrain Profile appear almost vertical. In reality, the difference between the original Flat Earth and modified Curved Earth versions of the Terrain Profile would barely be seen in an isometric diagram.

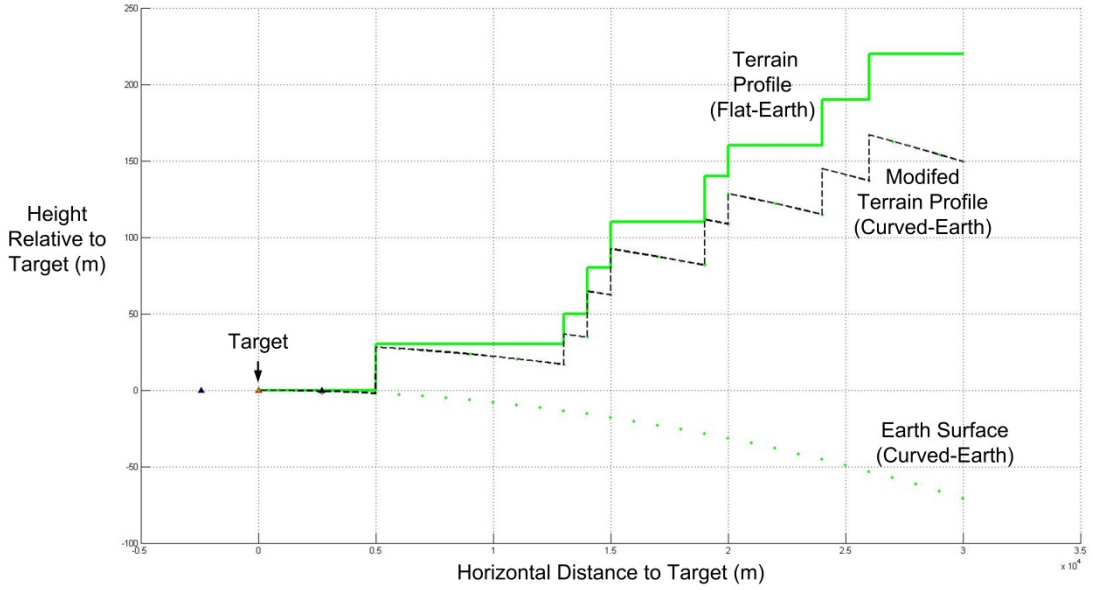

Figure 21: Modified Terrain Profile for a Curved Earth Geometry

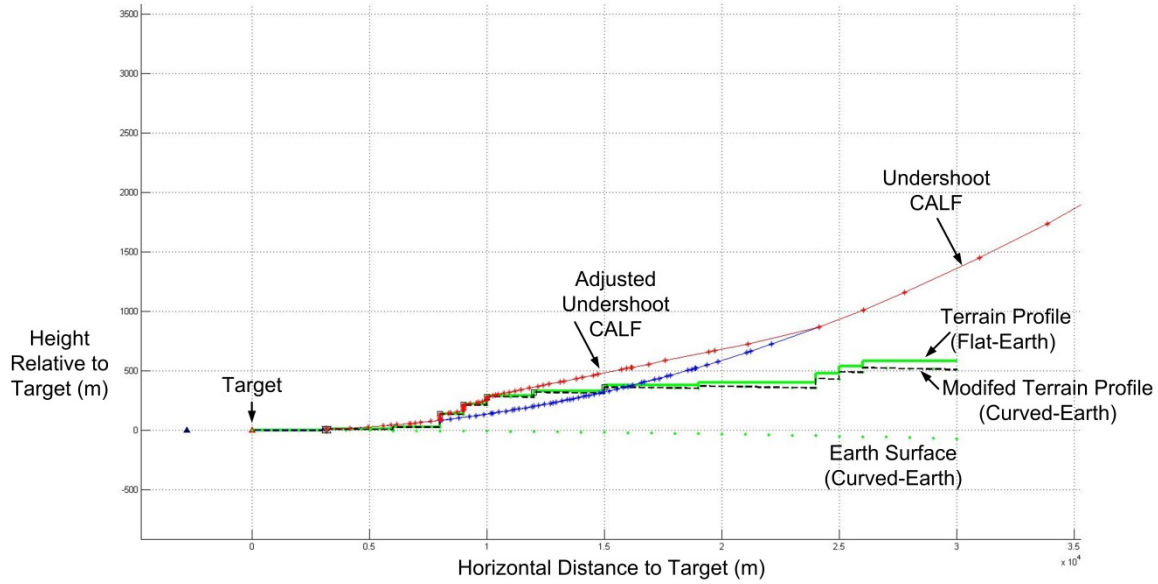

Figure 22: Undershoot CALF in a Curved Earth Model

Having calculated the Terrain Step coordinates of the modified Curved Earth Terrain Profile, the CALF geometry can be applied in exactly the same manner as for the Flat Earth Model. Figure 22 provides an illustration of an undershoot CALF for a Curved Earth Terrain Profile. In this case, it is necessary for the undershoot CALF to be adjusted in order to avoid intrusion of the modified terrain steps.

The algorithm for the undershoot CALF adjustment in the Curved Earth Model involves a similar procedure to that described in Section 3 for the Flat Earth Model. However, the calculation of the adjusted undershoot CALF co-ordinates will need to account for the Earth's curvature. Figure 23 provides an illustration of the undershoot CALF adjustment for a Curved Earth geometry.

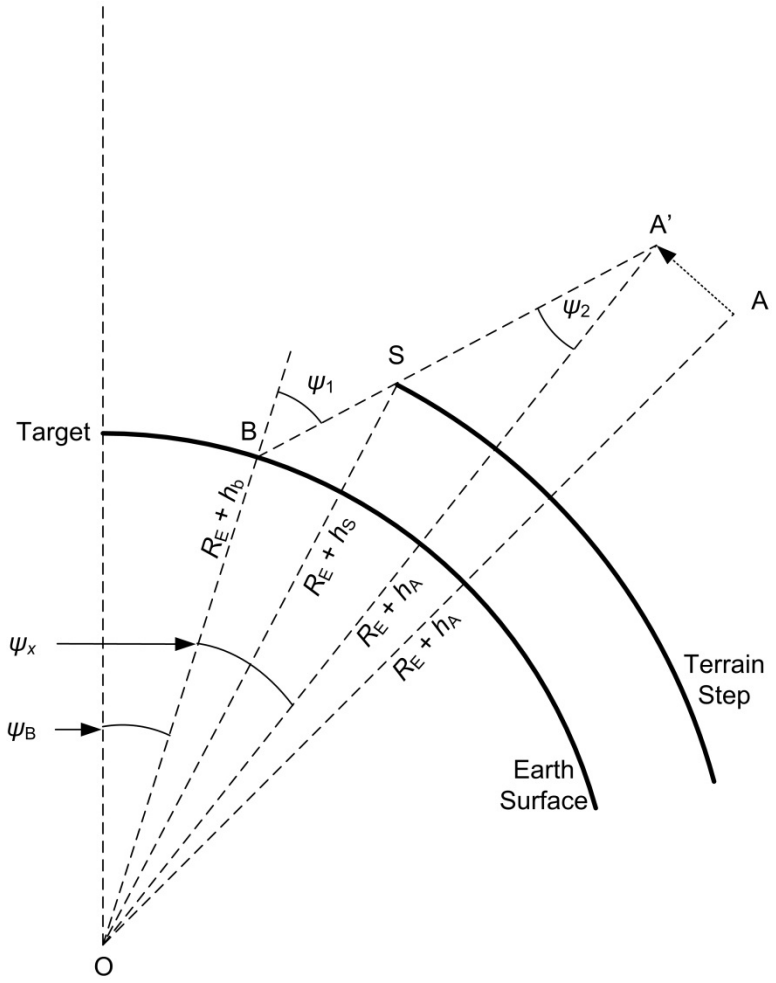

Figure 23: Undershoot CALF Adjustment for a Curved Earth Geometry

In the undershoot CALF adjustment shown in Fig. 23, the aircraft position is moved from point A to point A′, while maintaining the same altitude AMSL. This adjustment allows the maximum undershoot pointing error to fall between the Target and the undershoot boundary point B, without striking the edge of the Terrain Step at point S. Because the two aircraft positions have the same altitude AMSL, we have

$$OA' = OA = R_E + h_A \quad , \tag{4.2}$$

where R_{E} is the radius of the earth and h_{A} is the aircraft height AMSL. Once again h_s is the Terrain Step height AMSL and h_B is the boundary point height AMSL. The slant angle, ψ_2, from the adjusted aircraft position A' to the boundary point B, can be calculated from trigonometry, so that

$$\frac{R_{\mathrm{E}} + h_{\mathrm{A}}}{\sin(\pi - \psi_1)} = \frac{R_{\mathrm{E}} + h_{\mathrm{B}}}{\sin\psi_2} \quad , \tag{4.3}$$

which solves to

$$\psi_2 = \sin^{-1}\left(\frac{(R_{\mathrm{E}} + h_{\mathrm{B}})\sin(\pi - \psi_1)}{R_{\mathrm{E}} + h_{\mathrm{A}}} \right) \quad . \tag{4.4}$$

Trigonometry also yields the relationship, $\psi_1 = \psi_x + \psi_2$, giving

$$\psi_x = \psi_1 - \psi_2 \quad . \tag{4.5}$$

The vector connecting the Earth's Center point O and the adjusted aircraft position A' has horizontal and vertical components given by

$$\begin{aligned} x_u &= (R_{\mathrm{E}} + h_{\mathrm{A}})\sin(\psi_{\mathrm{B}} + \psi_{\mathrm{x}}) \\ z_u &= (R_{\mathrm{E}} + h_{\mathrm{A}})\cos(\psi_{\mathrm{B}} + \psi_{\mathrm{x}}) \end{aligned} \quad . \tag{4.6}$$

These values can be used to compute the aircraft's MICS coordinates (x_u , $z_u - R_E$). Finally, the small angle approximation yields the value

$$r_d = (R_{\mathrm{E}} + h_{\mathrm{A}})(\psi_{\mathrm{B}} + \psi_{\mathrm{x}}) \quad , \tag{4.7}$$

for the geodesic aircraft range-to-target at which laser firing is permitted to commence. Equation 4.7 represents the maximum undershoot laser firing range-to-target calculated from the adjusted undershoot CALF in the Curved Earth geometry. A similar analysis for the adjusted overshoot CALF in the Curved Earth geometry yields the maximum overshoot firing range.

4.2 FFLFZ for Curved Earth Model

The computational procedures described in Sections 3.3, 3.4, and 4.1 can now be used to define the (adjusted) undershoot and overshoot CALFs, in the Curved Earth geometry, for a given aircraft attack height and a given pair of undershoot and overshoot CRA boundary points lying along a given attack radial. The undershoot and overshoot CALF geometry parameter values can then be used to calculate the maximum undershoot and overshoot laser firing ranges-to-target, for an aircraft flying along that attack radial at that attack height. As in the Flat Earth Model, this process is repeated for every desired attack height and every radial passing through every CRA boundary point. Once again the maximum undershoot and overshoot firing ranges, computed for all attack heights and all attack radials, are used to generate the corresponding FFLFZs, using Eq. 3.12 and the method described in Section 3.5.

We illustrate the 3D-CALCZONE results (Curved Earth Model) by computing the FFLFZs for the same sample test range, target location, CRA, Terrain Surface Profile, and set of desired attack heights, used to generate the Flat Earth Model FFLFZs shown in Figs. 18 and 19. Figures 24 and 25 illustrate the FFLFZ contours for the Curved Earth Model, in three and two dimensions, respectively. It should be noted that these Figures have been generated by computing the Curved Earth FFLFZs expressed in MICS coordinates, transforming them into spherical latitude-longitude coordinates, and then transforming these into a "local map" 2-D coordinate system for plotting. Since these are the FFLFZs for a test scenario at the Tain Range in Scotland, the local map coordinate system used was the British National Grid (BNG) [21].

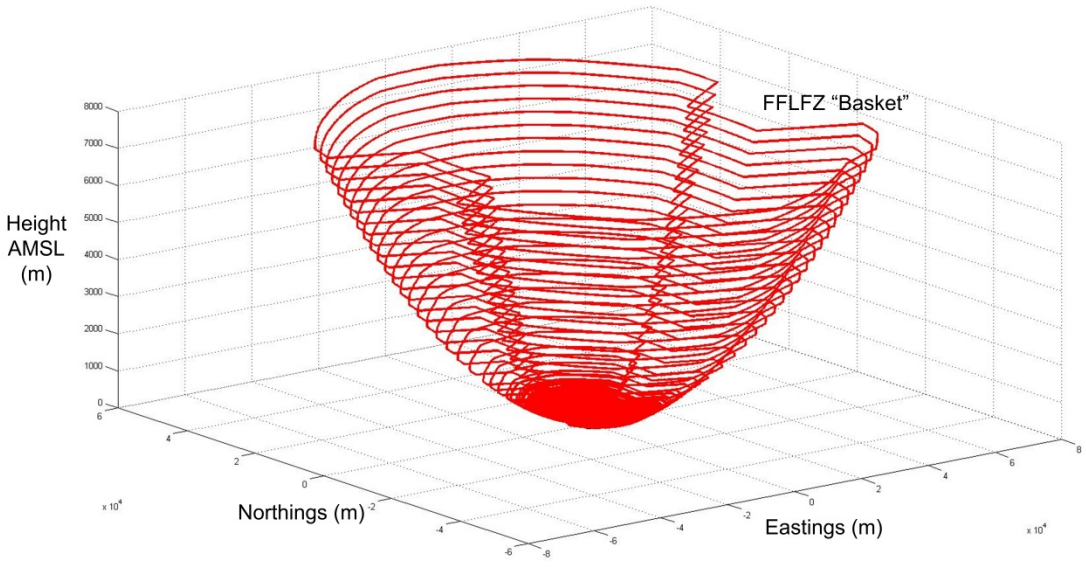

Figure 24: FFLFZ Contours "Basket" (Curved Earth Model)

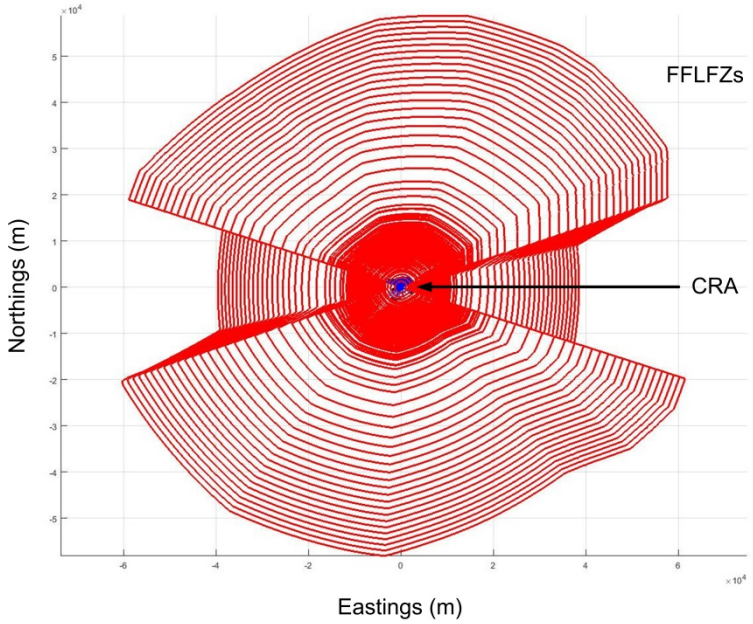

Figure 25: FFLFZ Contours "Bird's Eye" View (Curved Earth Model)

4.3 FFLFZ Comparison: Flat Earth vs. Curved Earth

Although it is not readily apparent when visually comparing Fig.19 to Fig. 25, the FFLFZs for the Flat Earth and Curved Earth Models do exhibit some minor differences. The differences would be even greater if the Curved Earth FFLFZs in Figure 25 had not been transformed from MICS coordinates into BNG coordinates prior to plotting. When this "flattening" factor is removed, the differences are much more apparent. Figure 26 provides a comparison of the "true" Curved Earth FFLFZ contours with the Flat Earth FFLFZs, when the curvature of the earth is taken into account. The FFLFZ contours produced by the Flat Earth Model are indicated by red lines, while those resulting from the Curved Earth Model are indicated by blue lines.

Note that the Curved Earth FFLFZs allow firing at greater ranges than the Flat Earth contours, since the curvature of the Earth's surface as we move away from the target makes it easier to avoid irradiating the Terrain Steps due to an undershoot pointing error. The Figure 26 contours indicate the additional distance an aircraft would fly when traveling at a constant altitude above the Curved Earth surface. However, it should be noted that the Figure 26 Curved Earth contours are based on a simple spherical Earth model, which is an approximation. Since the true shape of the Earth is an oblate spheroid, these results may differ somewhat from FFLFZ contours computed using the full transformation from three-dimensional geodetic (latitude-longitude-altitude) coordinates to a 2-D map based system [21].

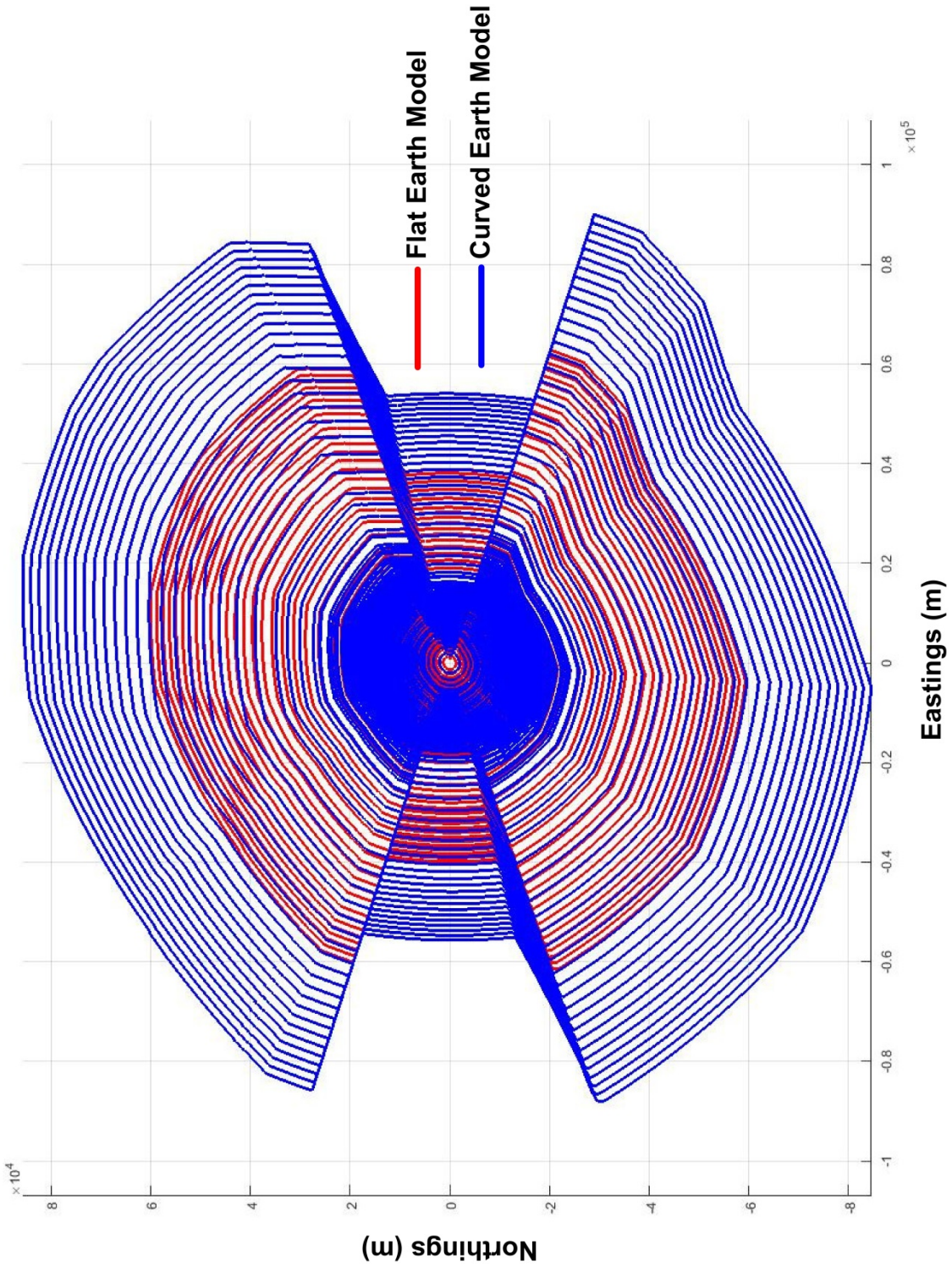

Figure 26: FFLFZ Comparison: Flat Earth vs. Curved Earth

5 3D-CALCTERT

The fourth step in hazard analyses performed with the Rough Earth TIALD Model is execution of the three-dimensional Tertiary Precaution module (3D-CALCTERT), which modifies the FFLFZ produced by 3D-CALCZONE. Once again the CALF method is applied, this time to produce FFLFZ restrictions arising from the Tertiary Precaution, which imposes a Minimum Separation Distance (MSD) to mitigate hazards arising from potential short range irradiation of unprotected observers. The result of the 3D-CALCTERT analysis is to create a low elevation Tertiary Precaution Surface, which effectively puts a "floor" under the FFLFZ "Basket" shown in Fig. 24, and prevents the use of low elevation attack tracks that violate the Tertiary Precaution. Before beginning our discussion, we should note that the material of Section 5 is only a condensed summary of the far more extensive documentation produced earlier by Dr. Brian Flemming, the TIALD model developer [22]. Readers are directed to earlier documentation for more mathematical detail and some derivations.

5.1 Tertiary Precaution Definition

As discussed in Section 2.1, the Tertiary Precaution is one of three safety measures applied in the UK Laser PRA Model. It is intended to guard against a potentially high risk of ocular damage from short range exposures being masked by a correspondingly low risk of laser misdirection or ocular irradiation; that is, it mitigates the hazards arising from high consequence/low probability events. The Tertiary Precaution makes two assumptions: first, that laser energy has definitely been misdirected to a point outside the CRA ($P_E = 1$), and second that an ocular irradiation of an unprotected observer has occurred at that point ($P_I = 1$). It then compares the *consequent* probability of ocular damage (P_{OD}) to a pre-defined maximum acceptable value. For the UK, a typical maximum acceptable value for the Tertiary Precaution is 10^{-1} probability of MOVL per attack.

The effect of the Tertiary Precaution is to impose a probabilistically defined Minimum Separation Distance (MSD) between the laser and any unprotected observer outside the CRA. The MSD must be applied at every laser firing point on the attack track and over the entire laser field of regard at each firing point. Laser firing is prohibited at any point on the attack track where the Tertiary Precaution is not satisfied. The MSD, defined as the parameter R_{CON3}, can be derived using the same method used to calculate the deterministic Nominal Ocular Hazard Distance (NOHD). That is, assuming a Gaussian beam profile,

$$R_{CON3} = \frac{1}{\phi_e}\sqrt{\frac{4E}{\pi H_{max}}} \quad , \tag{5.1}$$

where ϕ_e is the $1/e$ point beam divergence, E is the pulse energy and H_{max} is the energy density corresponding to a probability of 10^{-1} that the irradiated observer sustains a MOVL. The correct energy density for this probability of damage is calculated from the MATILDA dose-response model described in previous documentation [16, 18]. Depending on the pulse energy and beam divergence, the MSD can extend up to several kilometers from the laser source.

In the Smooth Earth TIALD Model the Tertiary Precaution was applied as part of the probabilistic fault/failure hazard analysis performed in CALCFAULT, with laser firing

prohibited at any point on the chosen attack track where the Tertiary Precaution was not satisfied. One problem with this procedure is that there is no prior guide to which attack tracks are acceptable. If the height of the attack track chosen for CALCFAULT analysis is too low, then the Tertiary Precaution may prohibit laser firing at all points, requiring the analyst to start over.

For the Rough Earth TIALD Model the 3D-CALCTERT module provides a prior guide to acceptable attack track heights by using the CALF method, along with the maximum *fault* laser pointing error, ε, to define a low elevation Tertiary Precaution Surface. Any aircraft flying at elevations above this surface will not have firing restrictions due to the Tertiary Precaution. Thus, in the fifth step of the Rough Earth TIALD Model, the attack track chosen for 3D-CALCFAULT analysis must be inside the FFLFZ and above the Tertiary Precaution Surface. In this sense the Tertiary Precaution Surface puts a "floor" under the FFLFZ.

As we saw in Sections 3 and 4, the application of the CALF geometry to definition of the FFLFZ was first done in a Flat Earth Model, and then adapted to the more complex Curved Earth geometry. The application of the CALF geometry to definition of the Tertiary Precaution Surface, described in the remainder of Section 5, has currently only been done for the case of a Flat Earth Model and a Flat Earth Terrain Profile [22]. This application has been incorporated into the 3D-CALCTERT module in MATILDA Version-2.0.3. Adaptation of 3D-CALCTERT to a Curved Earth geometry is a planned task for future MATILDA development. Fortunately, for range safety purposes the Flat Earth Model provides a more conservative safety analysis than the Curved Earth Model, with more restrictive firing zones. Since a more conservative analysis can always be used for safety purposes, the current Flat Earth implementation of 3D-CALCTERT is acceptable until further development can be done.

5.2 Circle of Allowed Laser Firing

The current application of the Circle of Allowed Laser Firing (CALF) geometry to definition of the Tertiary Precaution Surface uses the Flat Earth Terrain Profile and MICS coordinates, which have been previously described in Sections 3.1 and 3.2, respectively. Section 3.2 also gives a general discussion of the CALF geometry, illustrated in Fig. 6, and the geometry of the loci of equiangular points, illustrated in Figs. 7 and 8. That discussion was tailored for application of the CALF geometry to define the FFLFZ. For application of the CALF geometry to define the Tertiary Precaution Surface, some modification of the material in Section 3.2 is needed. Figs. 6 to 8 and Eqs. 3.1 to 3.4 still apply, but with changes to some parameter definitions.

Once again the Circle of Allowed Laser Firing, illustrated in Fig. 6, is a geometric construct that defines a locus of aircraft positions from which the laser can be fired at different aircraft heights. For each aircraft height, the laser firing position on the CALF is defined to ensure that, for a fixed laser pointing error, ϕ, all laser energy will fall between the Target and the CRA boundary. In the earlier discussion of Section 3.2, the angle ϕ represented a fault-free laser pointing error and the CALF could be used to define the FFLFZ for the special case where the fault-free laser pointing error equals the maximum value, $\phi = \alpha_{\max}$.

In contrast, for the Tertiary Precaution CALF application, the angle ϕ represents a *fault* laser pointing error and the CALF can be used to define the Tertiary Precaution Surface for the special case where the fault laser pointing error equals the maximum value, $\phi = \varepsilon$. The maximum fault laser pointing error is used here because the Tertiary Precaution was originally applied during the fault/failure hazard analysis performed in CALCFAULT. The MSD was applied at every laser firing point on the attack track and over the entire laser field of regard at each firing point, where the laser field of regard was determined by the maximum fault pointing error.

Referring to the geometry of the loci of equiangular points, illustrated in Fig. 7, we once again note that for the triangle *APB*, the sum of the interior angles is π, so that

$$2a + 2b + 2c = \pi \quad , \tag{5.2}$$

where *a* is the angle *OAB*, *b* is the angle *OPA* and *c* is the angle *OPB*. The angle *APB* is then given by

$$APB = b + c = (\pi/2) - a \quad , \tag{5.3}$$

and is constant for all points *P* on the circle. This relation remains true even if the circle center point *O* is outside the triangle *APB*, as shown in Fig. 8, provided the point *P* lies on the larger circular segment created by the chord *AB*. In this case, the angle *c* will effectively be "negative".

For the Tertiary Precaution CALF analysis, the angle APB corresponds to the maximum fault laser pointing error, ε, so that

$$b + c = \varepsilon \quad . \tag{5.4}$$

The angle *a* is then given by

$$a = \frac{\pi}{2} - \varepsilon \quad . \tag{5.5}$$

Note that Eqs. 5.4 and 5.5 are equivalent to Eqs. 3.3. and 3.4 in the special case where $\phi = \varepsilon$.

For an undershoot laser pointing error, the points B and A on the circle will correspond to the target and the undershoot ground point of interest, respectively, where the undershoot ground point of interest is typically the CRA undershoot boundary point. The line segment AP represents the separation distance between the laser and the undershoot ground point of interest. Conversely, for an overshoot laser pointing error, the target and the overshoot point of interest will be represented by A and B, respectively. Similarly, the line segment BP will represent the separation distance between the laser and the overshoot ground point of interest. For the Tertiary Precaution analysis, the distances AP and BP will be compared with the MSD.

5.3 Tertiary Precaution Analysis: Undershoot Risk

We begin our discussion of the application of the CALF geometry to define the Tertiary Precaution Surface by considering use of the CALF to mitigate undershoot laser pointing error

risk. The distance, R_{CON3}, given by Eq. 5.1, represents the MSD that must be maintained between the laser and populated areas outside the CRA, for all fault laser pointing errors up to the maximum fault laser pointing error, ε. In the Tertiary Precaution analysis the CALF will be used to determine the minimum altitude at which the aircraft is permitted to fire the laser so that the MSD is maintained. In the case of hilly terrain, this once again involves the use of the Terrain Profile Model and the intersection of undershoot laser pointing errors with the Terrain Profile Steps that cover all elevated terrain features.

The CALF laser undershoot geometry for an aircraft at point *P*, firing at a target at point *B*, with respect to an undershoot boundary point *A*, is shown in Figure 9 within Section 3.3. The edge of a Terrain Step is coincident with the undershoot boundary point *A*. The Terrain Step dimensions, the target height, and the Tertiary Precaution distance, R_{CON3}, can be used to determine the CALF center point and radius, *O* and r respectively, for an undershoot laser pointing error. The chord distance *AB* is derived from the target height, h_t , the terrain step height, h_s , and the terrain step distance from the target, r_s , so that

$$AB = \sqrt{r_s^{\,2} + \left(h_s - h_t\right)^2} \quad . \tag{5.6}$$

The slope, α , of the chord *AB* with respect to the local horizontal, can also be derived from the terrain step and target parameters:

$$\alpha = \tan^{-1} \frac{\left(h_s - h_t\right)}{r_s} \quad . \tag{5.7}$$

The radius r of the CALF can be calculated as a function of the chord length *AB* and the angle *a*,

$$r = \frac{AB}{2\cos a} \quad , \tag{5.8}$$

where *a* is given by Eq. 5.5. The coordinates $\left(x_c, z_c\right)$ of the undershoot CALF center point *O*, relative to the target position *B*, are now given by:

$$\begin{aligned} x_c &= r\cos\left(a+\alpha\right) \\ z_c &= h_t + r\sin\left(a+\alpha\right) \end{aligned} \quad . \tag{5.9}$$

In order to determine the minimum altitude at which the aircraft is permitted to fire the laser, the distance from the laser to the top of the undershoot boundary Terrain Step, *AP*, must be set to the Tertiary Precaution distance, R_{CON3}. The location (x_p, z_p) of the point, *P*, relative to the CALF centre, *O*, and hence the target position, *B*, can be derived from the triangle *AOP*. If the line segment $AP = R_{CON3}$ then, from triangle *AOP*,

$$\cos b = \frac{AP}{2r} = \frac{R_{CON3}}{2r} \quad . \tag{5.10}$$

From triangle *AOB*,

$$\cos a = \frac{AB}{2r} \quad , \tag{5.11}$$

so that

$$\cos b = \frac{R_{\mathrm{CON3}}}{AB}\cos a = \frac{R_{\mathrm{CON3}}}{AB}\sin \varepsilon \ , \tag{5.12}$$

since

$$\cos a = \cos\left(\frac{\pi}{2} - \varepsilon\right) = \sin \varepsilon \ . \tag{5.13}$$

Hence

$$b = \cos^{-1}\left(\frac{R_{\mathrm{CON3}} \sin \varepsilon}{AB}\right) \ . \tag{5.14}$$

The points A and P can hence be defined parametrically in terms of the CALF radius, r, and centre position (x_c, z_c). The coordinates (x_a, z_a) of the point A are

$$\begin{aligned} x_a &= x_c + r\cos\theta_1 \\ z_a &= z_c - r\sin\theta_1 \end{aligned} \quad , \tag{5.15}$$

where

$$\theta_1 = a - \alpha \ . \tag{5.16}$$

Similarly, the coordinates (x_p, z_p) of the point P are

$$\begin{aligned} x_p &= x_c + r\cos\theta_2 \\ z_p &= z_c + r\sin\theta_2 \end{aligned} \quad , \tag{5.17}$$

where

$$\theta_2 = \pi - 2b - \theta_1 \ , \tag{5.18}$$

so that

$$\theta_2 = \frac{\pi}{2} - 2b + \varepsilon + \alpha \ . \tag{5.19}$$

As can be seen from Fig. 9, the arc AP can be traced out by sweeping the CALF radius, r, through the angle $-\theta_1$ to $+\theta_2$. If the point A is populated, then the point P represents the Minimum Separation Distance from which the laser can be fired in order to satisfy the Tertiary Precaution. It follows that the aircraft elevation at point P, z_p , represents the minimum altitude at which the laser can be fired. Firing the laser at any lower altitude, for instance at any point on the CALF between the points A and P, would violate the Tertiary Precaution.

To summarize, Fig. 9 shows an aircraft approaching the Target along a particular attack radial, and at a point *P* in its attack track where the range-to-target puts it almost directly above the undershoot boundary Terrain Step. The equations above allow us to calculate the coordinates for a point *P* that represents the minimum firing altitude at this range-to-target. However, if the laser were fired at a different range-to-target along this attack radial, a different point *P* and a different minimum firing altitude would be computed. The locus of *all* points *P*, representing all possible firing ranges-to-target, will hence determine the set of minimum altitudes at which the laser can be fired for an attack track lying along this attack radial. Extending the computation to all attack radials, and combining all loci of points *P* obtained, produces the Tertiary Precaution Surface.

Figure 27 provides an illustration of the Tertiary Precaution geometry described above, as applied to a typical Terrain Profile lying along a particular attack radial. The *AP* arcs have been evaluated for all (r_s, h_s) Terrain Step coordinates in the Terrain Profile. We should note that the CALF circular arcs appear distorted in the diagram due to the use of non-isometric (i.e., differently-scaled) axes. The diagram is based on an MSD of R_{CON3} = 5 km and a maximum fault laser pointing angle of ε = 10°. The locations of the points *P*, representing various firing ranges-to-target, are indicated by the blue triangles. The slope of the laser-target vector steepens as the distance between the aircraft and the target decreases. The fault-pointing error cone will also tend towards the vertical, with the result that the minimum laser firing altitude will be increasingly dominated by the Tertiary Precaution distance. The diagram below illustrates effect of the Terrain Profile geometry on the locus of points *P*.

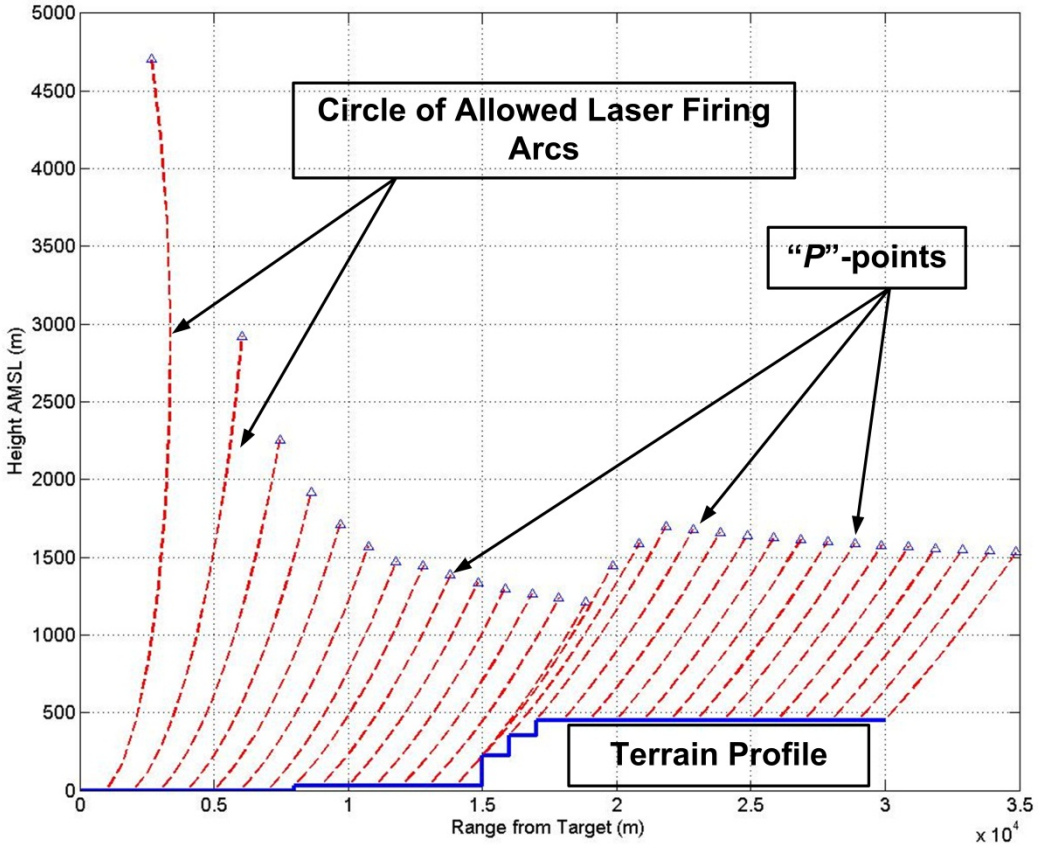

Figure 27: Tertiary Precaution Geometry for a Terrain Profile

5.4 Tertiary Precaution Analysis: Near-Target Geometry and Overshoot Risk

The basic Tertiary Precaution undershoot geometry described in Section 5.3 is only valid for sufficiently large distances of the aircraft from the target. The basic geometry breaks down at smaller ranges-to-target, depending on the values of R_{CON3} and ε. There are two critical positions in the Near-Target geometry. The first occurs when the maximum depression of the undershoot laser pointing error is vertical. The second occurs when the aircraft is directly over the target.

Figure 28 provides an illustration of the Near-Target geometry and the two critical positions. The target is assumed to be at point *B*. At the first critical position, P_1 , a maximum undershoot laser pointing error of ε results in the laser pointing vertically downwards towards the ground point, A_1. In this case a Terrain Step of height h_s is coincident with point A_1, so applying the MSD means the aircraft at P_1 must have a minimum height of $R_{CON3} + h_s$. As the aircraft passes P_1 and approaches the target, the laser vector at the maximum undershoot laser pointing error will start to point backwards, away from the target. At the second critical position, P_2 , the aircraft is directly above the target, where an undershoot laser pointing error of ε would cause the point A_2

to be irradiated. Applying the MSD here would give a minimum height of R_{CON3} plus the target height. It is assumed, however, that the target is unpopulated, so the target height need not be considered in the evaluation. The minimum aircraft height at P_2 is thus set to R_{CON3}. We note that laser energy can be fired in any direction within the fault pointing error cone. Thus, all ground points between B and A_1 should be at least the Tertiary Precaution distance, R_{CON3}, from the laser.

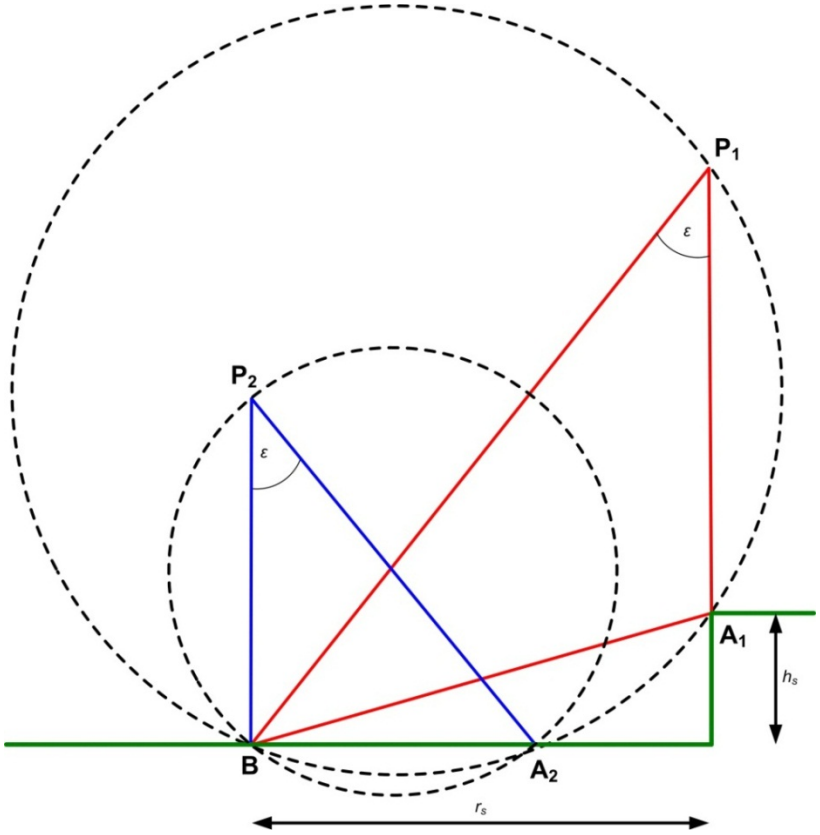

Figure 28: Near-Target Geometry

Figure 29 provides an illustration of how the modified minimum laser firing height geometry *could* appear for the Near-Target condition. In this example, the diagram illustrates the effect of a single terrain step. Additional terrain steps could result in a more complicated minimum laser firing height contour between P_1 and P_2.

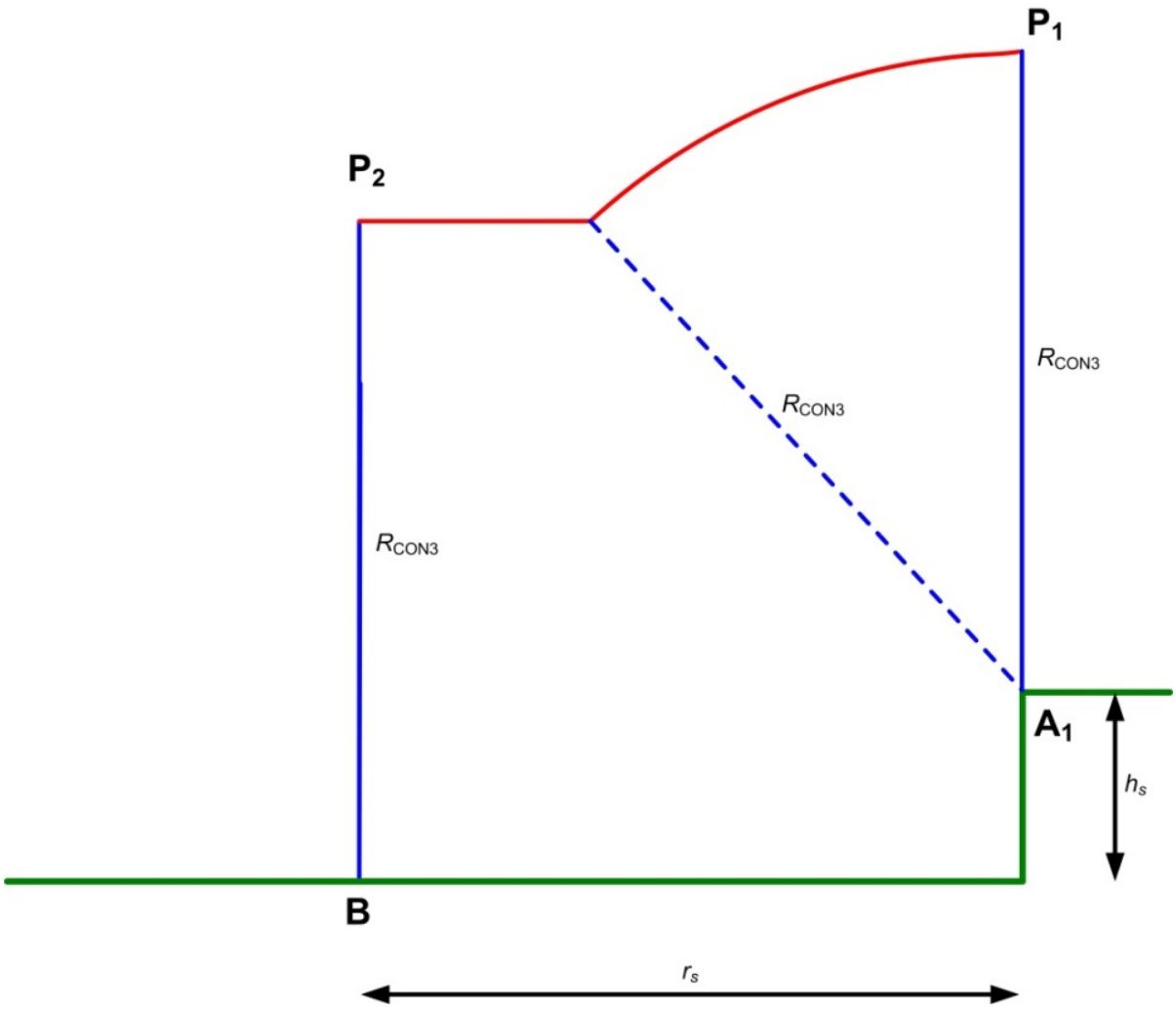

Figure 29: Near-Target Minimum Laser Firing Height

Figure 30 illustrates the locus of the computed Tertiary Precaution minimum firing altitude points *P* that ensure the MSD is maintained between the laser and populated ground areas. The diagram includes the application of the Near-Target Tertiary Precaution geometry described above. The locus of points *P* is indicated by the continuous blue line in the diagram and represents a cross-section of the Tertiary Precaution Surface along this attack radial.

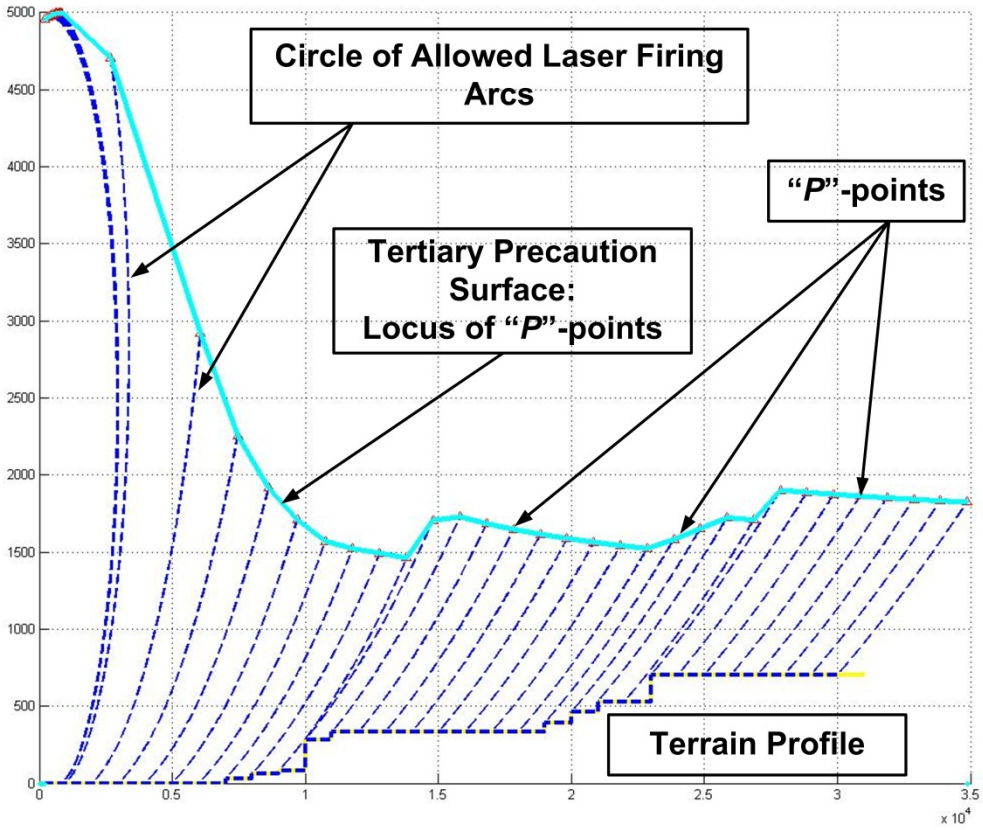

Figure 30: Locus of Tertiary Precaution Minimum Separation Distance Points

Up to this point, the Tertiary Precaution analysis has only considered use of the CALF to mitigate risks arising from *undershoot* laser pointing errors, which might cause short range irradiation of populated areas outside the CRA. The emphasis on undershoot laser pointing errors is due to the fact that these errors may strike the Terrain Steps closest to the approaching aircraft. Such exposures constitute the highest risk of ocular damage, since the potentially populated areas under these Steps are the closest to the laser source. In contrast, Terrain Steps struck by overshoot laser pointing errors do not generally pose a significant problem, since any populated areas under these Steps will be located beyond the target and at longer range. There could, however, be circumstances in which overshoot laser pointing errors become the predominant risk, due to the proximity of the target to the CRA overshoot boundary. Thus, any laser firing restrictions arising from Tertiary Precaution overshoot risk are best considered in an analysis which includes consideration of the CRA boundary location relative to the target. In the next section we will discuss the Tertiary Precaution analysis for an aircraft operating inside the CRA, which includes cases where the target is in close proximity to the CRA boundary.

5.5 Tertiary Precaution Analysis: Inside the CRA

Most range clearance assessments are predicated on the assumption that the target is located within a Controlled Range Area (CRA) from which unprotected persons are excluded. If the CRA is truly unpopulated, then the Tertiary Precaution condition would not apply to points inside the CRA boundary. Thus, Tertiary Precaution restrictions could potentially be relaxed, depending upon the extent of the CRA around the target relative to the values of the MSD and the maximum fault laser pointing error.

Although the CRA itself is typically assumed to be unpopulated, a Tertiary Precaution analysis for an aircraft operating inside the CRA should consider the possibility of laser energy irradiating populated areas beyond the Range boundary, as a result of an undershoot or overshoot fault laser pointing error. Restrictions might still have to be imposed on the permitted laser firing envelope *inside* the CRA to ensure that the MSD is maintained between the laser and populated areas *outside* the CRA.

Figure 31 illustrates the Tertiary Precaution Geometry for an aircraft operating inside the CRA. Both the laser undershoot and overshoot geometries are indicated, with respect to the undershoot and overshoot CRA boundary points, labeled RUB and ROB, respectively. The undershoot CALF (large solid blue circle) represents the locus of limiting aircraft positions, which ensure that an undershoot fault laser pointing error, up to the maximum value, ε, will remain within the CRA. For convenience, in future reference this CALF will be designated as the "CRA-Relaxation (Undershoot)" or "C-RX(U)".

Aside from aircraft positions on the CALF itself, an undershoot fault laser pointing error will always remain inside the CRA if the aircraft position is anywhere inside the circle designated C-RX(U). Conversely, an undershoot fault laser pointing error could cause laser irradiation of populated areas outside the CRA if the aircraft position is outside the circle C-RX(U). The irradiation of populated areas outside the CRA, however, would be deemed acceptable if the Tertiary Precaution is satisfied; that is, if the separation distance between the laser and any ground point outside the CRA, as measured along the laser line-of-sight, is greater than R_{CON3}.

The locus of points within the MSD, R_{CON3}, of the CRA undershoot boundary point, RUB, is indicated by the large dashed blue semi-circle, which for convenience will be designated as the "CRA-Restriction (Undershoot)" or "C-RT(U)". The shaded portion of this semi-circle, labelled C on the diagram, indicates the region of airspace that is outside the C-RX(U) but is also within R_{CON3} of the CRA undershoot boundary. Laser firing would hence not be permitted in this region of airspace. Tertiary Precaution restrictions on laser firing for populated areas short of the CRA, including the region labelled C, are discussed in the previous section.

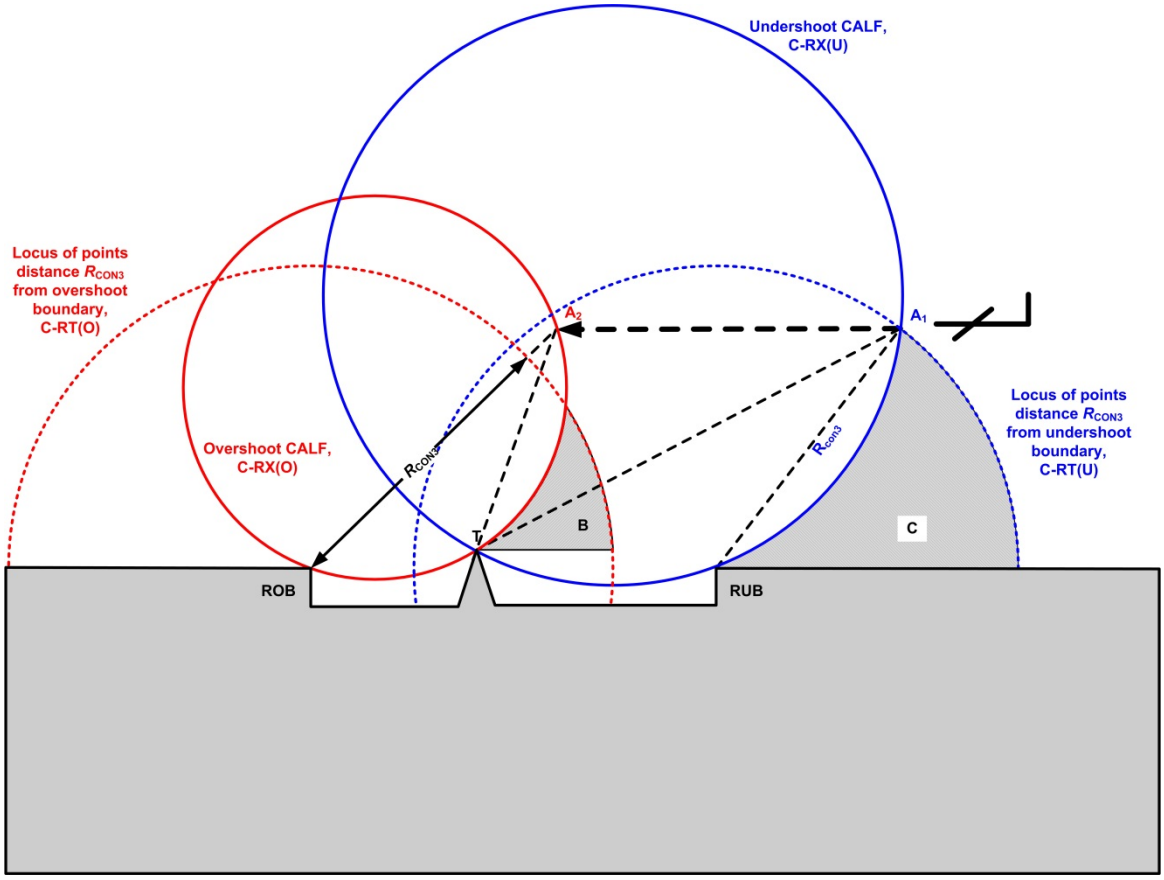

Figure 31: Tertiary Precaution Geometry for Operations Inside the CRA

Populated areas outside the CRA, and on the far side of the target, *could* become vulnerable to an overshoot fault laser pointing error as the aircraft traverses the CRA. Irradiation of populated areas beyond the CRA cannot occur once the aircraft enters the overshoot CALF (small solid red circle), which for convenience will be designated as the "CRA-Relaxation (Overshoot)", or "C-RX(O)". Once again, irradiation of populated areas outside the CRA is acceptable providing the separation distance of ground points from the aircraft remains greater than or equal to the MSD.

The locus of points within the MSD of the CRA overshoot boundary point, ROB, is indicated by the large dashed red semi-circle, which for convenience will be designated as the "CRA-Restriction (Overshoot)", or "C-RT(O)". It can be seen from Fig. 31 that there are possible aircraft positions, indicated by the shaded region labeled B, where an overshoot fault laser pointing error could cause irradiation of populated areas outside the CRA, but within the MSD of the laser. Once again, laser firing would not be permitted in this region of airspace.

The prohibited laser firing zone B can be quite extensive for some cases, as illustrated in Figure 32. Here the target is located close to the CRA overshoot boundary and the corresponding C-RX(O), indicated by the red circle, is quite small. In this instance, the whole of the C-RX(O) is contained within the C-RT(O) and is thus within R_{CON3} of the CRA overshoot boundary point.

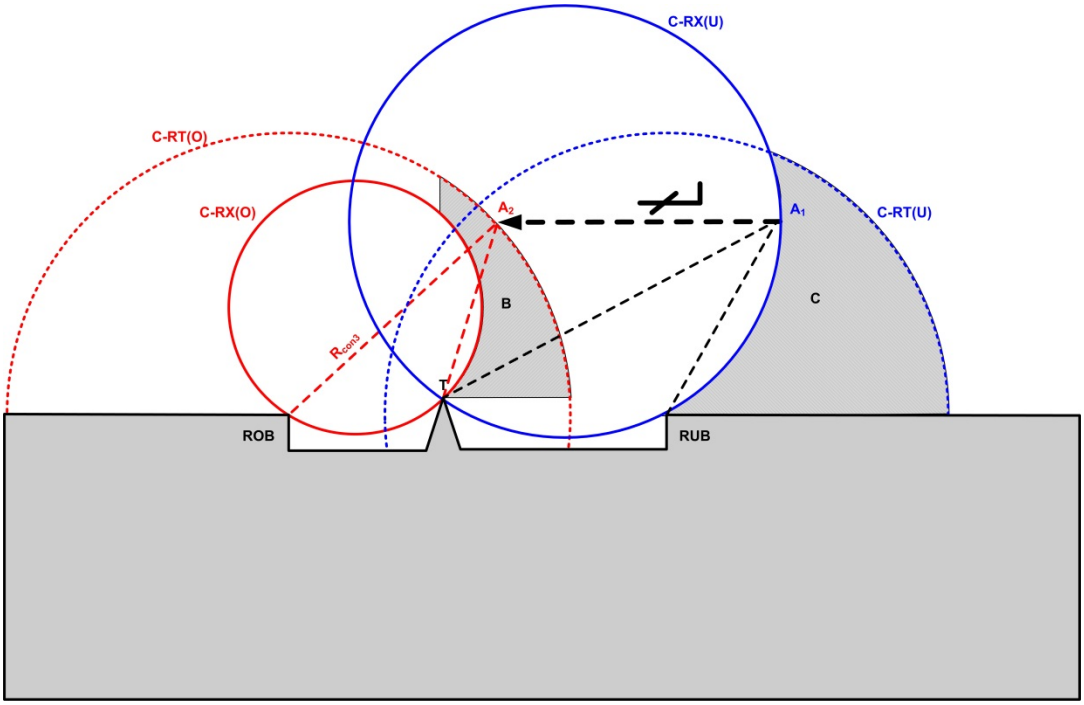

Figure 32: Small Overshoot CALF

It is assumed that the undershoot and overshoot geometries swap once the aircraft has passed over the target, or if the aircraft is approaching from the opposite side of the target. The corresponding reverse situation, in which the target is located closer to the CRA undershoot boundary than to the CRA overshoot boundary, is illustrated in Figure 33. In this case, the C-RX(U) will be smaller than the C-RX(O), reversing the situation seen in Figure 32. The whole of the C-RX(U) is now contained within the C-RT(U), with a correspondingly larger region (indicated by the shaded area C) in which laser firing would not be permitted.

Laser firing can be permitted within the CRA when the aircraft is within the undershoot or overshoot CALF circles for undershoot and overshoot fault laser pointing errors, respectively, subject to Tertiary Precaution restrictions for the CRA undershoot and overshoot boundary points. When the aircraft is approaching the target, laser firing would only be permitted when the aircraft is within the C-RX(U), but not within the C-RT(O). Similarly, when the aircraft is past the target, laser firing would only be permitted when the aircraft is within the C-RX(O), but not within the C-RT(U).

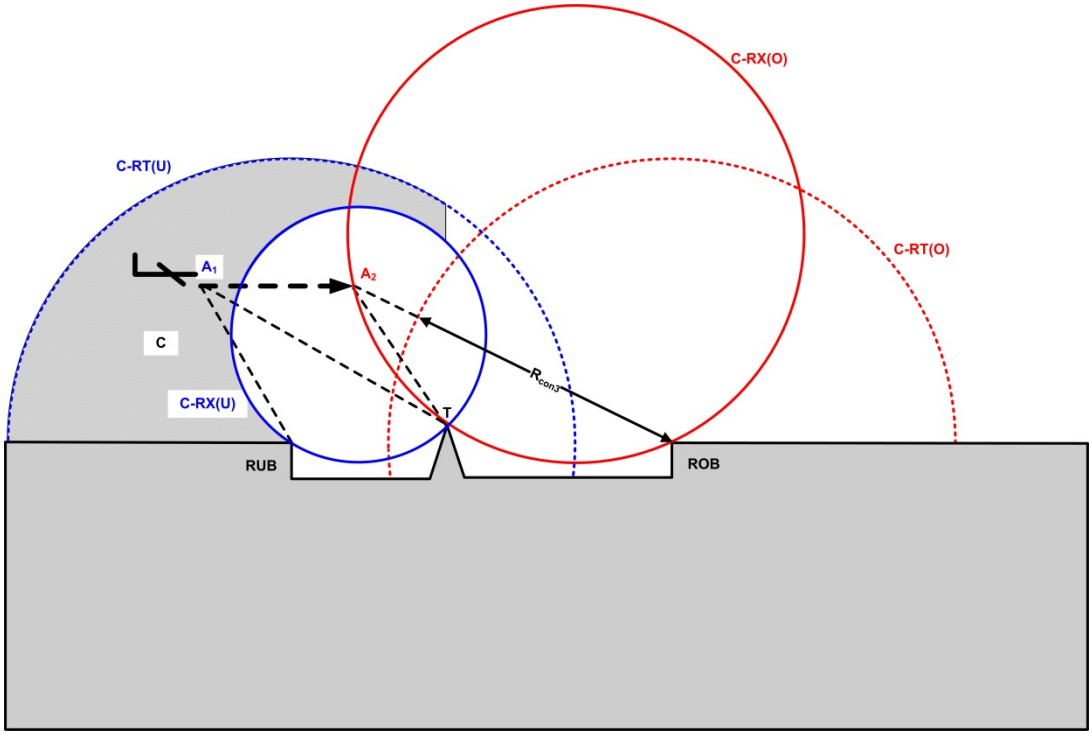

Figure 33: Small Undershoot CALF

The center point, (x_u, z_u), of the undershoot CALF, C-RX(U), is evaluated using the same geometry as described in Section 5.3. That is, we can slightly modify Eqs. 5.6 to 5.9 to obtain

$$\begin{aligned} x_u &= r_u \cos\left(a + \alpha_u\right) \\ z_u &= r_u \sin\left(a + \alpha_u\right) \end{aligned}, \tag{5.20}$$

where

$$r_u = \frac{AB_u}{2\cos a} \tag{5.21}$$

is the C-RX(U) radius, a is given by Eq. 5.5,

$$AB_u = \sqrt{{r_{bu}}^2 + \left(h_u - h_t\right)^2} \tag{5.22}$$

is the chord length between the target aim-point and the CRA undershoot boundary,

$$\alpha_u = \tan^{-1}\left(\frac{h_u - h_t}{r_{bu}}\right) \tag{5.23}$$

is the chord slope, and h_u, h_t, and r_{bu} are the CRA undershoot boundary height, the target aim-point height, and the CRA undershoot boundary distance from the target, respectively.

Figure 34 indicates the potential improvement produced in the Tertiary Precaution Surface (permitted laser firing envelope), as a result of a CRA boundary laser undershoot pointing error relaxation. In the diagram the dashed green line represents the undershoot CALF C-RX(U), corresponding to the CRA undershoot boundary. The magenta-coloured line represents the portion of the C-RX(U) circle that would contribute to the Tertiary Precaution Surface. Undershoot related laser firing restrictions within the green-coloured C-RX(U) can be ignored.

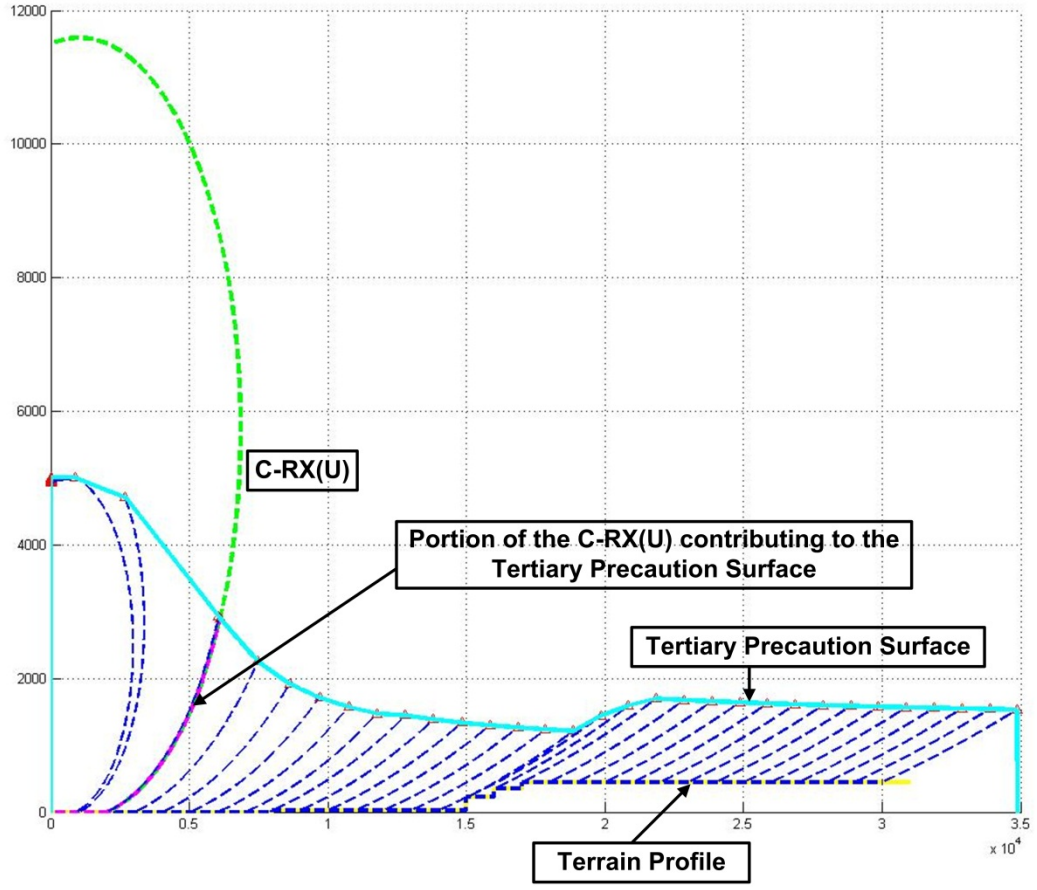

Figure 34: CRA Boundary Undershoot Relaxation

The center point, (x_o, z_o), of the overshoot CALF, C-RX(O), is similarly evaluated, so that

$$\begin{aligned} x_o &= -r_o \cos\left(a + \alpha_o\right) \\ z_o &= r_o \sin\left(a + \alpha_o\right) \end{aligned}, \tag{5.24}$$

where

$$r_o = \frac{AB_o}{2\cos a} \tag{5.25}$$

is the C-RX(O) radius,

$$AB_o = \sqrt{r_{bo} + \left(h_o - h_t\right)} \tag{5.26}$$

is the chord length between the target aim-point and the CRA overshoot boundary,

$$\alpha_o = \tan^{-1}\left(\frac{h_o - h_t}{r_{bo}}\right) \tag{5.27}$$

is the chord slope, and h_o and r_{bo} are the CRA overshoot boundary height and the CRA overshoot boundary distance from the target, respectively. If the observed convention is that undershoot distances, short of the target, are increasing from zero (positive), then overshoot distances, beyond the target, will be decreasing from zero (negative). This explains the minus sign in the expression for x_o in Eq. 5.24.

An aircraft whose range and altitude relative to the target are x_A and H_A, respectively, will be within the C-RX(U) when

$$r_A = \sqrt{\left(x_A - x_u\right)^2 + \left(H_A - z_u\right)^2} \le r_u \quad . \tag{5.28}$$

Similarly, an aircraft whose range and altitude relative to the target are x_A and H_A, respectively, will be within the C-RX(O) when

$$r_A = \sqrt{\left(x_A - x_o\right)^2 + \left(H_A - z_o\right)^2} \le r_o \quad . \tag{5.29}$$

From the above analysis, laser firing within the CRA would hence be permitted anywhere:

1. within the C-RX(U) short of the target, except when the aircraft is outside the C-RX(O) and within the C-RT(O).
2. within the C-RX(O) short of the target, except when the aircraft is outside the C-RX(U) and within the C-RT(U).

The CRA Tertiary Precaution relaxation criteria, described above, can be combined with the Tertiary Precaution Surface, described in Sections 5.3 and 5.4, to define a composite set of Tertiary Precaution Restrictions for laser firing operations on a “hilly” range.

Finally, in the case of the CRA boundary being within the critical distance AB^* of the target, the Tertiary Precaution Surface can also be relaxed to the C-RT(U) and C-RT(O) semi-circles, which define the MSD range from the CRA undershoot and overshoot boundary points, respectively. Figure 35 illustrates such a relaxation of the Tertiary Precaution Surface.

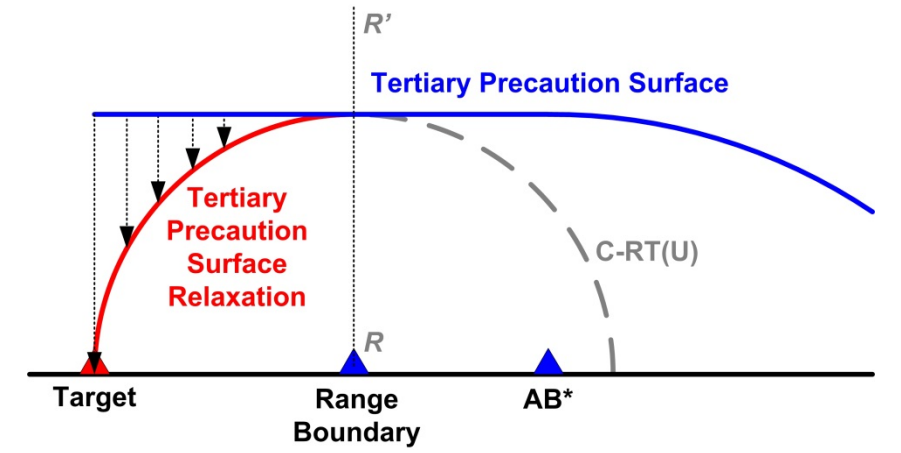

(a)

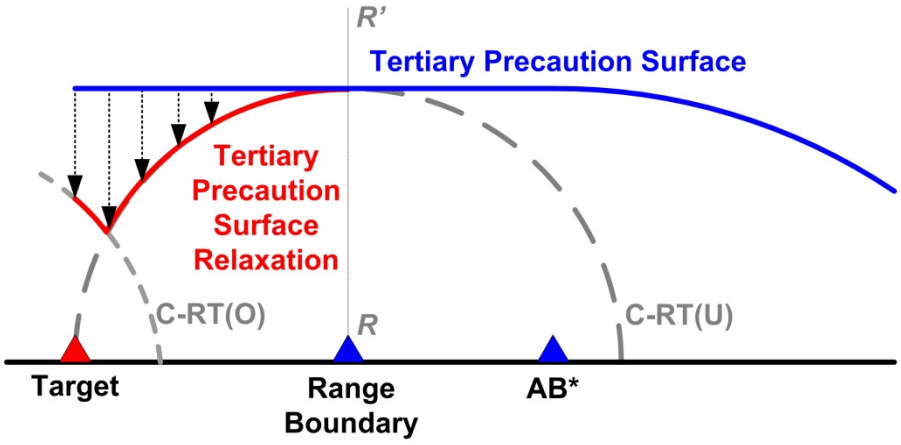

(b)

Figure 35: Tertiary Precaution Surface Relaxation for (a) CRA Undershoot Boundary and (b) CRA Overshoot Boundary

Figure 35 (a) illustrates the Tertiary Precaution Surface relaxation for the case where the target is within the critical distance AB^* of the CRA undershoot boundary. The semi-circle C-RT(U) defines the locus of points that are a distance of R_{CON3} from the CRA undershoot boundary. All points outside of this semi-circle that are also between the target and the CRA boundary (i.e., to the left of the line *RR'*) will be at a greater distance than the MSD from the CRA undershoot boundary. Hence, the Tertiary Precaution restrictions inside the CRA boundary can be relaxed to the C-RT(U) semi-circle, as shown. Figure 35 (b) illustrates the change in the relaxation produced by consideration of the CRA overshoot boundary (to the left of the target and not shown in the diagram). The Tertiary Precaution Surface inside the CRA boundary is now relaxed to the mutually-exclusive arcs of the semi-circles, C-RT(U) and C-RT(O).

5.6 Tertiary Precaution Surface Algorithm

An algorithm designed to implement the Tertiary Precaution analysis described in Sections 5.3 to 5.5 and create the Tertiary Precaution Surface must be able to accommodate a reasonably wide variation in values of the Minimum Separation Distance, R_{CON3}, and the maximum fault laser pointing error, ε. The algorithm must also be applicable to a reasonably wide range of Terrain Profiles. The purpose of this section is to provide a summary of the main considerations in the development of a Tertiary Precaution Surface algorithm for a "hilly" range.

The phrase "reasonably wide" is used in this context since it would be uneconomic to develop an algorithm to cope with every conceivable Terrain Profile or combination of R_{CON3} and ε. The algorithm described in this section has been successfully tested on the Terrain Profiles for two UK ranges: Garvie Island Range and Tain Range [22]. The algorithm has also been reliably tested for maximum fault laser pointing angles in the range $1^{\circ} \le \varepsilon \le 50^{\circ}$ and Minimum Separation Distances in the range from 4 km to 6 km.

To illustrate the results of the 3D-CALCTERT Tertiary Precaution analysis we once again use the test case previously used in Sections 3 and 4 to illustrate the 3D-CALCZONE results: a hypothetical airborne laser designator used in an attack maneuver during a training scenario at the UK's Tain Range in northern Scotland. Figure 36 illustrates the test case CRA, which is a modification of the Tain Range boundary made to ensure a "star-shaped" configuration relative to the target position [16]. In a "star-shaped" CRA, each radial emanating from the target cuts the boundary once only. For this test case we assume that the laser system parameters give a MSD of 5 km and a maximum fault laser pointing error of error of 20°.

In the diagram, the CRA boundary "near" side is populated with all relevant boundary points created for use in the 3D-CALCZONE computation. These include points relating to the shape of the boundary itself, to the Terrain Profile "Web" (see Figure 4), and to relevant features in the surrounding environment, such as urban areas. The various computational steps needed to define all relevant CRA boundary points has been described in previous documentation [16] and will not be repeated here. For the Tain Range Terrain Profile the terrain steps are defined at 1 km spacing and there are 36 sectors with an angular width of 10°. The Tertiary Precaution algorithm described in this section has also been applied to a Terrain Profile with a step spacing of 0.5 km (Garvie Island Range). Finer Terrain Profile Web resolutions are feasible, but are subject to the disadvantages of increased memory and computational time.

The high density of points on the "near" side boundary corresponds to a relatively large number of points spanning each of the angular sectors in the Terrain Profile. Consequently, only elevation pointing errors need be considered for the Tertiary Precaution analysis, since the effect of azimuth errors relative to adjacent Terrain Profile sectors will be negligible. For each CRA boundary point on the "near" side, a corresponding CRA boundary point on the "far" is calculated. These near and far side boundary point "pairs" define the possible attack radials. The Tertiary Precaution analysis is performed systematically for each attack radial and each point on the "near" and "far" CRA boundaries.

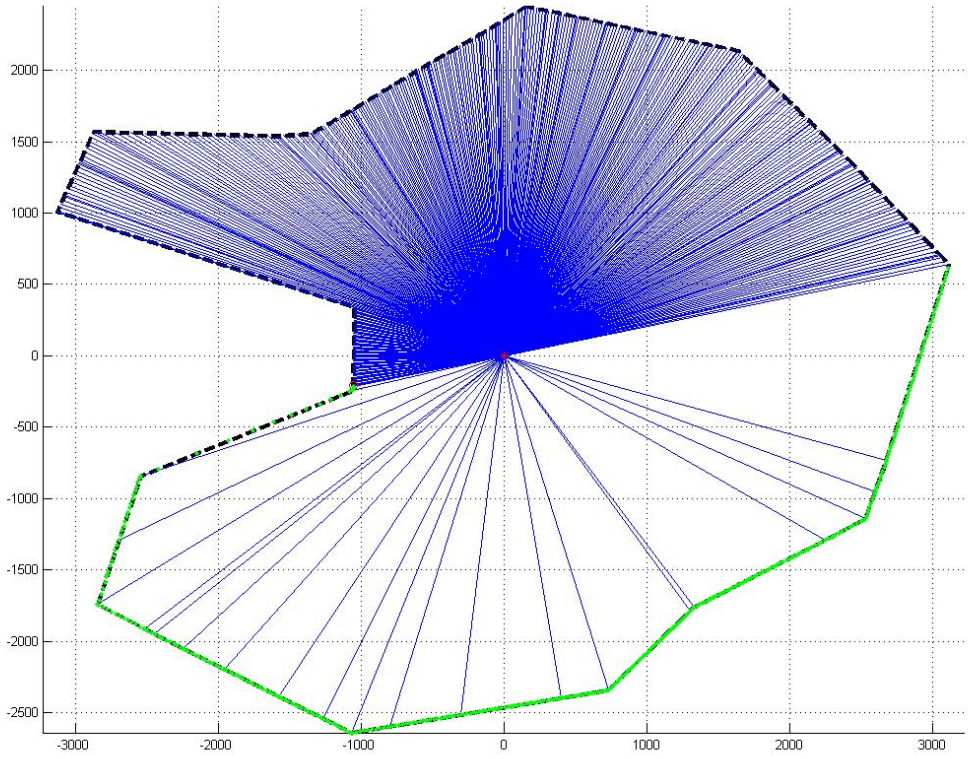

Figure 36: CRA Boundary "Near" and "Far" Side

Referencing the material of Sections 5.3 and 5.4, the initial Tertiary Precaution profile (the locus of points *P* that represent the minimum firing altitude at various ranges) for each radial direction from the target (attack radial) is essentially derived from a series of circular (CALF) arcs, the definition of which depend on the location of the critical point, A_1 (see Figures 27 and 28). For distances beyond A_1 the circular arcs are defined for each terrain step. Referring to the geometry of Figure 9, parametrical information for each CALF circular arc includes:

- The center of curvature, (x_c, z_c)
- The radius of curvature, r_c
- The angle, θ_1, corresponding to the Terrain Step
- The angle, θ_2, corresponding to the point *P*

The point *P* corresponds to the maximum height on the CALF circular arc which is used in defining the Tertiary Precaution profile. The location of each point *P* relative to *adjacent* arcs depends on the values of R_{CON3} and ε, and also on the Terrain Profile.

Figure 37 provides an illustration of the potential locations of the points P relative to an arbitrary Terrain Profile, in which the CALF circular arcs are indicated by a dashed red line, and the points P are identified by the blue triangles. In this case, some of the points P occur under the surface of the closest Terrain Step. A technique is therefore required to ensure that only the points P above the Terrain Profile Surface are included in the Tertiary Precaution profile**.**

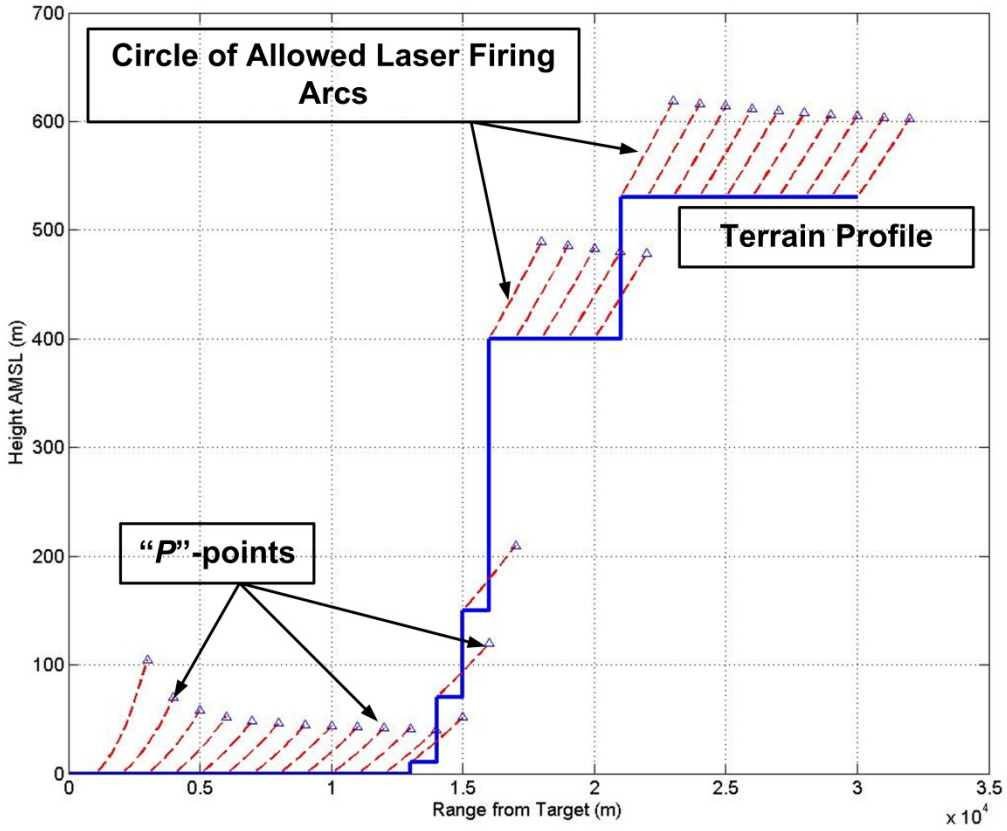

Figure 37 Tertiary Precaution Circular Arcs and Minimum Firing Altitude Points P

The Tertiary Precaution profile height at any given MICS point (*x*, *y*) is defined by the maximum *z* value from three different sources shown in Fig. 37:

- The locus of the points, *P*
- The Terrain Step heights
- CALF circular arcs passing through the point (*x*, *y*)

The locus of the points P can be estimated through the use of straight line segments, or by the application of more sophisticated curve-fitting techniques such as splines. If necessary, the

resolution of each of the three components listed above can be increased to every meter, in order to facilitate definition of the Tertiary Precaution profile.

Next, looking at near-target geometry, the circular arcs between the target and the critical point, A_1, are similarly defined. In this case, parametrical information for each CALF circular arc includes:

- The center of curvature, $(x_c, 0)$
- The radius of curvature, $r_c = R_{CON3}$.
- The angle, $\theta_1 = \pi/2$, corresponding to the point P at the zenith of each circular arc
- The angle, θ_2, corresponding to the point $x = 0$

The Tertiary Precaution profile height at any given MICS point (x, y) within the near-target geometry is defined by the maximum z value from two different sources:

- The locus of the points, P
- CALF circular arcs passing through the point (x, y)

Figure 38 provides an illustration of how the maximization procedures described above are used to define the Tertiary Precaution profile. The locus of the points P is indicated by a solid green line. The CALF circular arcs are indicated by a narrow dashed blue line. The cyan line indicates the maximum elevation of the CALF circular arcs. The Terrain Steps are indicated by a wide dashed blue line. The maximum locus, defining the Tertiary Precaution Surface for this attack radial, is indicated by the dashed red line. Note that the Tertiary Precaution Surface algorithm computes an initial Tertiary Precaution profile, based on the Locus of points P, and then adjusts it upwards in some locations based on the Terrain Profile Steps and the CALF circular arcs. This two-step computation of a "lower" and an "upper" Tertiary Precaution profile ensures that there is always a single z-coordinate for every x-value.

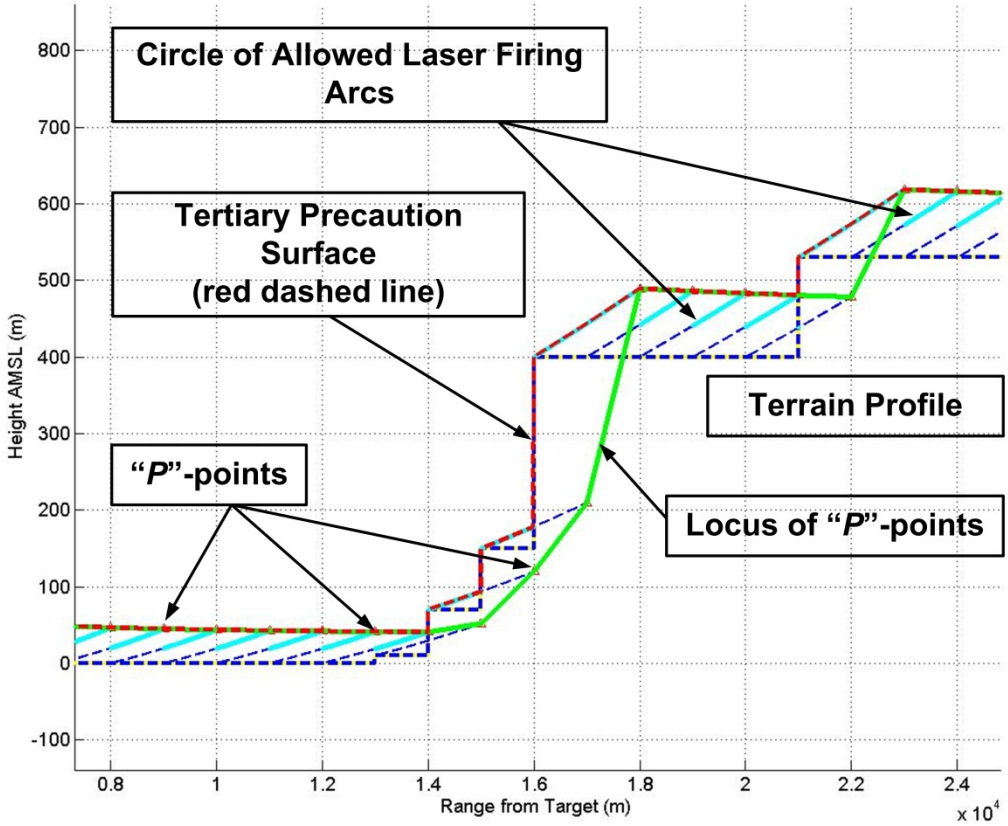

Figure 38: Tertiary Precaution Profile (Detail)

To illustrate how the Tertiary Precaution profile along an attack radial can vary, depending on variations in the Terrain Profile, and in the target location relative to the CRA boundary, we will now apply the Tertiary Precaution Surface algorithm described above to two illustrative examples taken from the Tain Range test case described earlier. Then we will apply the algorithm to derivation of the complete Tertiary Precaution Surface for the Tain Range test case. As mentioned previously, the Tain Range test case assumes a laser giving a MSD of 5 km and a maximum fault laser pointing error of 20°.

Example 1, shown in Figure 39, illustrates a relatively simple application of the algorithm. In this example the Terrain Profile is composed of a rising series of steps, the effect of which can be seen in the subsequent Tertiary Precaution Surface, which is designated by a solid red line. At the point *X* the Tertiary Precaution Surface intersects with the C-RT(U) semi-circle, designated by a dashed black line, which indicates the locus of points that are at distance R_{CON3} from the undershoot CRA boundary point *R*. In the absence of any CRA relaxations, the Tertiary Precaution Surface would continue along the C-RT(U) semi-circle. In this example, the critical point *A* lies within the CRA boundary. The solid green C-RX(U) arc is a portion of the undershoot CALF at the CRA undershoot boundary, which intersects with the corresponding C-

RT(U) semi-circle at the point *X*. All under-shoot restrictions between *X* and the target *T* can be relaxed back to the C-RX(U).

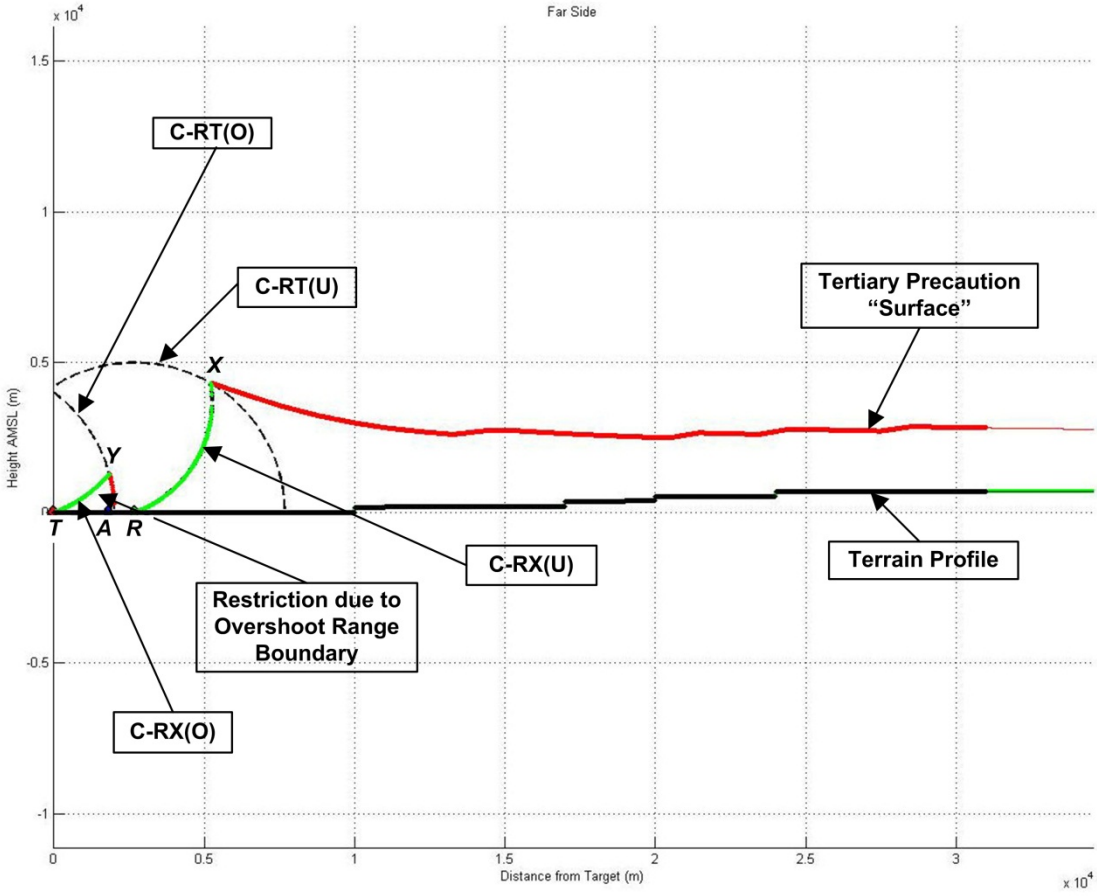

Figure 39: Tertiary Precaution Profile – Example 1

Within the CRA there is a further overshoot restriction to be considered, due to the proximity of the target to the overshoot CRA boundary (to the left of the target and not shown in the diagram). However, the corresponding C-RT(O) semi-circle intersects with the green portion of the overshoot CALF, C-RX(O), at the point *Y*, leaving a small "tooth-shaped" area within the CRA in which laser firing is not permitted. This "tooth-shaped" restriction becomes part of the overall Tertiary Precaution Surface, now shown as the combination of the red and green lines in the diagram. An aircraft flying above the Tertiary Precaution Surface along this attack radial could fire the laser without restriction, other than those imposed by the Fault Free Laser Firing Zones and the outcome of the 3D-CALCFAULT evaluation. An aircraft flying below the Tertiary Precaution Surface would not be permitted to fire the laser at all.

Example 2, shown in Figure 40, illustrates the case where the critical point *A* lies at the critical distance AB^* from the target *T*, and the CRA undershoot boundary point *R* occurs within the critical distance AB^* of the target. In this example the solid green C-RX(U) arc, representing a portion of the undershoot CALF at the CRA undershoot boundary, is almost a full circle. Moreover, the C-RX(U) arc lies completely within the Tertiary Precaution Surface, designated by the red line. The C-RX(U) thus creates a small "bubble," under the Tertiary Precaution Surface and inside the CRA, in which laser firing would be permitted,. On the other hand, laser firing is prohibited for areas under the Tertiary Precaution Surface which are *outside* the C-RX(U).

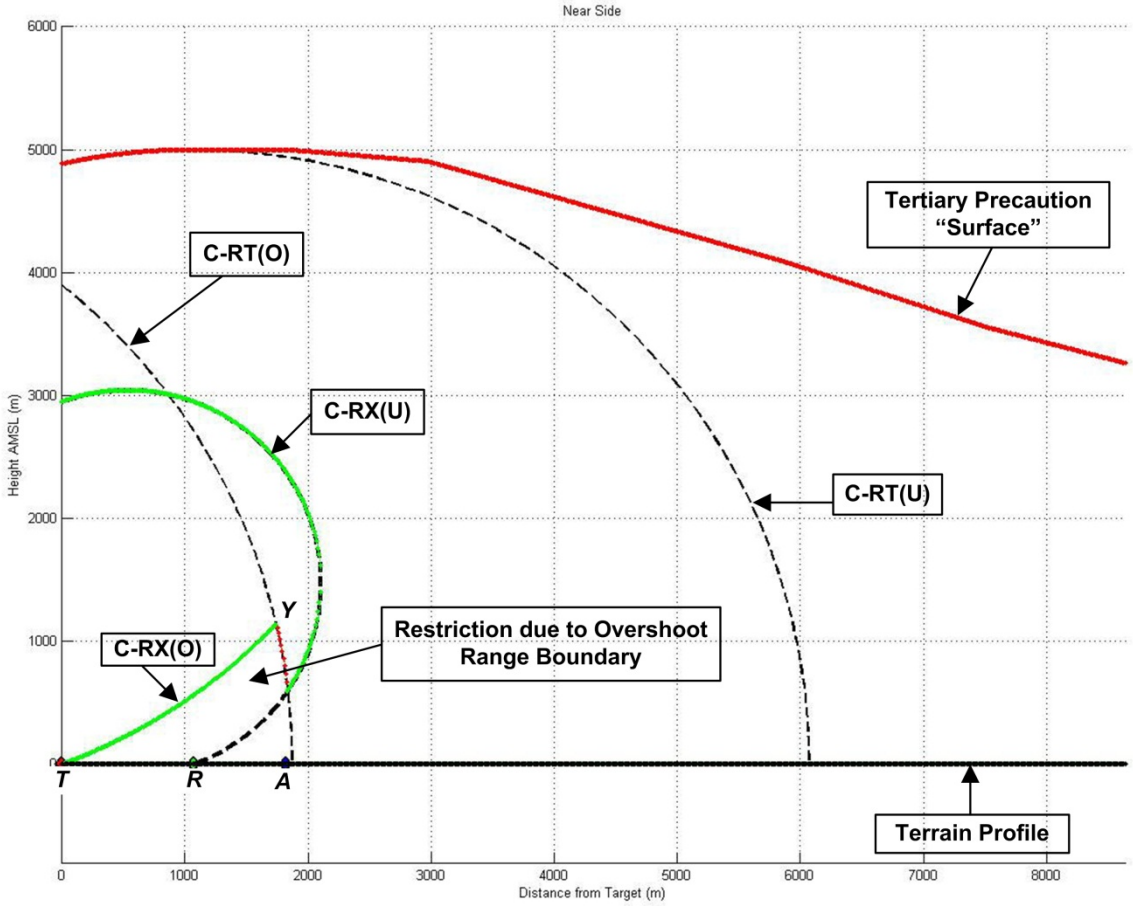

Figure 40: Tertiary Precaution Profile – Example 2

Figure 40 also shows that there is an additional restriction imposed on laser firing due to the overshoot CRA boundary (to the left of the target and not shown in the diagram). In this case, laser firing would not be permitted within a distance of R_{CON3} of the overshoot CRA boundary, including the portion of the C-RX(U) that lies within the C-RT(O) semi-circle. However, application of the C-RX(O) will permit laser firing within the region enclosed by the C-RT(O)

semi-circle, the C-RX(O) and the C-RX(U). The result is a small "tooth-shaped" intrusion into the C-RX(U), signifying an additional region where laser firing is prohibited. The rule for permitting laser firing under the Tertiary Precaution Surface, due to CRA relaxations, can be expressed as follows:

Laser firing is permitted when the aircraft is inside the C-RX(U), together with either of the following additional conditions:

1. The aircraft is inside the C-RX(O).
2. The aircraft is outside both the C-RT(O) and the C-RX(O).

As our final illustration, we now apply the Tertiary Precaution Surface algorithm to derivation of the complete Tertiary Precaution Surface for our main Tain Range test case. The algorithm is sequentially applied to all attack radials designated by "near" and "far" CRA boundary points on the Tain Range CRA shown in Figure 36. A Tertiary Precaution profile is generated for each attack radial. The overall Tertiary Precaution Surface is then generated by combining all these individual Tertiary Precaution profiles and interpolating between them to produce a continuous surface. The result is illustrated in Figure 41. Note that the coordinate axes are equally scaled.

The diagram illustrates the effect of the CRA relaxation, in which the outline of the CRA appears as a "crater" within the central "bump" in the Tertiary Precaution Surface. An aircraft flying above the Tertiary Precaution Surface along any attack radial can fire the laser without restriction, other than those imposed by the Fault Free Laser Firing Zones and the outcome of the 3D-CALCFAULT evaluation. An aircraft flying below the Tertiary Precaution Surface is not permitted to fire the laser at all. Thus, the Tertiary Precaution Surface puts a "floor" under the FFLFZ and prevents the use of low elevation attack tracks that violate the Tertiary Precaution.

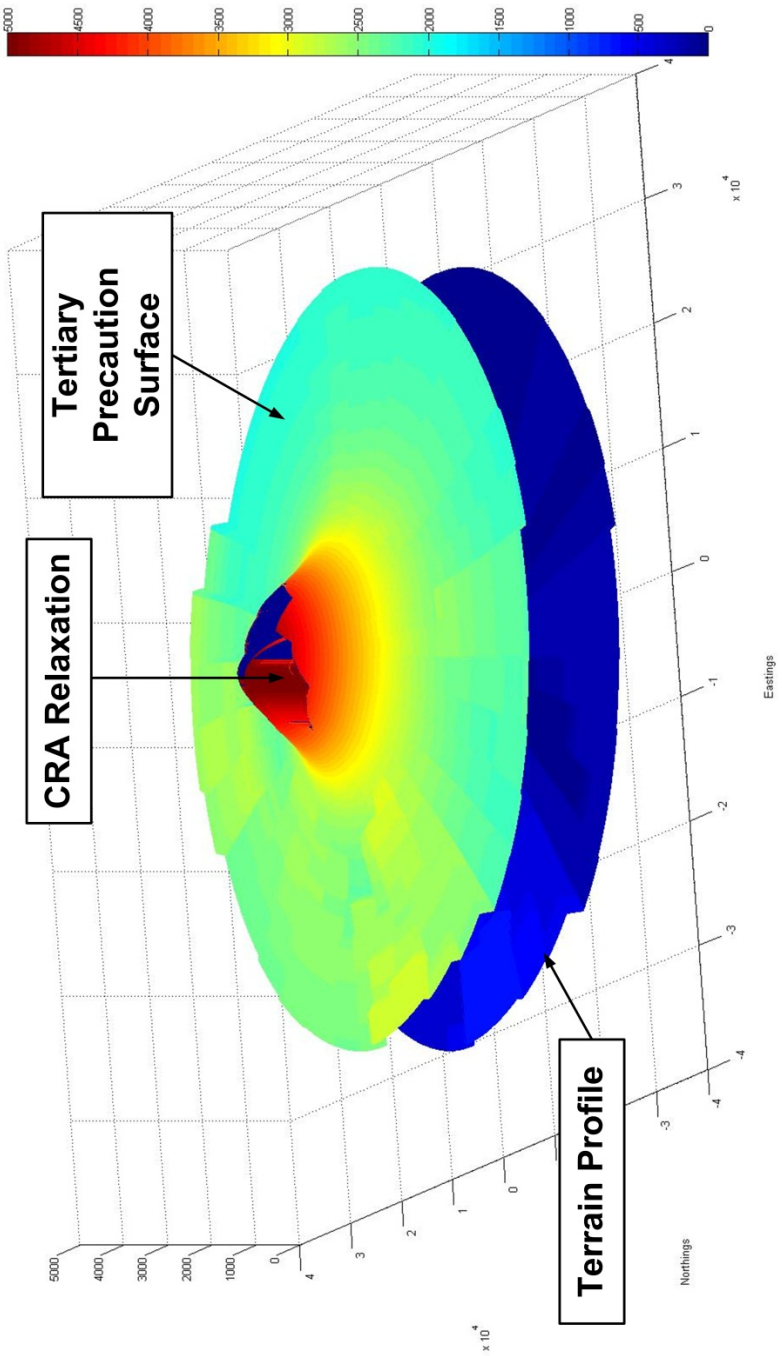

Figure 41: Tertiary Precaution Surface

6 CONCLUSIONS

Over the past 15 years, the United Kingdom (UK) Ministry of Defence (MoD) and the United States (US) Air Force Research Laboratory (AFRL) have collaborated to develop a US-UK laser range safety tool, the Military Advanced Technology Integrated Laser hazarD Assessment (MATILDA) tool. MATILDA uses Probabilistic Risk Assessment (PRA) techniques to perform laser safety and hazard analysis in support of airborne laser designator use during test and training exercises on military ranges. The initial MATILDA tool, MATILDA PRO Version-1.6.1, was based on the 2007 PRA model developed to perform range safety clearances for the UK Thermal Imaging Airborne Laser Designator (TIALD) system. The 2007 TIALD model was an approximation that assumed flat terrain on the range (Smooth Earth TIALD Model), a conservative approximation valid in all terrain. Over the past five years, however, an enhanced version, MATILDA PRO Version-2.0.3, has been produced. The enhanced tool is based on an updated (2012) TIALD model, which has more complex PRA algorithms appropriate for hilly terrain (Rough Earth TIALD Model).

The Rough Earth TIALD Model has four major computational modules: 3D-RBPROG, 3D-CALCZONE, 3D-CALCTERT, and 3D-CALCFAULT. The first module, 3D-RBPROG, deals with creation of a three-dimensional Controlled Range Area (3D-CRA). The second module, 3D-CALCZONE, performs the laser hazard analysis for fault-free laser operation. The product of the fault-free laser hazard analysis is the Fault-Free Laser Firing Zones (FFLFZ), a geometric area within which an aircraft flying at a designated altitude can fire freely at the target. The third module, 3D-CALCTERT, modifies the FFLFZ by applying restrictions arising from the Tertiary Precaution. The product of the Tertiary Precaution analysis is the Tertiary Precaution Surface, which puts a “floor” under the FFLFZ and prevents the use of low elevation attack tracks that violate the Tertiary Precaution. The fourth module, 3D-CALCFAULT, performs a probabilistic hazard analysis for laser operation in the fault/failure condition. The product of the probabilistic fault/failure laser hazard analysis is the expectation value: the likelihood that an unprotected observer outside the CRA will suffer ocular injury as a result of the directional control failure.

For reasons of length, documentation of the mathematical algorithms and computational procedures incorporated in MATILDA PRO Version-2.0.3 has been divided between two AFRL Technical Reports, which will provide the mathematical basis for future code development. The first Technical Report, designated Part I [18], documented the computational procedures for the probabilistic fault/failure laser hazard analysis performed by the fourth module of the Rough Earth TIALD Model, 3D-CALCFAULT. This Technical Report, designated Part II, documents the computational procedures for the fault-free laser hazard analysis, performed by the first three modules: 3D-RBPROG, 3D-CALCZONE, and 3D-CALCTERT.

Section 3 briefly discusses the 3D-RBPROG module, before reviewing algorithms for the 3D-CALCZONE module, in a geometry which assumes a Flat Earth, but a hilly terrain on and surrounding the range. A new method, the Circle of Allowed Laser Firing (CALF) geometry, is used to determine the FFLFZ in hilly terrain. The 3D-CALCZONE computation for a Flat Earth Model is inherently conservative, and overestimates the hazard of short range exposure of an observer on a hill, due to neglect of the Earth’s curvature. Section 4 documents modifications to the 3D-CALCZONE algorithms required for the more complex Curved Earth Model, and compares the FFLFZ for the Flat Earth and Curved Earth calculations. The Curved Earth

FFLFZs allow firing at greater ranges than the Flat Earth FFLFZs, since the curvature of the Earth's surface as we move away from the target makes it easier to avoid irradiating the Terrain Steps due to an undershoot pointing error.

Section 5 documents the 3D-CALCTERT module, which modifies the FFLFZ produced by 3D-CALCZONE. Once again the CALF method is applied, this time to produce FFLFZ restrictions arising from the Tertiary Precaution, which imposes a Minimum Separation Distance (MSD) to mitigate hazards arising from possible short range irradiation of unprotected observers on elevated terrain features. The result of the 3D-CALCTERT analysis is to create a low elevation Tertiary Precaution Surface. An aircraft flying above the Tertiary Precaution Surface can fire the laser without violating the Tertiary Precaution. An aircraft flying below the Tertiary Precaution Surface is not permitted to fire the laser at all. The attack track chosen for 3D-CALCFAULT analysis must therefore be inside the FFLFZ and above the Tertiary Precaution Surface. In this sense the Tertiary Precaution Surface puts a "floor" under the FFLFZ.

It should be noted that the 3D-CALCTERT module incorporated into MATILDA Version-2.0.3 uses a Flat Earth Model. Adaptation of 3D-CALCTERT to a Curved Earth geometry is a planned task for future MATILDA development. Fortunately, the Flat Earth Model provides a more conservative safety analysis than the Curved Earth Model, with more restrictive firing zones. Since a more conservative analysis can always be used for safety purposes, the current Flat Earth implementation of 3D-CALCTERT is acceptable until further development can be done.

7 REFERENCES

1. *MIL-HDBK-828A: Laser Safety on Ranges and in Other Outdoor Areas*, DOD Handbook, Department of Defense, Washington, DC (1996).

2. *JSP 390, Military Laser Safety: Volume 2 – Laser Safety Management System (2012 Edition)*, UK Ministry of Defence, London, UK (2012).

3. American National Standards Institute, *ANSI Standard Z136.1-2014: American National Standard for Safe Use of Lasers*, Laser Institute of America, Orlando, Florida (2014).

4. International Electrotechnical Commission, *IEC 60825-1-2015: Safety of Laser Products, Part 1 – Equipment Classification and Requirements*, Geneva, Switzerland (2015).

5. Bedford, T. and Cooke, R. M., *Probabilistic Risk Analysis: Foundations and Methods*, Cambridge University Press, Cambridge, UK (2001).

6. Kummamoto, H. and Henley, E. J., *Probabilistic Risk Assessment and Management for Engineers and Scientists (Second Ed.)*, Institute of Electrical and Electronic Engineers, Inc., New York, NY (1996).

7. Smith, P. A., "Probability and Risk in Laser Safety," *J. Laser Appl.* **6**, 101 (1994).

8. Sliney, D. H., "Risk Assessment and Laser Safety," *Optics and Laser Tech.* **27**, 279 (1995).

9. Gardner, R. and Smith, P. A., *Optics and Laser Tech.* **27**, 15 (1995).

10. Smith, P. A., Van Veldhuizen, D. A. and Polhamus, G. D., "High-Energy Laser Systems: Analytical Risk Assessment and Probability Density Functions," *Proceedings of the SPIE* **4246**, 145 (2001).

11. Flemming, B. K., "A Probabilistic Risk Assessment Process for High-Power Lasers on Outdoor Ranges," *Proceedings of the International Laser Safety Conference* **12**, 171 (2015).

12. Flemming, B. K., Kennedy, P. K., Huantes, D. F., and Flower, M. D., "Probabilistic Risk Assessment Process for High-Power Laser Operations in Outdoor Environments," *DEPS Journal of Directed Energy* **5**, 381 (2016).

13. Flemming, B. K., Huantes, D. F. and Kennedy, P. K., "MATILDA: A Laser Range Hazard Assessment Utility," *Proceedings of the International Laser Safety Conference* **10**, 239

(2011).

14. Flemming, B. K., Grieve, L. M., Huantes, D. F., Kennedy, P. K. and Flower, M. D., "Laser System Safety Investigations for PRA Model Development," *Proceedings of the International Laser Safety Conference* **11**, 118 (2013).

15. Flemming, B. K., Kennedy, P. K., Huantes, D. F., and Flower, M. D., "MATILDA: A Military Laser Range Safety Tool Based on Probabilistic Risk Assessment Techniques," *DEPS Journal of Directed Energy* **5,** 237 (2014).

16. Kennedy, P. K., Flemming, B. K., Huantes, D. F., and Flower, M. D., "MATILDA: A Miltary Laser Range Safety Tool Based on Probabilistic Risk Assessment (PRA) Techniques," DOD Technical Report No. AFRL-RH-FS-TR-2014-0035, U. S. Air Force Research Laboratory, Fort Sam Houston, TX (2014).

17. Huantes, D. F., Kennedy, P. K., Flemming, B. K., and Flower, M. D., "PRA Analysis of Attack Track Suitability," *Proceedings of the International Laser Safety Conference* **12**, 126 (2015).

18. Kennedy, P. K., Flemming, B. K., Huantes, D. F., and Flower, M. D., "MATILDA Version-2: Rough Earth TIALD Model for Laser Probabilistic Risk Assessment in Hilly Terrain – Part I," DOD Technical Report No. AFRL-RH-FS-TR-2017-0009, U. S. Air Force Research Laboratory, Fort Sam Houston, TX (2017).

19. *Health and Safety at Work Act 1974 (c. 37)*, Her Majesty's Stationary Office, London, UK (1974).

20. Covello, V.T. and Merkhofer, M.W., *Risk Assessment Methods: Approaches for Assessing Health and Environmental Risks*, Plenum Press, New York, NY (1993).

21. Flemming, B. K., and Harding, S. J., *Hilly Range CALCZONE for Flat and Curved Earth Models*, Leonardo Airborne & Space Systems Technical Report: AP50090206, Revision 3, Leonardo MW Ltd., Edinburgh, UK (2017).

22. Flemming, B. K., and Harding, S. J., *Application of the Tertiary Precaution to a "Hilly" Range*, Leonardo Airborne & Space Systems Technical Report: AP50078956, Revision 3, Leonardo MW Ltd., Edinburgh, UK (2017).